High-resolution Early Triassic ammonoid biostratigraphy of South Tibet, China and implications for global correlations.

Xu Dai, Arnaud Brayard, David Ware, Shouyi Jiang, Mingtao Li, Fengyu Wang, Xiaokang Liu, Haijun Song

High-resolution Early Triassic ammonoid biostratigraphy of South Tibet, China and implications for global correlations

Xu Dai[1, 2]*, Arnaud Brayard[2], David Ware[3], Shouyi Jiang[1], Mingtao Li[4], Fengyu Wang[1], Xiaokang Liu[1], Haijun Song[1]*

[1]State Key Laboratory of Biogeology and Environmental Geology, School of Earth Sciences, China University of Geosciences, Wuhan 430074, China

[2]Biogéosciences, UMR 6282, CNRS, Université de Bourgogne, 6 Boulevard Gabriel, 21000 Dijon, France

[3]Museum für Naturkunde, Otto-von-Guericke-Straße 68–73, 39104 Magdeburg, Germany

[4]School of Geosciences, Yangtze University, Wuhan 430100, China

*Correspondence: xudai@cug.edu.cn; haijunsong@cug.edu.cn

Abstract. Ammonoids are key fossil indexes for Triassic biochronology, as all Triassic stages and substages were initially defined on ammonoid faunas. In recent decades, the temporal resolution of ammonoid biostratigraphical scales for the Early Triassic has been greatly improved. However, many uncertainties in zones correlation and superpositions remain, mainly due to sampling heterogeneities, preservation biases and faunal endemicity. In this work, we present the first comprehensive Early Triassic ammonoid zonation from the South Tibet, China, a previously poorly investigated region. Ammonoids were sampled from the Kangshare Formation at four sections (Selong, Paizi, Qubu and Xialong), representing a total of 140 species, ranging from the Griesbachian to the Smithian. These new robust data allow the construction of a high-resolution biostratigraphy using the Unitary Association (UA) method. A total of 22 Unitary Association zones (UAZs) were recognized, including

two UAZs for the Griesbachian, nine for the Dienerian, and 11 for the Smithian. Then, we integrated data from neighboring basins, i.e., Spiti (India) and the Salt Range (Pakistan), and the new data from South Tibet to construct synthetic, laterally reproducible Dienerian-Smithian ammonoid UAZs, which include 12 UAZs for the Dienerian and 16 UAZs for the Smithian. Based on the newly obtained data and high-resolution biostratigraphic scales, we revised global correlations known for the ammonoid biostratigraphy in the Griesbachian, Dienerian and Smithian. Finally, the high-resolution ammonoid zones are generally in agreement with conodont zones in defining stage/substage boundaries. They also provide a robust and accurate time calibration for Early Triassic carbon isotope trend and temperature changes.

Keywords: South Tibet, Neotethys, Unitary Association zone, Griesbachian, Dienerian, Smithian

1 Early Triassic ammonoid biostratigraphy: state of the art

1.1 Early Triassic and its subdivisions

The Early Triassic was a crucial time interval (~251.9 Ma to ~247.1 Ma, Burgess et al., 2014; Ovtcharova et al., 2015) in geological history. The Permian-Triassic mass extinction (PTME) is the most severe known biotic catastrophe of the Phanerozoic, which wiped out more than 80% of marine species (Raup, 1979; Stanley, 2016; Dal Corso et al., 2022). After the PTME, the Early Triassic was characterized by a series of environmental and climate upheavals, including large perturbations of the carbon cycle (Payne et al., 2004; Galfetti et al., 2007a; Tong et al., 2007), recurrent anoxic-euxinic conditions in oceans (Song et al., 2012; Grasby et al., 2013), repeated warming events (Sun et al., 2012; Romano et al., 2013; Goudemand et al., 2019), and dramatic increases in atmospheric CO_2 concentrations (Wu et al., 2021; Joachimski et al., 2022). Coinciding with these environmental changes, life in the Early Triassic experienced significant evolutionary turnovers, for instance, the transition from the

Paleozoic Evolutionary Fauna to the Modern Evolutionary Fauna and the rise of modern marine ecosystems (Sepkoski, 1981; Brayard et al., 2017; Smith et al., 2021; Benton and Wu, 2022; Dai et al., 2023), the transition from non-motile dominated marine ecosystems to ones dominated by nektonic clades (Song et al., 2018).

To study the deep-time biotic-abiotic co-evolution, a robust and accurate timescale is a prerequisite. Formally, the Early Triassic is divided into two stages, i.e., the Induan and Olenekian, in ascending order, which were proposed by Kiparisova and Popov (1956) based on ammonoid assemblages. This two-stage subdivision of the Early Triassic was adopted by the Subcommission on Triassic Stratigraphy in 1991 (Visscher, 1992). The Induan corresponds to the Griesbachian and Dienerian, and the Olenekian corresponds to the Smithian and Spathian (Fig. 1). The four stages model was initially proposed by Tozer (1965, 1967) based on the ammonoid record from Arctic Canada, which was regarded as substages when the two stages model was accepted. During recent decades, conodonts have also played a significant role in the Early Triassic biostratigraphy (Orchard, 2010). However, the heterogeneous fossil record between tropical and boreal domains and between the Tethyan and Panthalassic basins, as well as the different standards among conodont and ammonoid workers, lead to intense debates on definitions of the Early Triassic stages and substages (see e.g., Jenks et al., 2015; Zhang et al., 2019). In this work, we use the four substage subdivision, as it well reflects major ammonoid evolutionary events during the Early Triassic and especially highlights the importance of the late Smithian crisis. The Induan/Olenekian (or Dienerian/Smithian) boundary has not yet been formally defined and is highly debated among different proposals. Here, we tentatively use the definition proposed by Brühwiler et al. (2010c) based on the occurrence of *Flemingites bhargavai* in bed 10 in the Mud section, Spiti, northern India. The bed 10 also corresponds to the first appearance of two Smithian ammonoid families, the Flemingitidae and Kashmiritidae (Brühwiler et al., 2010c). Other proposals include the basal *Hedenstroemia hendenstroemi* Zone in the high-latitude regions (Dagys, 1994a, 1994b; Tozer, 1994) and the basal *Hedenstroemia bosphorensis* Zone in South Primorye (Zakharov et al., 2000). Conodont proposals include the first appearance

datum of *Novispathodus waageni* in the Chaohu section, South China (Tong et al., 2005; Zhao et al., 2007), and the first appearance datum of *Novispathodus waageni* or *Eurygnathodus costatus* in the Mud section (Krystyn et al., 2007; 2017).

1.2 Early Triassic substages and characteristic ammonoids

Ammonoids exhibit high evolutionary rates in the Triassic and are also widely distributed in Triassic fossiliferous exposures. They therefore constitute an unavoidable index fossil for biostratigraphic zonations and correlations, as well as evolutionary studies at different geographic scales (Balini et al., 2010; Jenks et al., 2015). All Triassic stages and substages were initially defined on ammonoid evolutionary events (Mojsisovics, 1895; Tozer, 1965; Balini et al., 2010). The resolution and robustness of Triassic ammonoid biostratigraphic scales were largely improved during the last decades, especially for the Early Triassic and Anisian, leading to highly resolved zonations in some basins (Monnet and Bucher, 2005; Brühwiler et al., 2010a; Ware et al., 2015). For example, 13 UAZs have been recognized for the Smithian in the Salt Range, Pakistan (Brühwiler et al., 2010a, 2011). However, the application of such high-resolution biozonation at a global scale is more limited owing to the sometimes lack of bed-rock-controlled samplings, taxonomical homogenization, and marked biotic provinciality (Brayard et al., 2006; Dai and Song, 2020).

Based on ammonoid assemblages, the Griesbachian can be subdivided into two parts (early and late; Tozer, 1965, 1967). The early Griesbachian is mainly dominated by Permian holdovers, e.g., xenodiscids and otoceratids, while the late Griesbachian assemblages contain newly-originated families, such as ophiceratids, proptychitids, and mullericeratids (Ware et al., 2015; Fig. 1).

The Dienerian substage was erected by Tozer (1965, 1967) based on ammonoid records from Arctic Canada, with two ammonoid zones, the *Proptychites candidus* Zone and the *Paranorites sverdrupi* Zone, in ascending order. Recently, Ware et al. (2015) proposed an exhaustive revision of the Dienerian ammonoid taxonomy and

biochronology based on extensive sampling of Dienerian ammonoids from the Salt Range (Pakistan) and Spiti (India). A total of 12 ammonoid UAZs have been established in these regions (Ware et al., 2015). This exceptionally high resolution ammonoid zonation allows the subdivision of the Dienerian into three parts: lower, middle and late (Ware et al., 2015). The early Dienerian is represented by the co-occurrence of *Gyronites* and *Ussuridiscus* together with the youngest representative of ophiceratids (*Ghazalaites*) (Ware et al., 2015). The middle Dienerian is characterized by the co-occurrence of *Ambites* and *Mullericeras* (note that *Mullericeras* occurs earlier in South China; Dai et al., 2019). The late Dienerian corresponds to the oldest occurrences of paranoritids (e.g., *Vavilovites*, *Koninckites*, and *Awanites*) and hedenstroemiids (*Clypites* and *Pseudosageceras*).

The Smithian substage was also proposed by Tozer (1965, 1967) and initially comprised two ammonoid zones in Arctic Canada, *Euflemingites romunderi* Zone and *Wasatchites tardus* Zone. In recent decades, Smithian ammonoids have been intensively sampled and studied in the western USA basin (Brayard et al., 2013; Jattiot et al., 2017; Jenks and Brayard, 2018; Brayard et al., 2020, 2021), the Salt Range (Brühwiler et al., 2011, 2012c), Spiti (Brühwiler et al., 2010c, 2012b), North Vietnam (Shigeta et al., 2014), South Primorye (Shigeta et al., 2009; Zakharov et al., 2013; Zakharov et al., 2021), and South China (Brayard and Bucher, 2008; Dai et al., 2021). Among these sites, the Salt Range and Spiti show the most complete Smithian ammonoid successions so far, comprising 14 UAZs (Brühwiler et al., 2010a, 2011). Based on these zones, threefold subdivisions (early, middle and late) of the Smithian have been proposed by Brühwiler et al. (2010a, 2011). The early Smithian is characterized by the dominance of flemingitids, kashmiritids, and paranoritids. During the middle Smithian, the relative dominance of these 3 families largely decreased, and newly originating families, such as Arctoceratidae, Galfettitidae, Aspenitidae, and Inyoitidae, became dominant. The late Smithian witnessed severe ammonoid extinction, with many families flourishing in the early and middle Smithian being wiped out (Brühwiler et al., 2010a; Brayard et al., 2021). The early late Smithian was strongly dominated by Prionitidae, while the second part of the late Smithian was

characterized by the co-occurrence of a few xenoceltitids (e.g., *X. subevolutus*, *Glyptophiceras sinuatum*) and *Pseudosageceras* species (Brayard et al., 2021; Dai et al., 2021). Recently, a potential third zone representing the latest Smithian was mentioned (Widmann et al., 2020), but its faunal content and correlation have not been published yet.

The Spathian substage was proposed by Tozer (1965, 1967) based on two ammonoid zones in Arctic Canada, the *Olenikites pilaticus* Zone and the *Keyserlingites subrobustus* Zone. After the Tozer's proposal, the temporal resolution of the Spathian ammonoid biozonations has been greatly improved based on the extensive fieldworks conducted within the western USA basin (Guex et al., 2010; Jenks et al., 2013; Brayard et al., 2019), Japan (Ehiro et al., 2016; Ehiro, 2022; Shigeta, 2022), Western Tethys (Gaetani et al., 1992; Posenato, 1992), and South China (Galfetti et al., 2007b; Ji et al., 2015). However, many uncertainties remain for large-scale correlations, partly reflecting the marked endemism existing during the middle and late Spathian (Brayard et al., 2006; Dai and Song, 2020). To date, the most complete succession of Spathian ammonoid faunas has been documented from the western US basin (Guex et al., 2010; Jenks et al., 2013). It presently contains 8 zones and 23 horizons. According to this succession, the Spathian can be subdivided into three parts: early, middle and late. The early Spathian was dominated by tirolitids and columbitids. The middle Spathian contains two zones, the *Fengshanites*/*Prohungarites* Zone and the *Silberlingeria* Zone. The late Spathian is represented by two zones as well, the *Neopopanoceras haugi* Zone and the *Keyserlingites subrobustus* Zone (Guex et al., 2010). However, the correlation of these high-resolution Spathian ammonoid zonations in the western USA basin awaits similar high-resolution biostratigraphical scales from other regions.

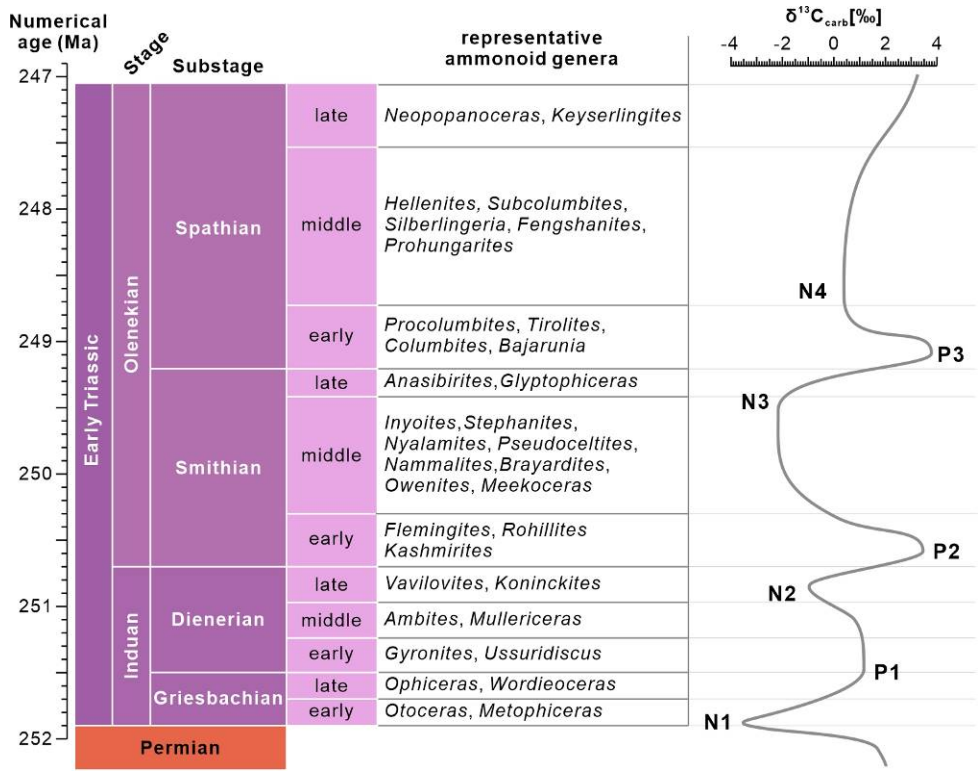

Figure 1. Early Triassic subdivisions and their representative ammonoid genera, associated with simplified carbon isotopic curve for the Early Triassic. Numerical ages for each stage/substage are from Burgess et al. (2014), Ovtcharova et al. (2015), Widmann et al. (2020) and Dai et al. (2023). Note that in the latest version of the ICS International Chronostratigraphic Chart (v2022/10), the age of the Induan/Olenekian boundary is 251.2 Ma based on sample CHIN40 (Ovtcharova et al., 2006). Recently, this sample has been re-analyzed and the new resulting age is 250.647 ± 0.064 Ma (2σ) (Widmann et al., 2020). Subdivisions and respective representative ammonoid genera for the Griesbachian are from Tozer (1965, 1967), for the Dienerian are from Ware et al. (2015), for the Smithian are from Brühwiler et al. (2010a), and for the Spathian are from Guex et al. (2010). Carbon isotopic curve is modified from Galfetti et al. (2008), Hermann et al. (2011), and Sun et al. (2021). The definition of the carbon isotopic excursions (N1-N4, P1-P3) refers to Song et al. (2013)

2 New Early Triassic ammonoid data from South Tibet

2.1 Geological settings

The Tibetan Plateau is a complex assembly of blocks and terranes separated by major suture zones. These are, from south to north, the Tethyan Himalaya, the Yarlung-Zangbo suture zone, the Lhasa Block, the Bangong-Nujiang suture zone, the

Qiangtang Block, the Longmu Co-Shuanghu-Lancangjiang suture zone, the Qamdo Block, and the Jinshajiang suture zone (Yin and Harrion, 2000). South Tibet is located in the Tethyan Himalaya, which was situated on the northern Gondwana passive margin during the Early Triassic (Fig. 2).

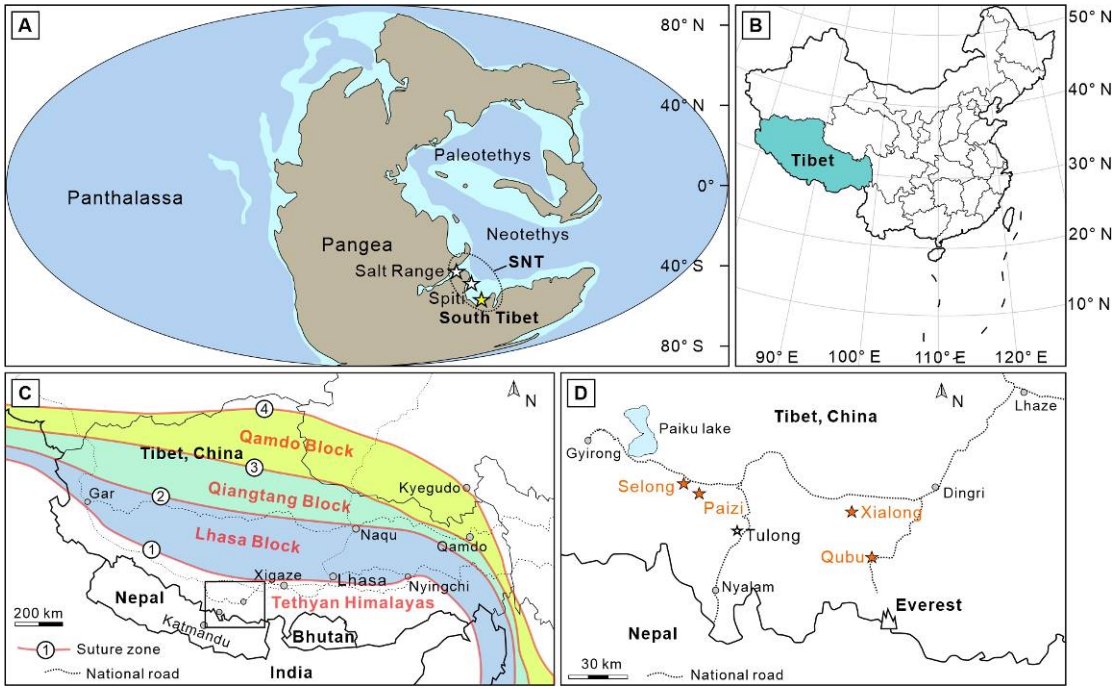

Figure 2. Locations of the studied region and sections. (A) Early Triassic paleogeographic map modified from Scotese (2014). SNT, Southern Neotethys. (B) Present-day position of Tibet, China. (C) Simplified tectonic map of Tibet and location of the study area (rectangle), modified from Zhang et al. (2013). Suture zones: 1, Yarlung-Zangbo; 2, Bangong-Nujiang; 3, Longmu Co-Shuanghu-Lancangjiang; 4, Jinshajiang. (D) Locations of the four studied sections (yellow stars) and the Tulong section (white star), which is a reference section previously studied by Brühwiler et al. (2010b).

The regional Permian-Triassic lithological succession is represented by the Permian Selong Group, the Lower Triassic Kangshare Formation and the Middle Triassic Laibuxi Formation (Wang et al., 1980). The Kangshare Formation is dominated by carbonate and shale deposits formed in middle to outer ramp settings (Li et al., 2019a, 2019b). After careful field observations and correlations, we can divide the Kangshare Formation into six lithological units (Figs. 3, 4).

Unit A is Griesbachian and is composed of thin- to medium-bedded, yellowish dolomites (Fig. 4A). It corresponds to unit Ia at Tulong (Brühwiler et al., 2009). This

unit is usually barren of macrofossils. However, at some sites (e.g., Selong), it contains common but poorly preserved ammonoids. The formation of this dolomitized unit is assumed to have been induced by sulphate-reducing bacteria under elevated seawater alkalinity caused by sulphate reduction coupled with elevated surface ocean temperatures (Li et al., 2018a, 2019b).

Unit B covers the Griesbachian-Dienerian transition and is characterized by thin-bedded, grey limestones, with a total thickness of ~ 1 m (Fig. 4A, B), identical to unit Ib at Tulong (Brühwiler et al., 2009). Unit B contains abundant ammonoids and occasionally bivalve-rich beds. However, these limestones are usually highly cemented, preventing easy excavation and preparation of ammonoid specimens.

Unit C is Dienerian and Smithian in age. It is dominated by shales, with rare occurrences of thin-bedded limestones (Fig. 4C), identical to unit II at Tulong (Brühwiler et al., 2009). Shales are usually barren of fossils, while limestone beds sometimes contain abundant ammonoids and some bivalve specimens.

The bottom of Smithian unit D is characterized by brown ferruginous limestone beds containing poorly preserved ammonoids (Fig. 4C). These ferruginous limestone beds are overlain by thin- to medium-bedded, light-grey, ammonoid-rich limestones (Fig. 4D). Ammonoids from these upper limestones are usually well preserved and easy to excavate and prepare. Bivalve-rich beds are also common in these upper beds. Overlying units E and F are Spathian in age.

Unit E is similar to unit C and is dominated by shales intercalated with a few limestone beds (Fig. 4E). This unit is barren of macrofossils. This unit straddles the Smithian/Spathian boundary (Brühwiler et al., 2009).

Unit F includes medium-bedded, grey (sometimes red, such as at Tulong; see (Brühwiler et al., 2009; Li et al., 2019a), nodular limestones (Fig. 4F) containing moderately abundant ammonoids that are hard to excavate due to the high cementation of enclosing rock.

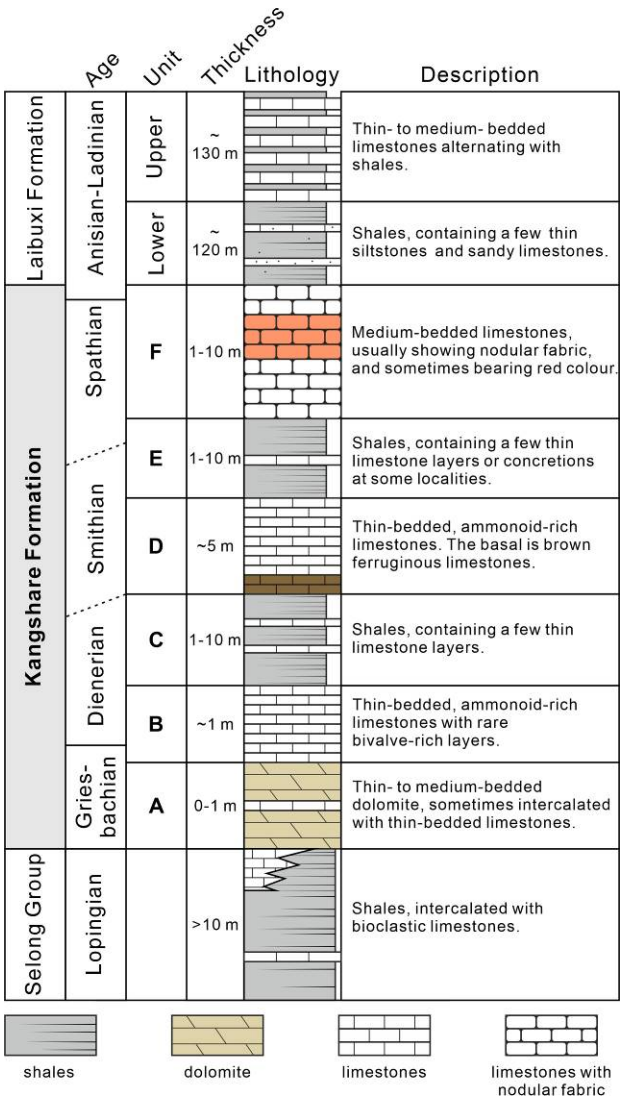

236

237 Figure 3. Synthetic lithological succession of the Kangshare Formation in South
238 Tibet.

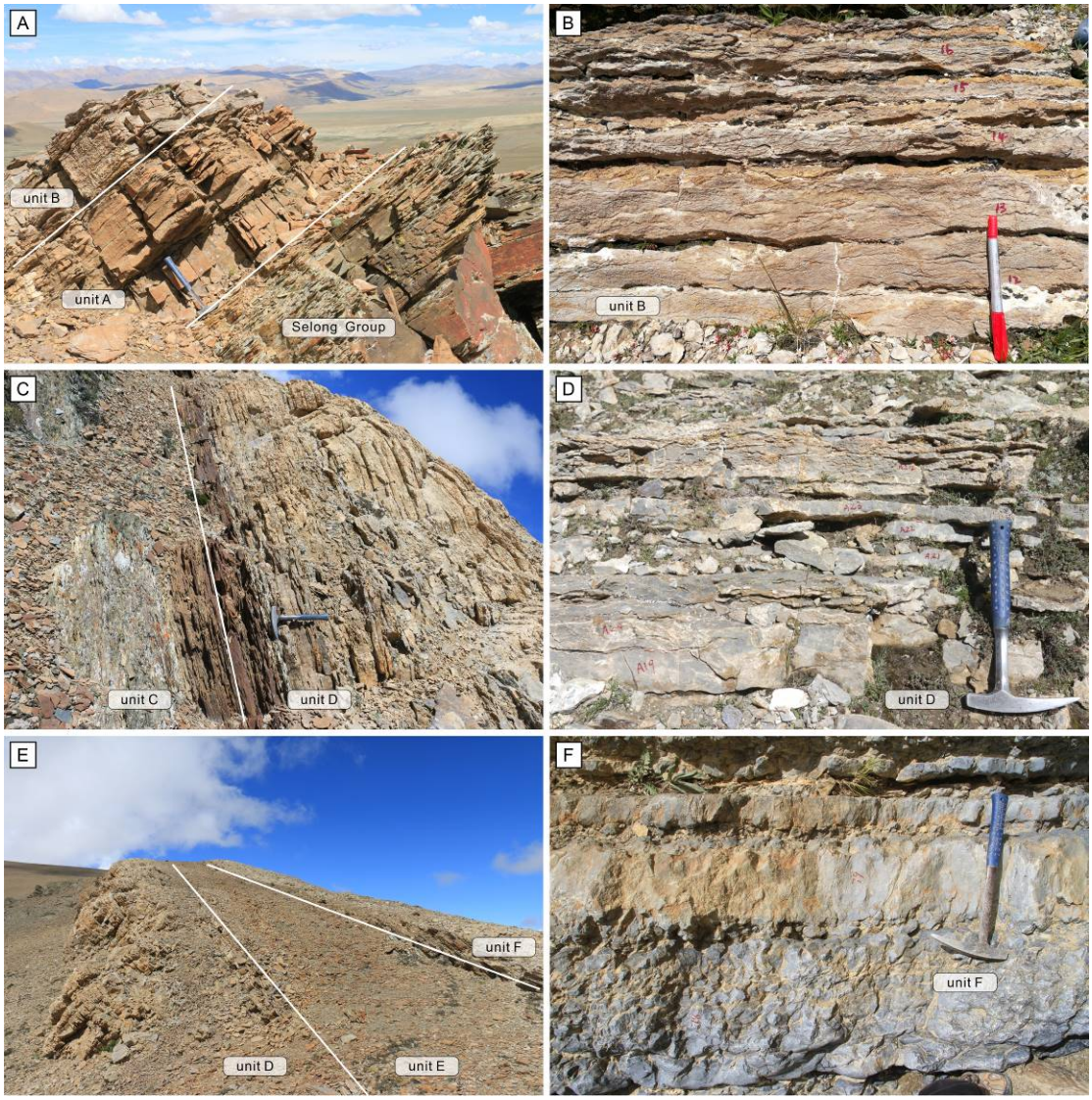

Figure 4. Field observations for lithological units of the Kangshare Formation. (A) ~~The b~~Boundary between the Kangshare Formation and Selong Group at Paizi. (B) Unit B showing thin-bedded limestones at Selong. (C) Units C and D in Paizi, showing dark brown ferruginous beds at the base of unit D. (D) Thin bedded ammonoid-rich limestones of unit D at Paizi. (E) Units D, E and F at Paizi. (F) Unit F medium-bedded limestones bearing nodular fabric at Xialong.

2.2 Historical studies on Early Triassic ammonoids from South Tibet

The Himalayan Early Triassic ammonoids have been known since the pioneering works of Griesbach (1880), Diener (1897), and Krafft and Diener (1909). However, detailed studies of the Lower Triassic exposures from South Tibet were only performed nearly one hundred years later (Mu et al., 1973; Wang and He, 1976; Wang et al., 1980). Since then, numerous works on ammonoids (Brühwiler et al., 2010b;

Zhang et al., 2017), conodonts (Orchard et al., 1994; Wang and Wang, 1995; Wang et al., 2017) and sedimentological and geochemical contexts (Brühwiler et al., 2009; Li et al., 2018a, 2018b, 2019a, 2019b) have been published, leading South Tibet to be a potentially significant area to decipher the PTME and its subsequent biotic recovery (Shen et al., 2006; Li et al., 2019a).

Wang and He (1976) originally recognized five ammonoid zones within the study area: the *Otoceras latilobatum* and *Ophiceras sakuntala* zones in the Griesbachian, the *Gyronites psilogyrus* Zone in the Dienerian, the *Owenites* Zone in the Smithian, and the *Procarnites-Anasibirites* Zone ranging from the late Smithian to the Spathian, in ascending order. Brühwiler et al. (2010b) established a high-resolution middle-late Smithian ammonoid biostratigraphy based on data from the Tulong section (Fig. 2D), which includes six ammonoid beds. Zhang et al. (2017) also described a few Griesbachian-Dienerian ammonoids from the Qubu section (Fig. 2D) and identified three zones: the *Otoceras woodwardi* and *Ophiceras tibeticum* zones in the Griesbachian and the *Ambites* Zone for the middle Dienerian. Overall, compared with adjacent regions such as Spiti and the Salt Range (Brühwiler et al., 2010a; Ware et al., 2015), the resolution of the South Tibet ammonoid zonation is much lower.

2.3 Studied sections

2.3.1 Selong

The Selong section (Figs. 2D, 5A) was first reported by the Scientific Survey of the Everest area (1966 to 1968) [Wang and He, 1976]. Since then, this site has been thoroughly studied for brachiopods (Shen et al., 2000, 2001), ammonoids (Wang and He, 1976), and conodonts (Orchard et al., 1994; Wang and Wang, 1995; Wang et al., 2017; Yuan et al., 2018) and for geochemical purposes (Shen et al., 2006). Selong was also proposed as a candidate for the Permian/Triassic boundary Global Boundary Stratotype Section and Point (GSSP) (Jin et al., 1996). The Permian is represented by

the Selong Group and contains shales and bioclastic limestones, with thicknesses greater than 20 m. It yields abundant brachiopods, corals, and bryozoans (Shen et al., 2000; Shen et al., 2001; Sakagami et al., 2006). The uppermost part of the Selong Group contains late Changhsingian conodonts (Orchard et al., 1994; Wang et al., 2017; Yuan et al., 2018). Unit A of the Lower Triassic Kangshare Formation at Selong corresponds to a lenticular dolomite bed with a maximum thickness of ~1 m, including crinoid fragments and a few poorly preserved ammonoids. This unit also yields *Hindeodus parvus*, a conodont marker of the Permian/Triassic boundary (Yin et al., 2001). Wang and He (1976) recognized five Early Triassic ammonoid zones at Selong.

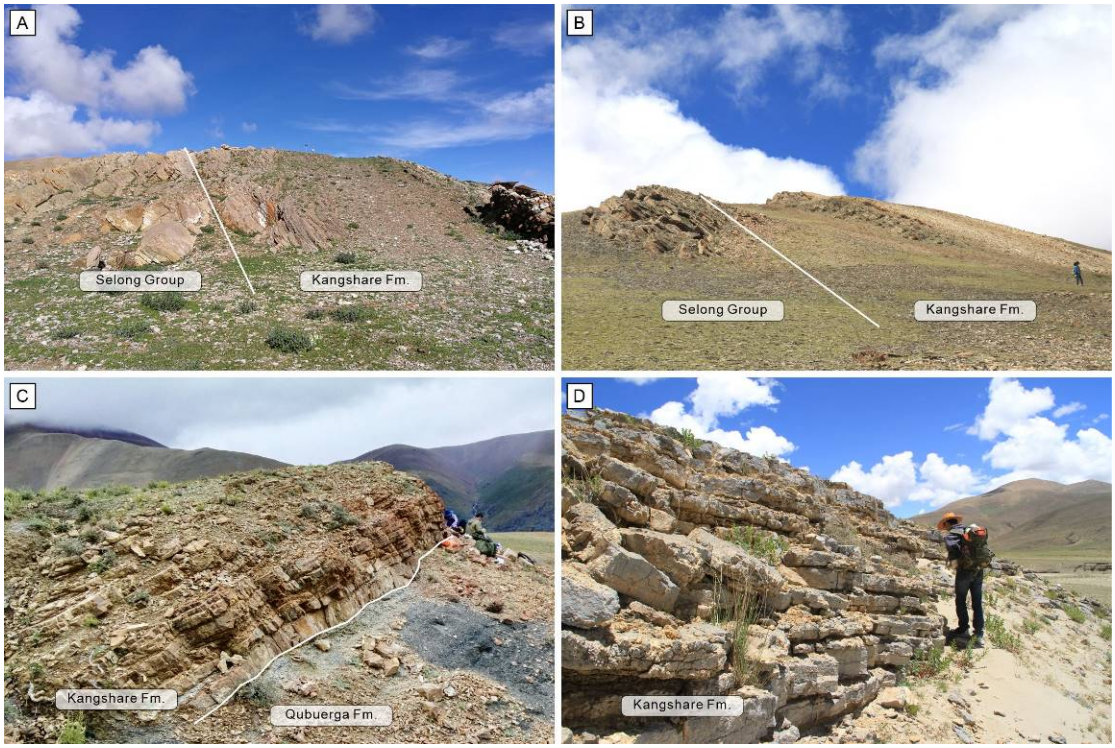

Figure 5. Landscape views of the studied sections. (A) Selong section (GPS: 28°39'52.8"N, 85°49'19.7"E). (B) Paizi section (GPS: 28°34'15.5"N, 85°57'50.9"E). (C) Qubu section (GPS: 28°18’43.6”N, 86°49’38.1”E). (D) Xialong section (GPS: 28°30'60.0"N, 86°41'13.7"E). Fm. Formaton.

2.3.2 Paizi

The Paizi section (Figs. 2D, 5D) is located ca. 20 km southeast of the Selong section. This section was discovered during a 2019 fieldwork. The lithological succession of the Kangshare Formation at Paizi is nearly identical to that of the

Selong section, with only minor differences in thickness. Abundant ammonoids were sampled from units B and D.

2.3.3 Qubu

The Qubu section (Figs. 2D, 5B) is situated approximately 15 km north of the Mt. Everest Base Camp, near Mt. Everest Road. The lithostratigraphic succession includes the Permian Qubu and Qubuerga Formations and the Early Triassic Kangshare Formation. The Qubu Formation is made of quartzose sandstone, alternating with black silty shales, yielding a *Glossopteris* flora (Hsu, 1976; Shen et al., 2003a). The overlying Qubuerga Formation is composed of siltstones interbedded with shales and bioclastic limestones, containing abundant brachiopods, bryozoans, corals, gastropods, bivalves and a few ammonoids (Shen et al., 2003b, 2004; Pan and Shen, 2008). The ammonoid *Roadoceras xizangense* was sampled from the lower part of the Qubuerga Formation, indicating a Late Capitanian-Early Wuchiapingian age (Shen et al., 2004). Unit A of the Kangshare Formation is dominated by ~1 m thick dolomite alternating with shales. The overlying unit B is characterized by thin-bedded limestones and shales, yielding abundant ammonoids (Zhang et al., 2017). This unit also includes the occurrence of a helicoprionid shark (Zhang, 1976).

2.3.4 Xialong

The Xialong section is located ~10 km southeast of Gangga, Tingri (Figs. 2D, 5C). A small outcrop of unit D in the Kangshare Formation, ~ 4.2 m thick, was sampled. This succession is dominated by bioclastic limestones, yielding abundant but usually weathered ammonoids, bivalves and rare orthoconic nautiloids.

2.4 Methods and data

The four studied sections were logged and sampled bed by bed (Figs. 6–11). Specimens were extracted by mechanically decomposing dm-sized blocks from fossiliferous beds. Mechanical techniques, e.g., pneumatic air scribes, were also later

performed in the laboratory to work out morphologic details facilitating species-level identification. Specimens were whitened by magnesium, then photographed using a Canon 70D camera with a micro-lens EF 100 mm f/2.8. Systematic works mainly follow the classification established by Tozer (1994) and revised by Brühwiler et al. (2012a, 2012b, 2012c) and Ware et al. (2018a, 2018b). A total of 140 species were identified in the four studied sections from the Griesbachian to the Smithian (Figs. 6–11). Representative ammonoid species of each substage are illustrated in Figures 12–14. All studied specimens are housed at the Yifu Museum, China University of Geosciences (YFMCUG). Inventory numbers of the figured specimens are reported in respective captions.

The Unitary Associations (UA) method was used to construct the ammonoid biostratigraphical scale. A detailed description of the UA method is available in Guex et al. (2016). Compared with classical interval zones, which are based on first and last occurrences of specific taxa, the UA method utilizes the associations and superpositions of a set of taxa and provides more robust discrete biozones with a higher lateral reproducibility (Guex et al., 2016). The UA method has therefore been used in many regional and global biostratigraphic works (Brühwiler et al., 2010a; Ware et al., 2015; Klein and Korn, 2016; Jattiot et al., 2017; Xiao et al., 2018; Wu et al., 2020). The UA method implemented in PAST 3.0 (Hammer et al., 2001) was used in this study.

Taxa lacking a firm species-level identification, long-ranging taxa, occurrences based on poorly preserved material, and occurrences from potential condensed/reworked levels were omitted in our analyses, except some taxa from the Griesbachian, due to the rarity of ammonoid specimens from this substage. A total of 59 species covering the Griesbachian-Smithian interval were included in the UA analyses. Previously removed taxa were reinserted into reconstructed UAZs. We performed a first set of analyses using the dataset of the four studied sections plus data from the Tulong section (Brühwiler et al., 2010b), providing a synthetic UA zonation for South Tibet. Then, we ran a second set of analyses using the South Tibet data together with published datasets from Spiti and the Salt Range (Brühwiler et al.,

2010b, 2010c, 2011; Ware et al., 2015; Krystyn et al., 2017; Fig. 2A). A total of 93 species were included in this second set of analyses. This allows the construction of integrated Dienerian and Smithian ammonoid UAZs for the Southern Neotethys (SNT). Griesbachian ammonoids were not integrated in the second set of analyses owing to their poorly documented occurrences and the lack of thorough taxonomic revisions. Additionally, we did not integrate in our analyses ammonoid faunas from the neighboring Nepal (Waterhouse, 1994….) as these specimens are very poorly preserved and calibrated, and require thorough taxonomic revisions.

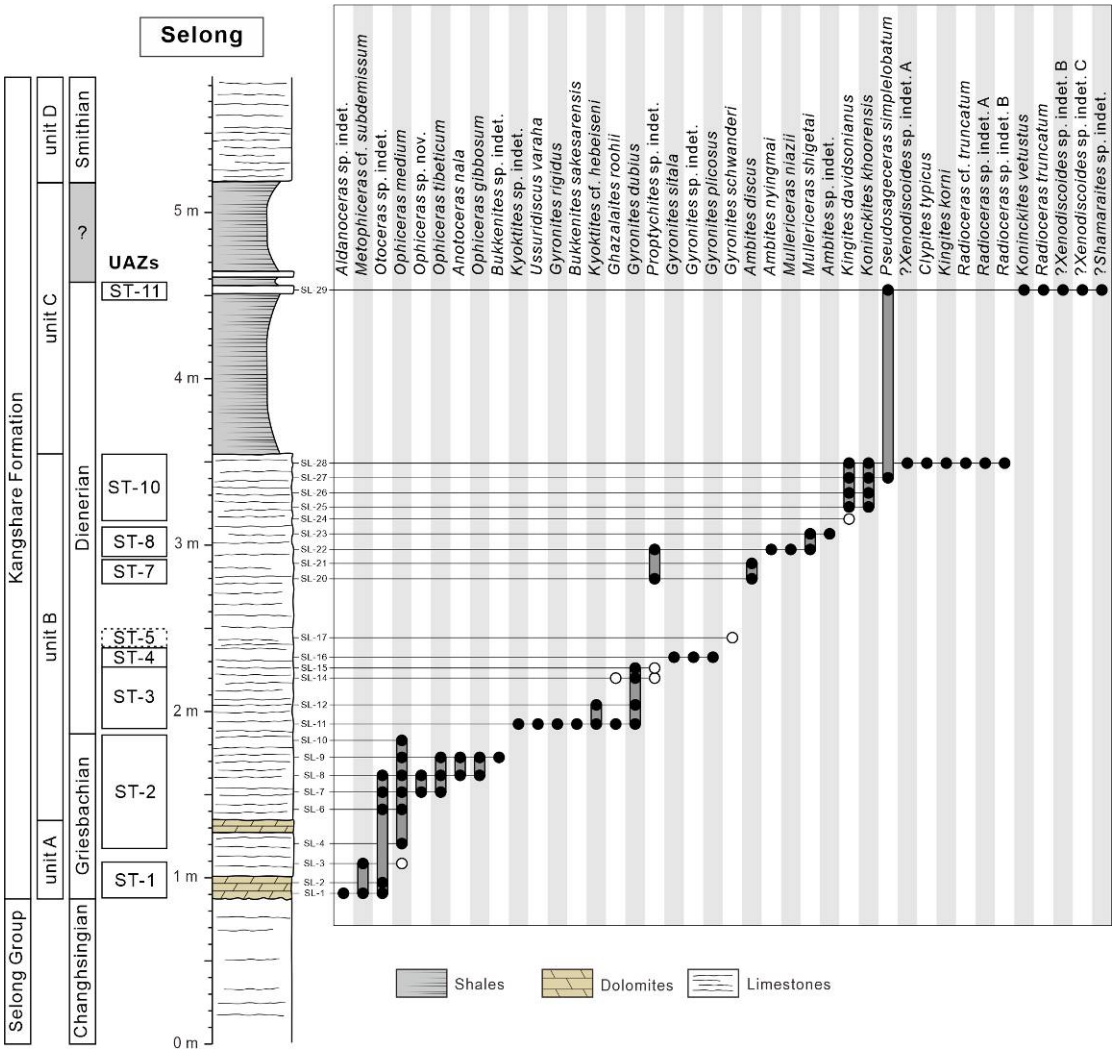

Figure 6. Ammonoid distribution within units A to C of the Kangshare Formation at Selong. Open circles represent occurrences based only on fragmentary or poorly preserved material.

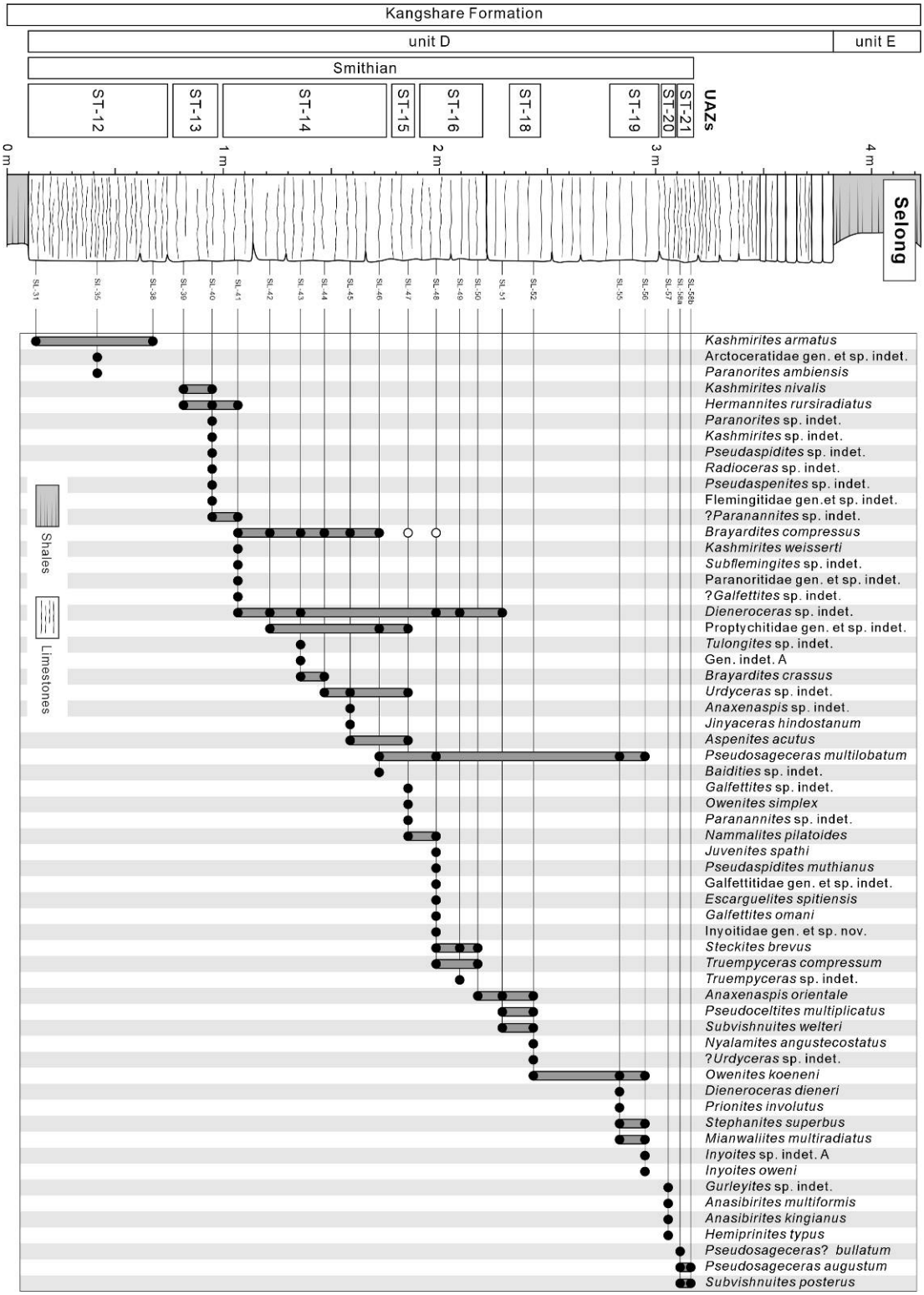

Figure 7. Ammonoid distribution in unit D of the Kangshare Formation at Selong. Open circles represent occurrences based only on fragmentary or poorly preserved material.

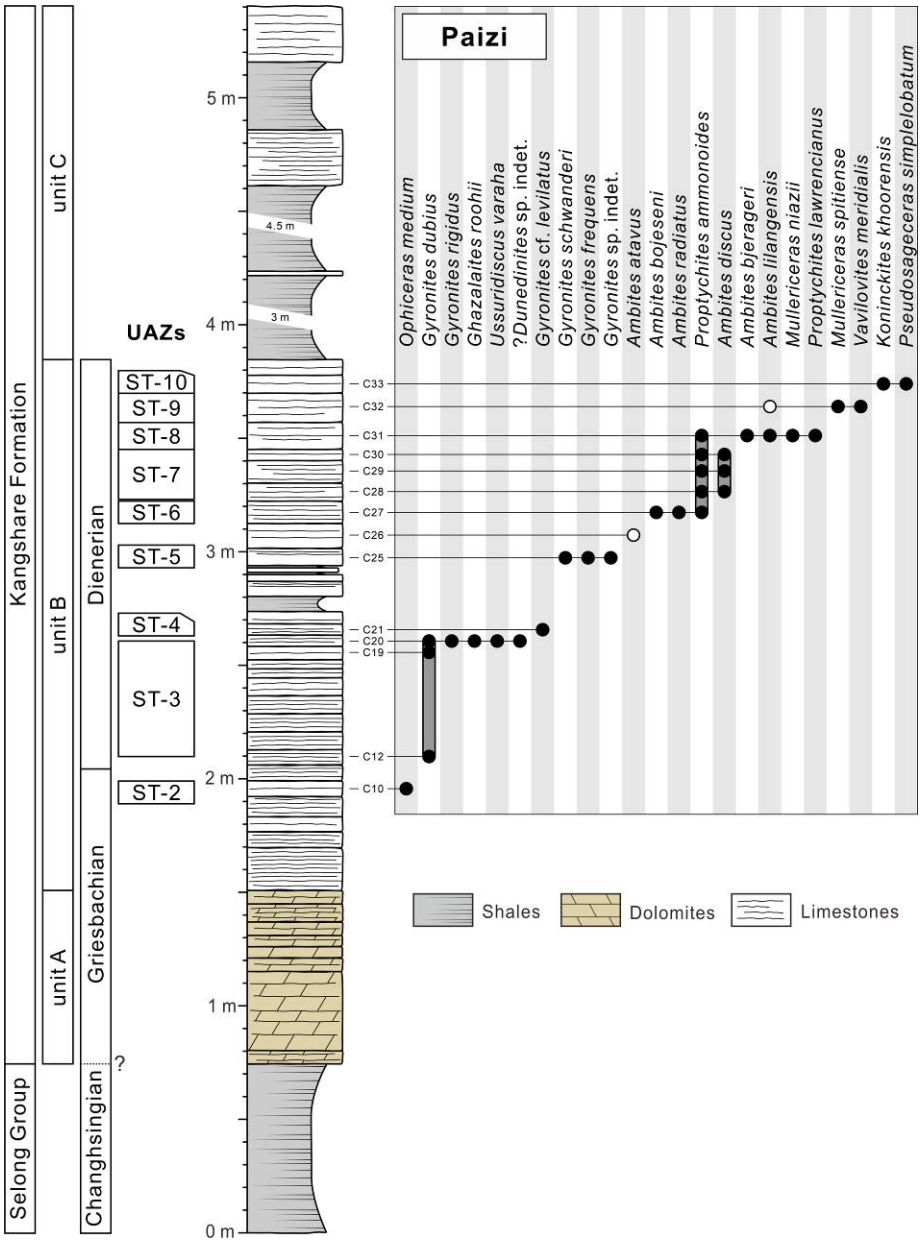

Figure 8. Ammonoid distribution in unit B of the Kangshare Formation at Paizi. Open circles represent occurrences based only on fragmentary or poorly preserved material.

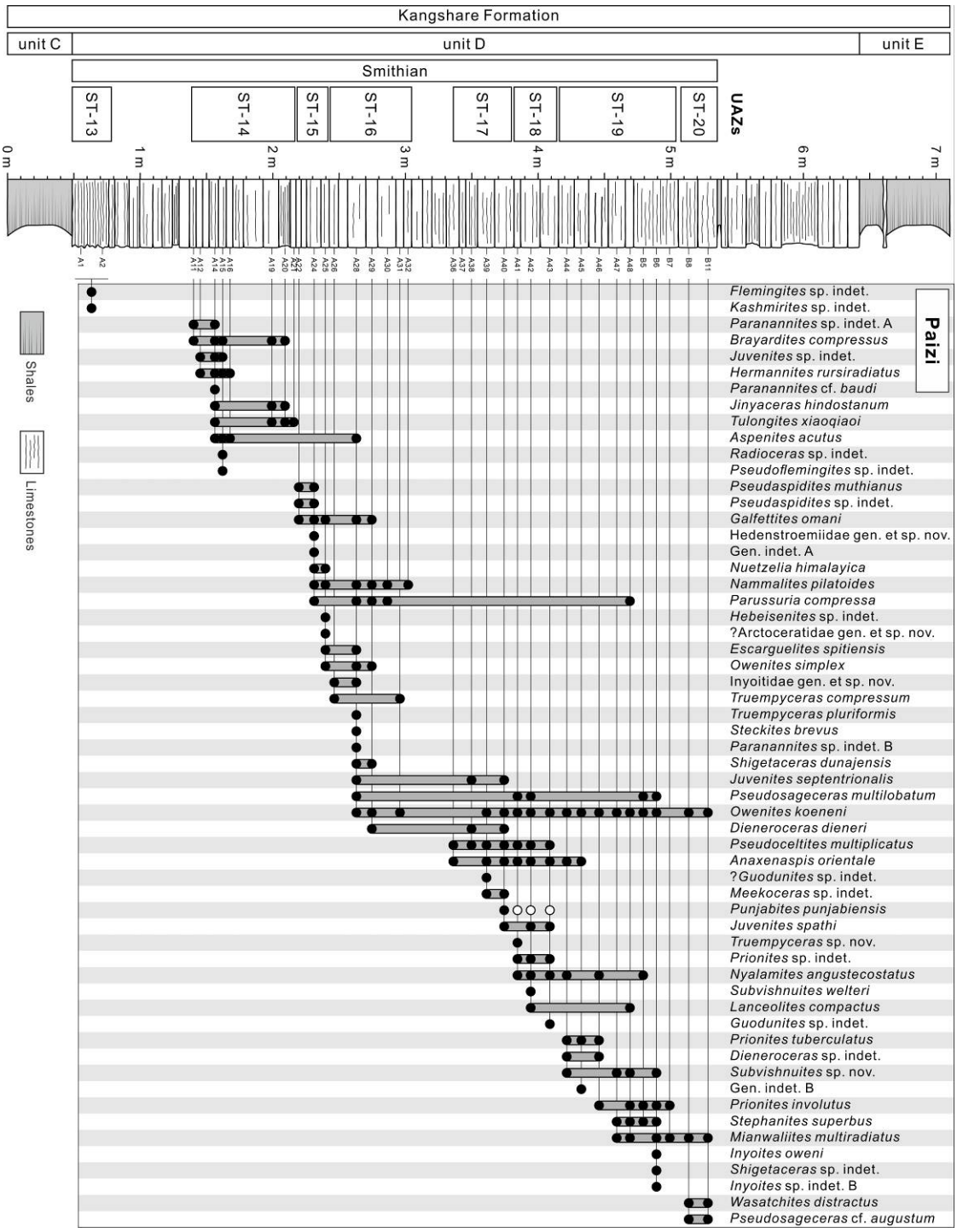

Figure 9. Ammonoid distribution in unit D of the Kangshare Formation at Paizi. Open circles represent occurrences based only on fragmentary or poorly preserved material.

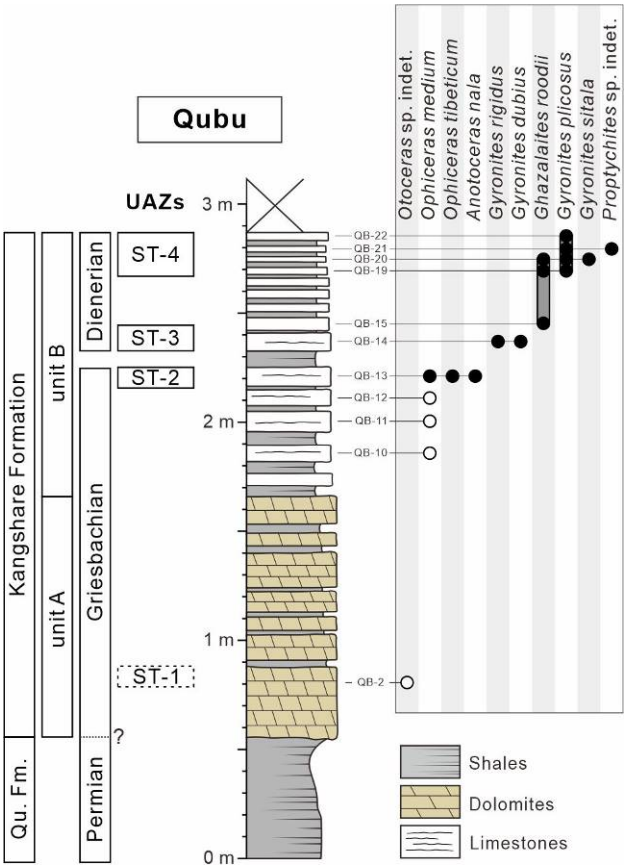

Figure 10. Ammonoid distribution in units A and B of the Kangshare Formation at Qubu. Open circles represent occurrences based only on fragmentary or poorly preserved material.

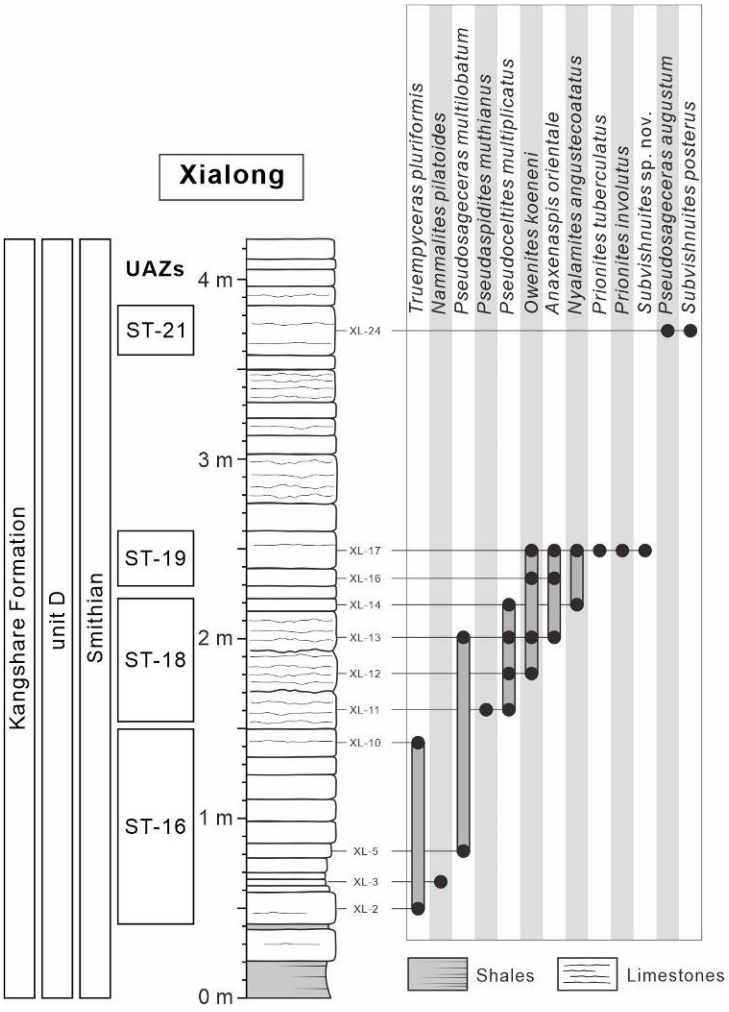

382

383 Figure 11. Ammonoid distribution in unit D of the Kangshare Formation at Xialong.

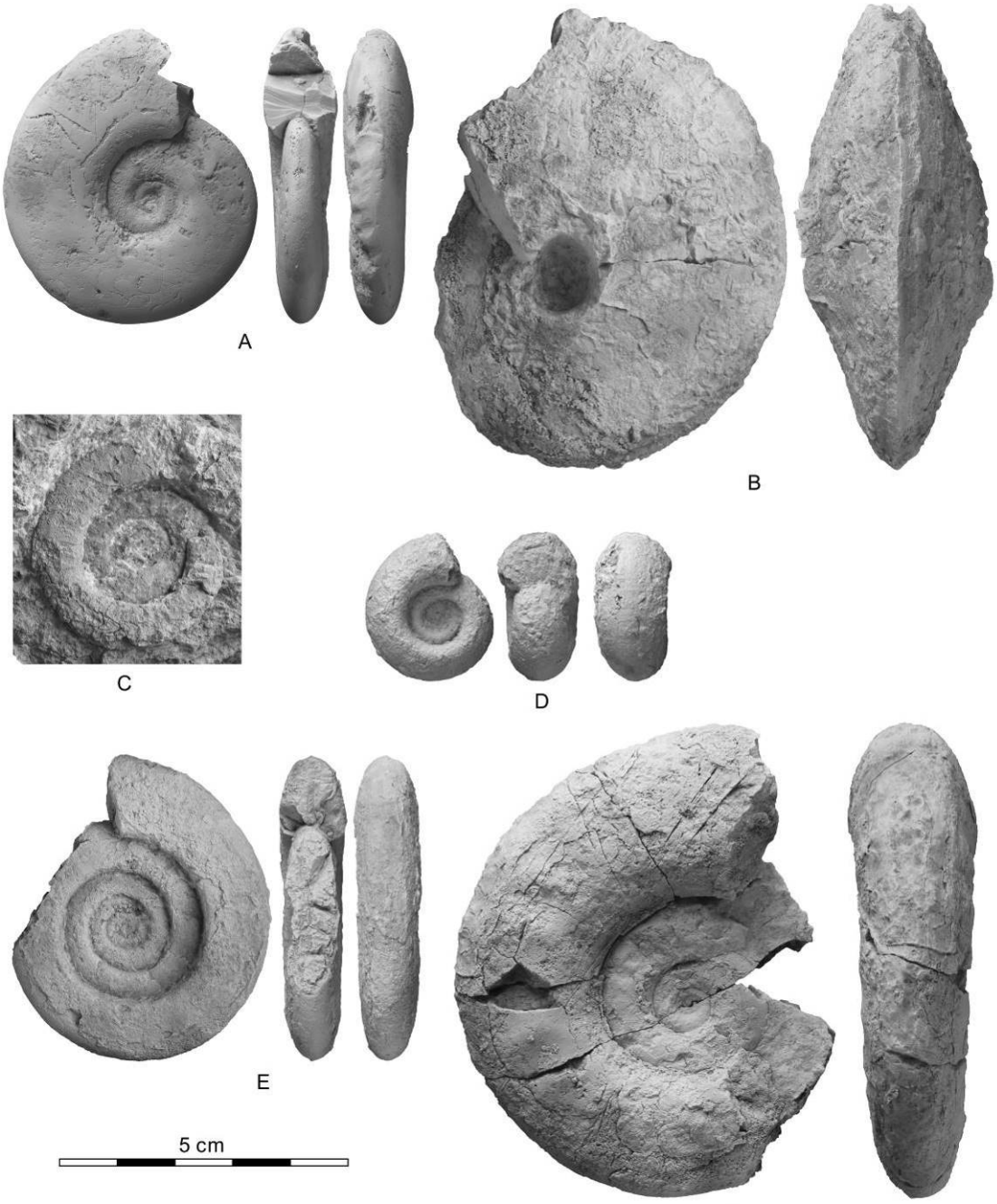

Figure 12. Representative Griesbachian ammonoids from South Tibet. (A) *Ophiceras medium*, YFMCUG 00304, from sample SL-8, Selong. (B) *Otoceras* sp. indet., YFMCUG 00305, from sample SL-8, Selong. (C) *Metophiceras* cf. *demissum*, YFMCUG 00306, from sample SL-3, Selong. (D) *Anotoceras nala*, YFMCUG 00307, from sample SL-8, Selong. (E) *Ophiceras tibeticum*, YFMCUG 00308, from sample SL-9, Selong. (F) *Ophiceras gibbosum*, YFMCUG 00309, from sample SL-8, Selong.

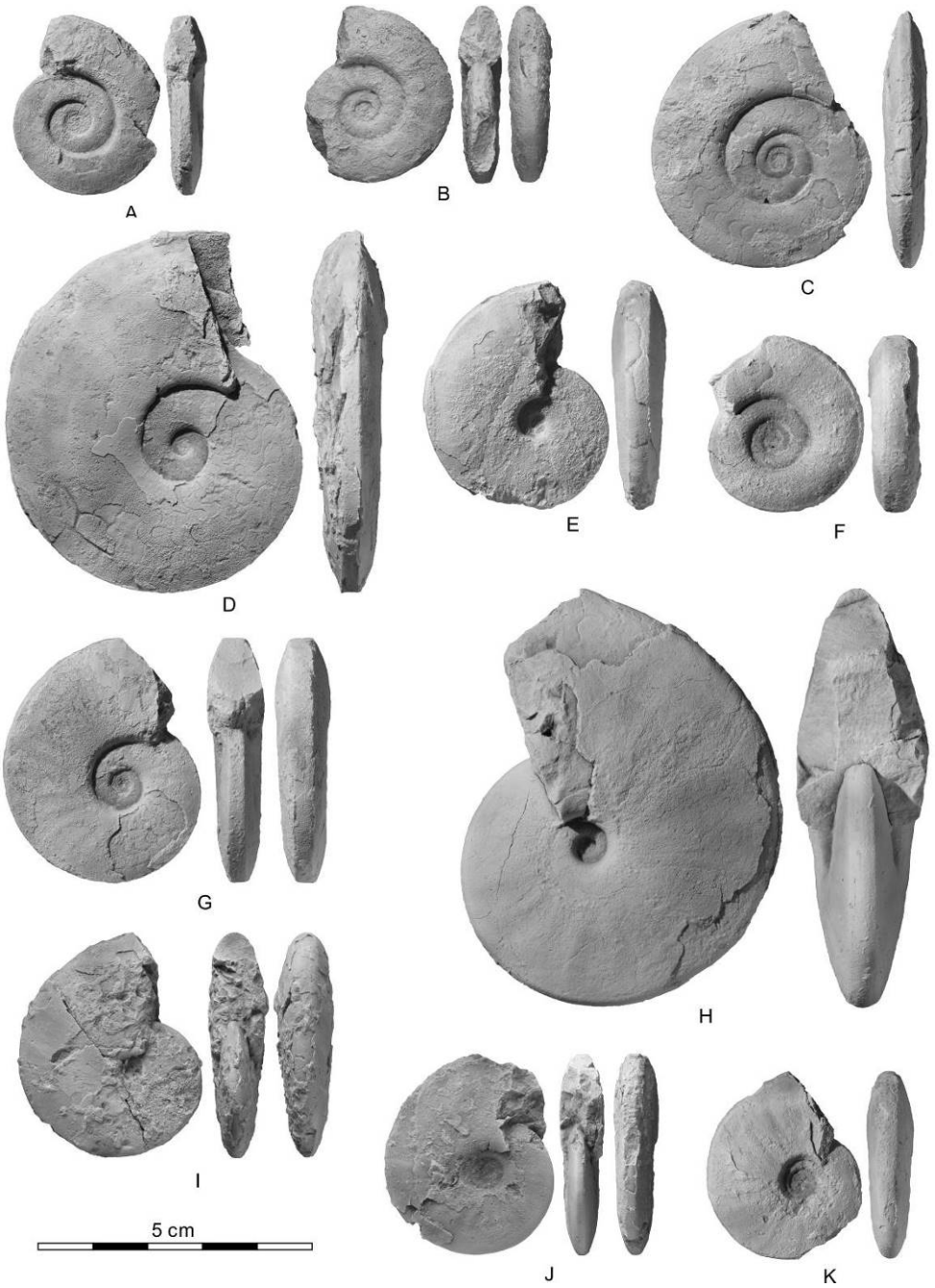

Figure 13. Representative Dienerian ammonoids from South Tibet. (A) *Gyronites dubius*, YFMCUG 00310, from sample C20, Paizi. (B) *Gyronites plicosus*, YFMCUG 00311, from sample SL-16, Selong. (C) *Gyronites frequens*, YFMCUG 00312, from sample C25, Paizi. (D) *Ambites discus*, YFMCUG 00313, from sample C28, Paizi. (E) *Ambites lilangensis*, YFMCUG 00314, from sample C31, Paizi. (F) *Ambites bjerageri*, YFMCUG 00315, from sample C27, Paizi. (G) *Ambites bojeseni*, YFMCUG 00316, from sample C31, Paizi. (H) *Vavilovites meridialis*, YFMCUG 00317, from sample C32, Paizi. (I) *Kingites davidsonianus*, YFMCUG 00318, from sample SL-27, Selong; (J) *Koninckites vetustus*, YFMCUG 00319, from sample C33, Paizi. (K) *Koninckites khoorensis*, YFMCUG 00320, from sample SL-29, Selong.

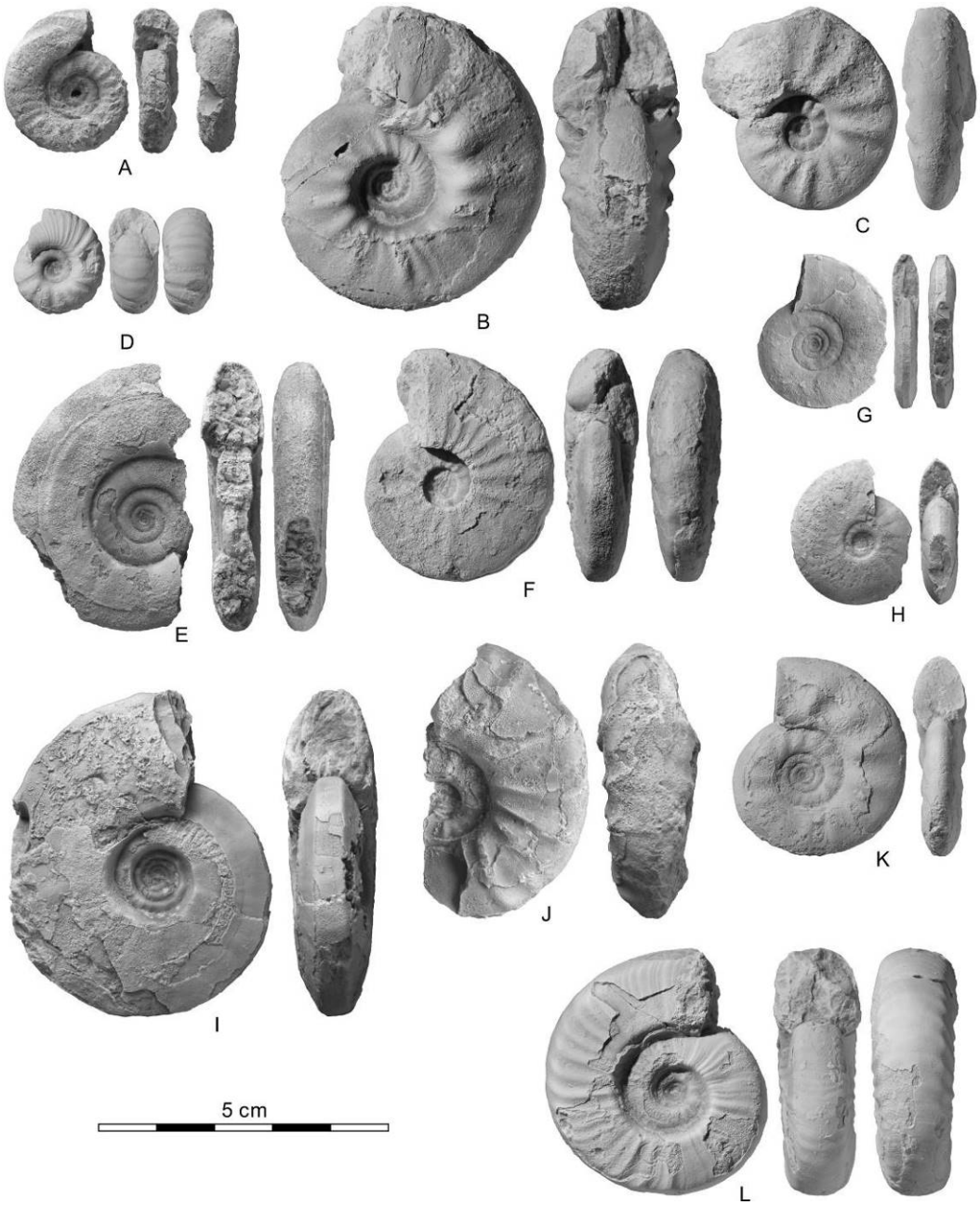

Figure 14. Representative early and middle Smithian ammonoids from South Tibet. (A) *Kashmirites armatus*, YFMCUG 00321, from sample SL-38, Selong. (B) *Brayardites compressus*, YFMCUG 00322, from sample A15, Paizi. (C) *Nammalites pilatoides*, YFMCUG 00323, from sample A25, Paizi. (D) *Juvenites septentrionalis*, YFMCUG 00324, from sample A28, Paizi. (E) *Baidites* sp. indet., YFMCUG 00325, from sample SL-46, Selong. (F) *Truempyceras pluriformis*, YFMCUG 00326, from sample A28, Paizi. (G) *Galfettites omani*, YFMCUG 00327, from sample SL-48, Selong. (H) *Owenites simplex*, YFMCUG 00328, from sample SL-47, Selong. (I) *Truempyceras compressum*, YFMCUG 00329, from sample SL-51, Selong. (J) *Escarguelites spitiensis* YFMCUG 00330 from sample SL-48, Selong. (K) *Anaxenaspis orientale*, YFMCUG 00331, from sample A41, Paizi. (L) *Pseudoceltites multiplicatus*, YFMCUG 00332, from sample A40, Paizi.

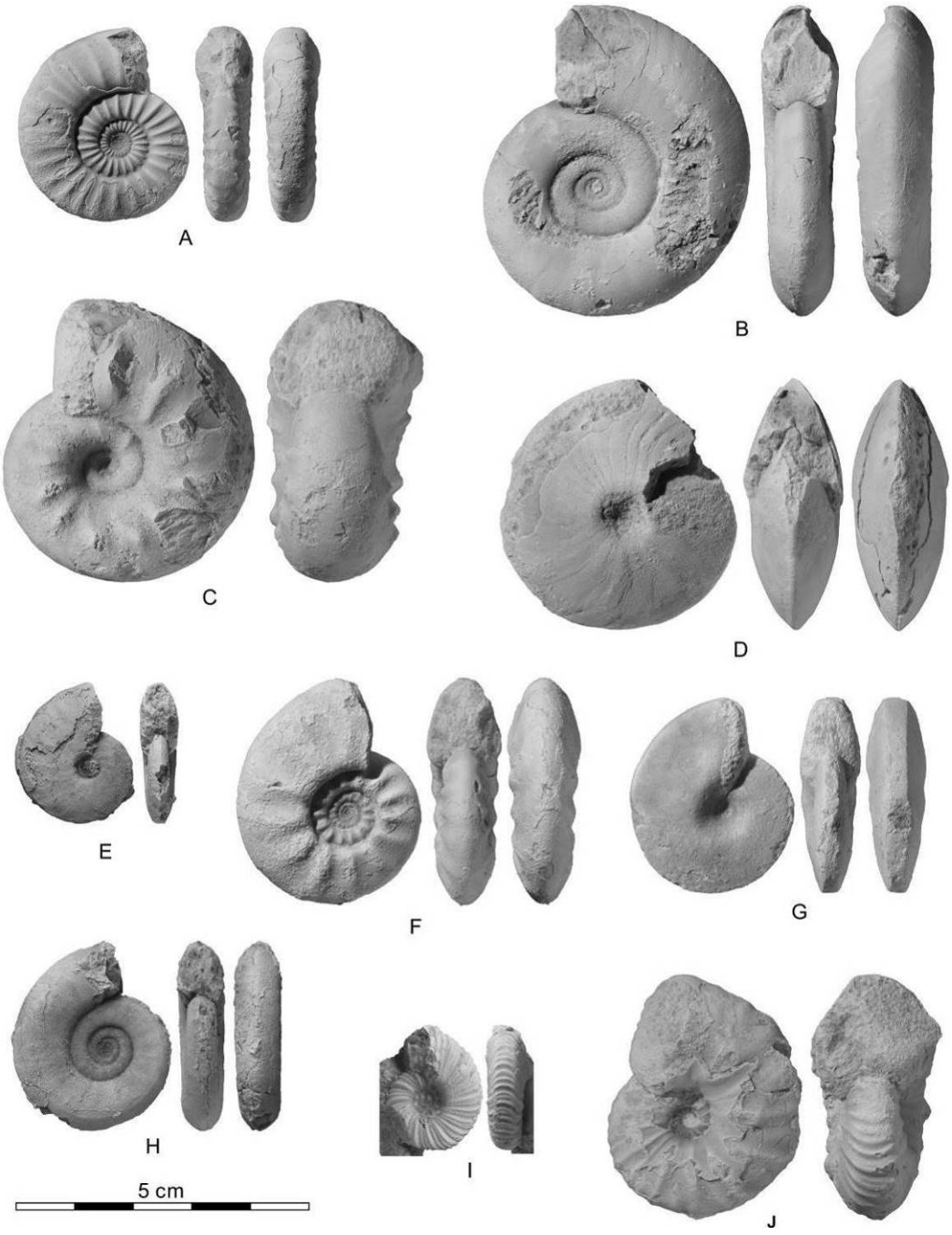

Figure 15. Representative middle and late Smithian ammonoids from South Tibet. (A) *Nyalamites angustecostatus*, YFMCUG 00333, from sample A42, Paizi. (B) *Subvishnuites welteri*, YFMCUG 00334, from sample A42, Paizi. (C) *Stephanites superbus*, YFMCUG 00335, from sample A47, Paizi. (D) *Owenites koeneni*, YFMCUG 00336, from sample A41, Paizi. (E) *Hemiprionites typus*, YFMCUG 00337, from sample SL-57, Selong. (F) *Mianwaliites multiradiatus*, YFMCUG 00338, from sample B6, Paizi. (G) *Prionites tuberculatus*, YFMCUG 00339, from sample A44, Paizi. (H) *Subvishnuites posterus*, YFMCUG 00340, from sample SL-58b, Selong. (I) *Anasibirites kingianus*, YFMCUG 00341, from sample SL-57, Selong. (J) *Wasatchites distractus*, YFMCUG 00342, from sample B11, Paizi.

2.5 A new ammonoid zonation for South Tibet

The first set of UA analyses based on the 59 species from South Tibet led to a first UA ammonoid zonation comprising 24 associations for the Griesbachian-Smithian interval without contradictions. UAs 19 and 20 were lumped together, resulting from their low lateral reproducibility. UAs 21 and 22 were also merged because they cannot be separated in adjacent regions, e.g., the Salt Range and Spiti (Brühwiler et al., 2010a). The final UA zonation thus includes 22 ammonoid UAZs: two for the Griesbachian, nine for the Dienerian, and 11 for the Smithian. The lateral reproducibility of the UAZs is indicated in Fig. 16, and their faunal content in Fig. 17.

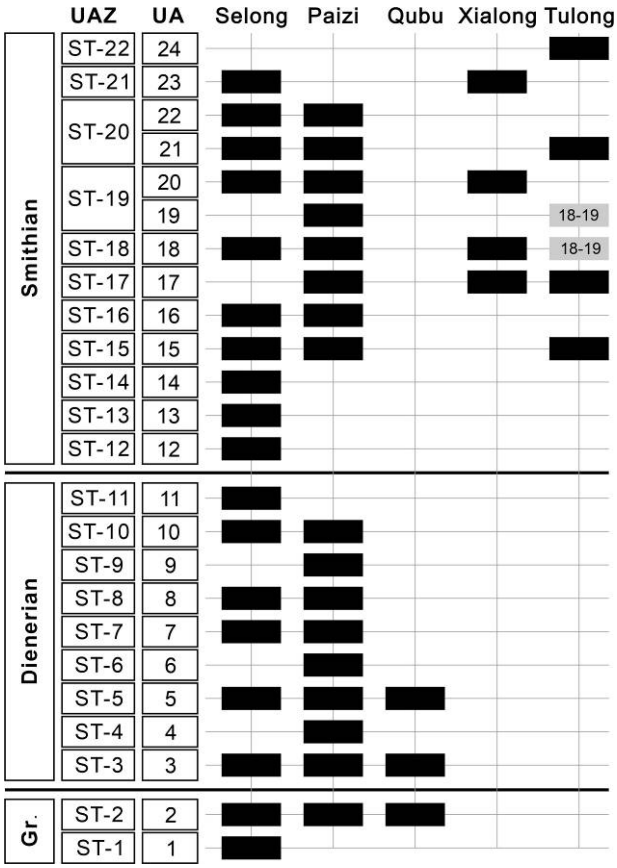

Figure 16. Lateral reproducibility of the UAs and UAZs at the five analyzed sections in South Tibet. Grey rectangles indicate uncertain UA assignment ranges.

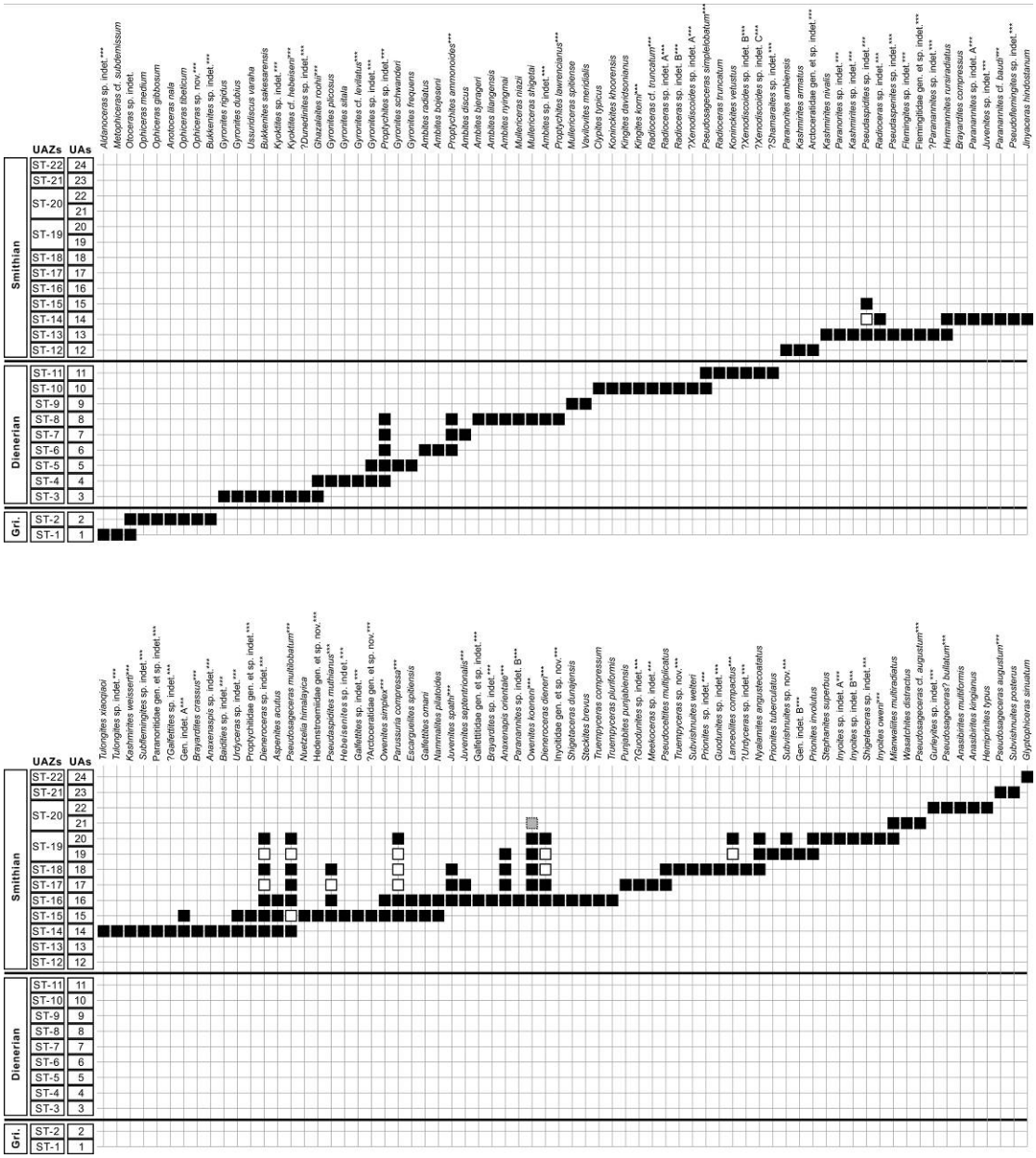

Figure 17. Synthetic range chart of Griesbachian to Smithian ammonoids in South Tibet. Species marked by asterisks (***) were omitted in UA analyses. White squares indicate virtual occurrences. The grey square of *Owenites koeneni* in UA 21 represents a unique occurrence, which probably resulted from condensation or reworking.

3 Integration at the Southern Neotethys scale

The newly obtained UA zonation largely improves the resolution of the Early Triassic ammonoid biochronology in South Tibet (Fig. 17). Based on these new data and previously published data from the neighboring basins of Spiti and the Salt Range (Brühwiler et al., 2010b, 2011; Ware et al., 2015; Krystyn et al., 2017), we

constructed a synthetic Dienerian-Smithian ammonoid zonation. Twenty-eight UAZs were identified, most of which showed strong lateral reproducibility (Figs. 18, 19).

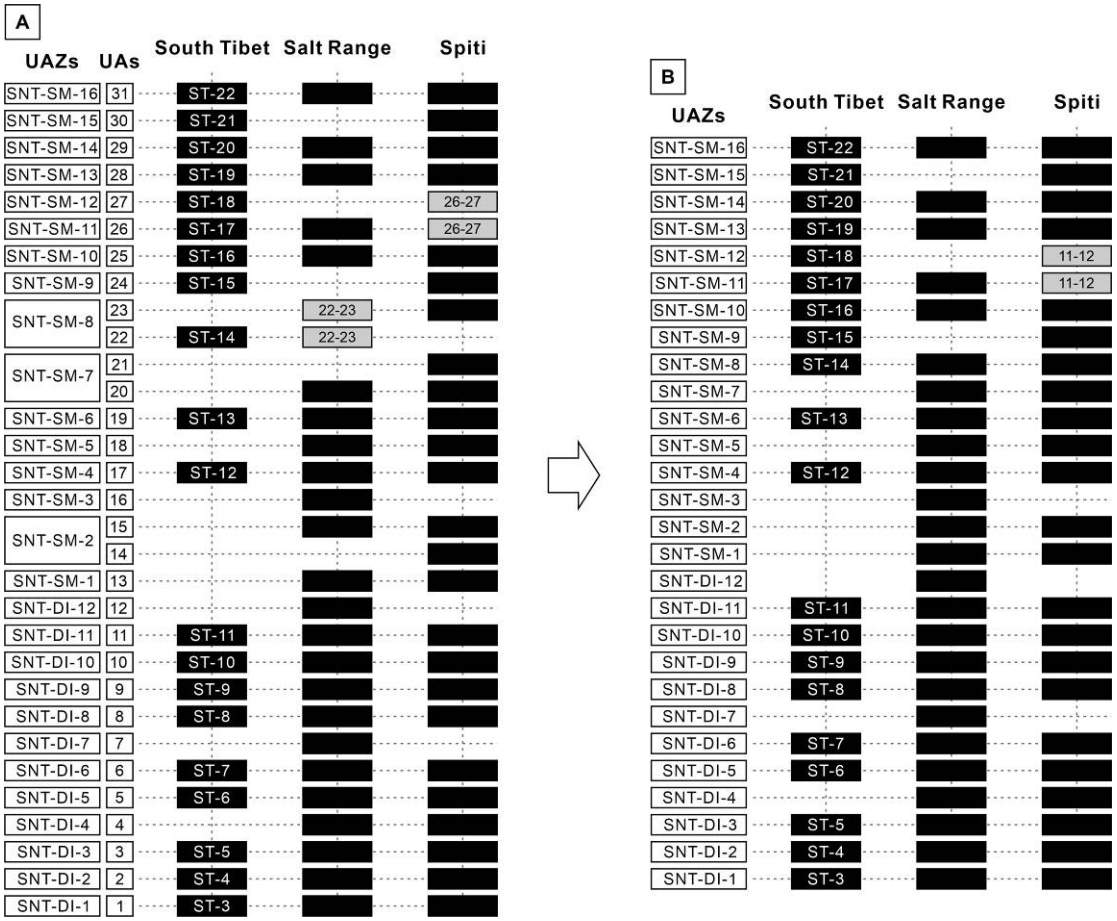

Figure 18. Lateral reproducibility of UAs and UAZs within the SNT. Grey rectangles indicate uncertain UA assignment ranges in (A) and uncertain UAZ assignment ranges in (B).

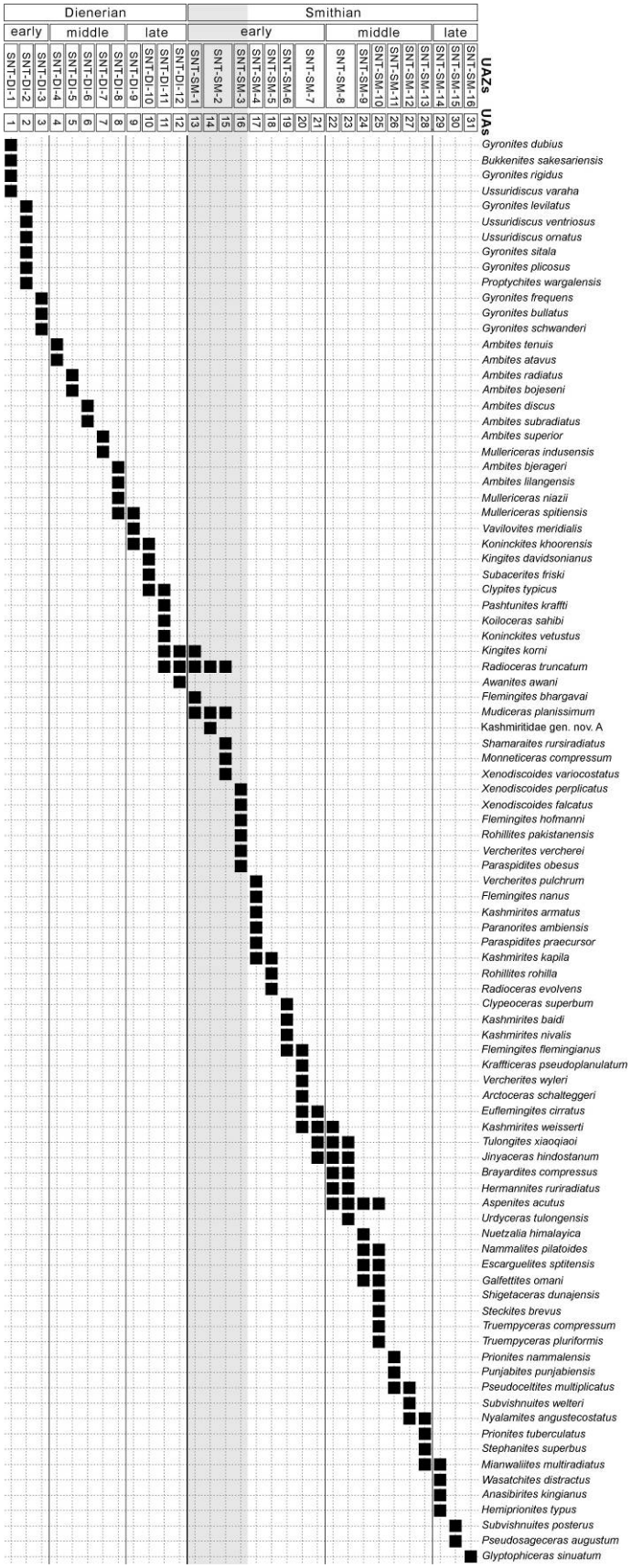

Figure 19. Synthetic range chart of Dienerian and Smithian ammonoids used in the UA analysis for the SNT. The grey area indicates the interval of uncertainty for the

placement of the Dienerian/Smithian boundary among different proposals (see section XXX).

3.1 Griesbachian

Griesbachian ammonoids are not well documented in the SNT. Thus, correlations with other basins for this time interval are rather rough (Fig. 20). Overall, SNT Griesbachian ammonoids can be divided into two successive assemblages, the older assemblage being dominated by xenodiscids and *Otoceras* and the younger assemblage being characterized by common occurrences of ophiceratids and a few *Otoceras* specimens.

In the seminal work of Griesbach (1880), the author introduced *Otoceras* and *Ophiceras* from the Shalshal Cliff in the central Himalayas, and coarsely grouped them into the *Otoceras* beds. Later, Diener (1897) published a more comprehensive taxonomic work based on Griesbach's specimens and his own new collections. However, Diener did not further subdivide the *Otoceras* beds.Wang and He (1976) initially established two zones in South Tibet: the *Otoceras latilobatum* and *Ophiceras sakuntala* Zones. The former zone contains *Otoceras latilobatum*, *Otoceras* sp. indet., and *Glyptophiceras* sp. (here, reassigned to *Metophiceras* sp.). It should be noted that the holotype of *Otoceras latilobatum* is a weathered fragment, without clear morphological details, thus questioning the taxonomic assignment of this species. Regardless of the taxonomic uncertainties, this zone most likely correlates with the newly defined ST-1, according to the association of *Otoceras* and *Metophiceras*. The *Ophiceras sakuntala* Zone of Wang and He (1976) undoubtedly correlates with ST-2.

At Qubu, Zhang et al. (2017) also distinguished the successive *Otoceras woodwardi* and *Ophiceras tibeticum* Zones. The former includes *Otoceras woodwardi* (the reader should note that the taxonomy of *Otoceras* in the Himalayas needs in-depth revisions) and *Ophiceras* sp. The latter contains *Ophiceras demisum*, *Ophiceras tibeticum and Discophiceras wordiei*. However, these two zones cannot be

492 distinguished at Selong (Fig. 6) and Shalshal Cliff (Griesbach, 1880; Diener, 1897).
493 Thus, the two zones of Zhang et al. (2017) can be merged into one single zone and
494 correlate with the ST-2.

495 Griesbachian ammonoid successions are almost identical between South Tibet
496 and Spiti. Two distinct zones were recognized in Spiti (Krystyn and Orchard, 1996).
497 The lower one is characterized by *Otoceras woodwardi* and "*Ophiceras bandoi*" (this
498 taxon probably rather belongs to *Metophiceras*, because it is ribbed and more evolute).
499 In the upper part of this zone, i.e., in bed E3 at Muth, *Ophiceras* cf. *tibeticum*
500 co-occurs with *Otoceras woodwardi and* "*Ophiceras bandoi*". Thus, the *Otoceras*
501 *woodwardi* - "*Ophiceras bandoi*" Zone in Spiti probably correlates with the ST-1 plus
502 the lower ST-2 in South Tibet (Fig. 20). The second zone established by Krystyn and
503 Orchard (1996) is represented by an assemblage of *Ophiceras*, *Discophiceras* and
504 *Bukkenites*. This zone correlates with the ST-2 in South Tibet (Fig. 20).

505 In the Manang district, Nepal, Waterhouse (1994) introduced two successive
506 Griesbachian ammonoid zones. The lower one is the *Otoceras woodwardi* Zone,
507 which can be correlated with the ST-1. The upper one is the *Ophiceras tibeticum* Zone,
508 corresponding to the ST-2.

509 In the Salt Range, Griesbachian ammonoids can be divided into three regional
510 zones (Ware et al., 2018b). The oldest is represented by a single specimen of
511 *Hypophiceras* aff. *gracile*, which most likely correlates with the ST-1 in South Tibet
512 and the *Otoceras woodwardi* - "*Ophiceras bandoi*" Zone in Spiti. The second zone is
513 also characterized by a single species, *Ophiceras connectens*, and probably correlates
514 with the lower ST-2 in South Tibet. The youngest zone is documented in a condensed
515 bed, as indicated by the co-occurrence of *Ophiceras sakuntala* and the earliest
516 Dienerian taxa, such as *Gyronites dubius*. This zone probably partly correlates with
517 the upper ST-2 in South Tibet.

518 ## 3.2 Dienerian

519 Integrated Dienerian ammonoid datasets from South Tibet, Spiti and the Salt

Range led to the construction of 12 UAZs without any contradiction, a resolution rather similar to the basinal UA zonation from Spiti and the Salt Range (Fig. 20). Most of these UAZs are documented in South Tibet, except SNT-DI-4, SNT-DI-7 and SNT-DI-12 (Figs. 18, 20). SNT-DI-4 (corresponding to sample C26) probably occurred at Paizi (Fig. 8) with several sampled fragments resembling *Ambites atavus*. The new resulting UAZs in this work is highly congruent with Ware et al. (2015).

Poorly preserved Dienerian ammonoids are reported from the Sabche and Jargeng members of the Khangsar Formation in the Manang district, Nepal (Waterhouse, 1996a). They may represent a complete Dienerian ammonoid succession similar to the synthetic SNT UAZs. However, precise correlation with this area require a bed-by-bed sampling and thorough taxonomic revisions of this material.

3.3 Smithian

A total of 19 UAs were constructed for the SNT with no contradiction. Three can be merged with temporally close associations, according to poor lateral reproducibility or marked taxonomic similarities (Fig. 18). Finally, a new zonation with 16 UAZs is constructed for the entire Smithian.

Compared with the 14 UAZs established by Brühwiler et al. (2010b, 2011), we identified an additional middle Smithian UAZ, i.e., SNT-SM-12, located between the previously named *Pseudoceltites multiplicatus* and *Nyalamites angustecostatus* UAZs (i.e., S-10 and S-11 of Brühwiler et al., 2011, respectively). This UAZ (ST-18, see detailed assemblage description in section 2.5.18 and Fig. 17) is notably characterized by the co-occurrence of *Subvishnuites welteri*, *Pseudoceltites multiplicatus* and *Nyalamites angustecostatus*. *Subvishnuites welteri* was chosen as the index species of this zone, owing to its restricted occurrence within this zone in the SNT. This association was also found in Oman (Brühwiler et al., 2012a) and possibly in Timor (Jattiot et al., 2020). Another modification is that the UA 30, characterized by *Subvishnuites posteri*, is now considered as a UAZ because this UA can be recognized in both Spiti and South Tibet. Overall, the temporal resolution of the Smithian scale

has been improved from 14 to 16 UAZs.

At Paizi , we found an unusual association in upper Smithian beds B8 and B11 (Fig 9), *Owenites koeneni* co-occurring with *Wasatchites distractus*. In other basins worldwide, *Wasatchites* distinctly overlies assemblages containing *Owenites* (Brühwiler et al., 2012b, 2012c; Jenks and Brayard, 2018). We interpret this uncommon association as a probable consequence of small condensation or reworking. Indeed, the Paizi section is somewhat condensed and some ammonoids from bed B11 are inclined or even vertical to the bedding plane, possibly indicating a local weak reworking. Additionally, a superposition between Wasatchites distractus and Anasibirites kingianus is observed in the studied sections, although these two taxa occur together in other regions, e.g., Spiti and the Salt Range (Brühwiler et al., 2012a, 2012b). This could be explained by a sampling or preservation bias. We therefore merged the UAs 21 and 22.

Successive Smithian ammonoid assemblages were also reported from the Manang Group, Manang district, Nepal, by Waterhouse (1996b, 1999). However, their very poor preservation and the near absence of any detailed superpositions prevent precise correlations with the SNT.

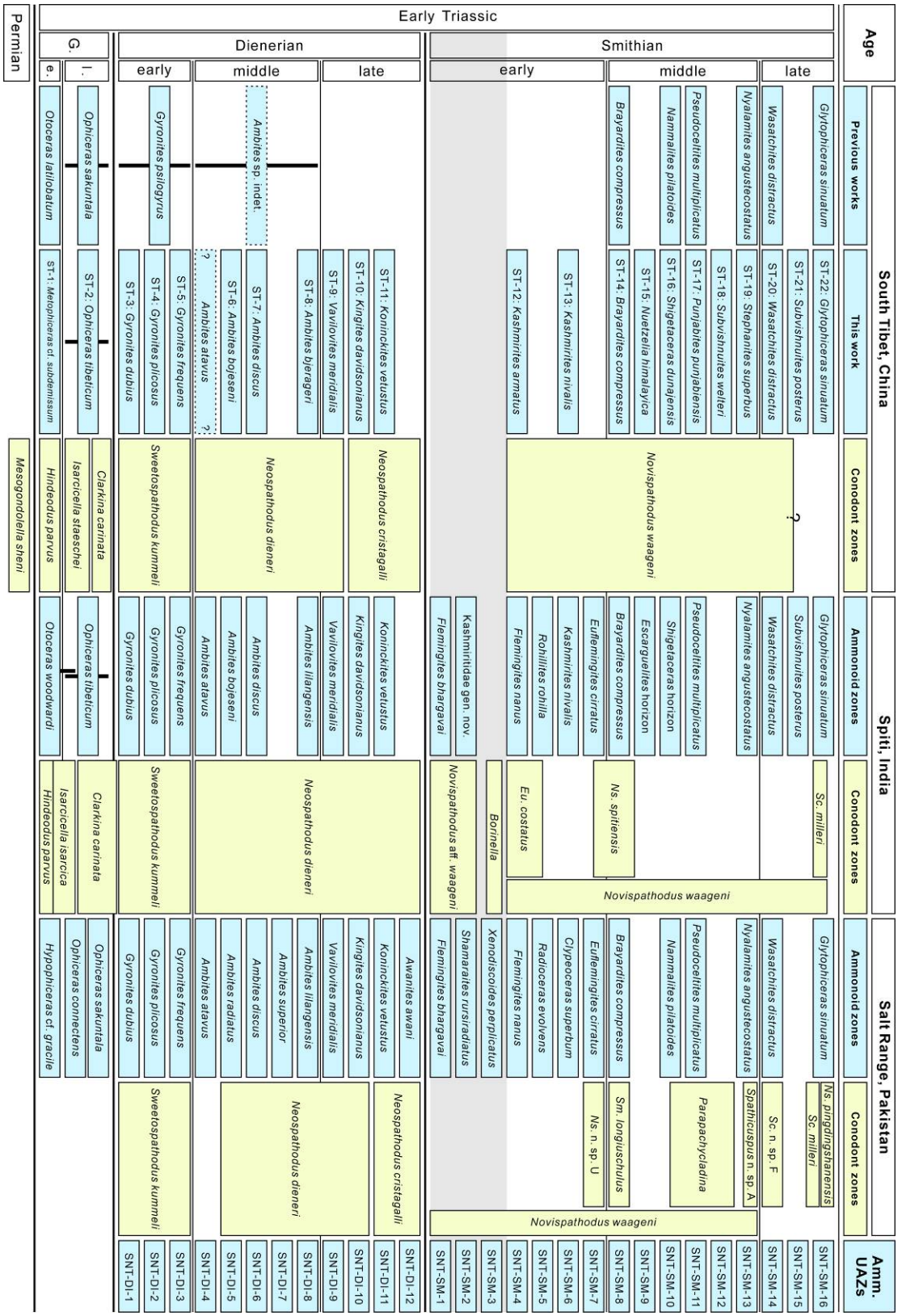

Figure 20. Correlation of Griesbachian-Smithian ammonoid and conodont zonations within the SNT. Previous works in South Tibet refer to Wang and He (1976), Brühwiler et al. (2010b), and Zhang et al. (2017). Spiti ammonoid data from Krystyn and Orchard (1996), Brühwiler et al. (2010c, 2012b), Ware et al. (2018a), and Krystyn et al. (2017). Salt Range ammonoid data from Brühwiler et al. (2011, 2012c) and

Ware et al. (2018b). South Tibet conodont data from Wang and Wang (1995); Salt Range conodont data from Romano et al. (2013) and Goudemand et al. (2019), Spiti conodont data from Krystyn and Orchard (1996), Krystyn et al. (2007, 2017), Goudemand (2014), and Sun et al. (2021). Grey area indicates an uncertain interval for the Dienerian/Smithian boundary among different proposals.

4 Global correlations for the Griesbachian, Dienerian, and Smithian ammonoid biostratigraphy

The worldwide distribution (Fig. 21), fast evolutionary rates and abundant fossil record of Early Triassic ammonoids allow their use as ideal index fossils for large-scale stratigraphic correlations (Balini et al., 2010; Jenks et al., 2015). Thanks to the bed-rock-controlled extensive samplings and detailed taxonomic revisions in the past decades (e.g., Brayard and Bucher, 2008; Shigeta et al., 2009; Brühwiler et al., 2011), the resolution of the Early Triassic ammonoid biostratigraphical scales has been significantly improved, and their correlations have been strengthened. However, some uncertainties remain in large-scale correlations (Figs. 22–23).

4.1 Griesbachian

Generally, the Griesbachian can be subdivided into two parts (early and late) based on ammonoid assemblages from Arctic Canada (Tozer, 1965, 1967, 1994). Currently, Griesbachian ammonoid biostratigraphy is still rough with many uncertainties in long distance correlation and in need of revision and more detailed study. Sections with good Griesbachian ammonoid record are exceedingly rare, particularly for low latitudes.

4.1.1 Oman

Griesbachian ammonoids are sporadically reported from exotic limestone blocks (Krystyn et al., 2003; Brosse et al., 2019). These assemblages include *Ophiceras*, *Episageceras*, *Metophiceras*, *Aldanoceras*, *Anotoceras* and *Discophiceras*, correlating

with the late Griesbachian assemblages in other basins (Fig. 22). However, the presence of *Metophiceras* could represent the late early Griesbachian, or an indication of condensation.

4.1.2 Afghanistan

Griesbachian ammonoids have been poorly documented from Afghanistan thus far. Some highly recrystallized, poorly preserved ophiceratid ammonoids were reported at Khojia Ghare Wali, approximately 30 km east of Kabul (Ishii et al., 1971). This ophiceratid assemblage could be of late Griesbachian age, but with many uncertainties (Fig. 22).

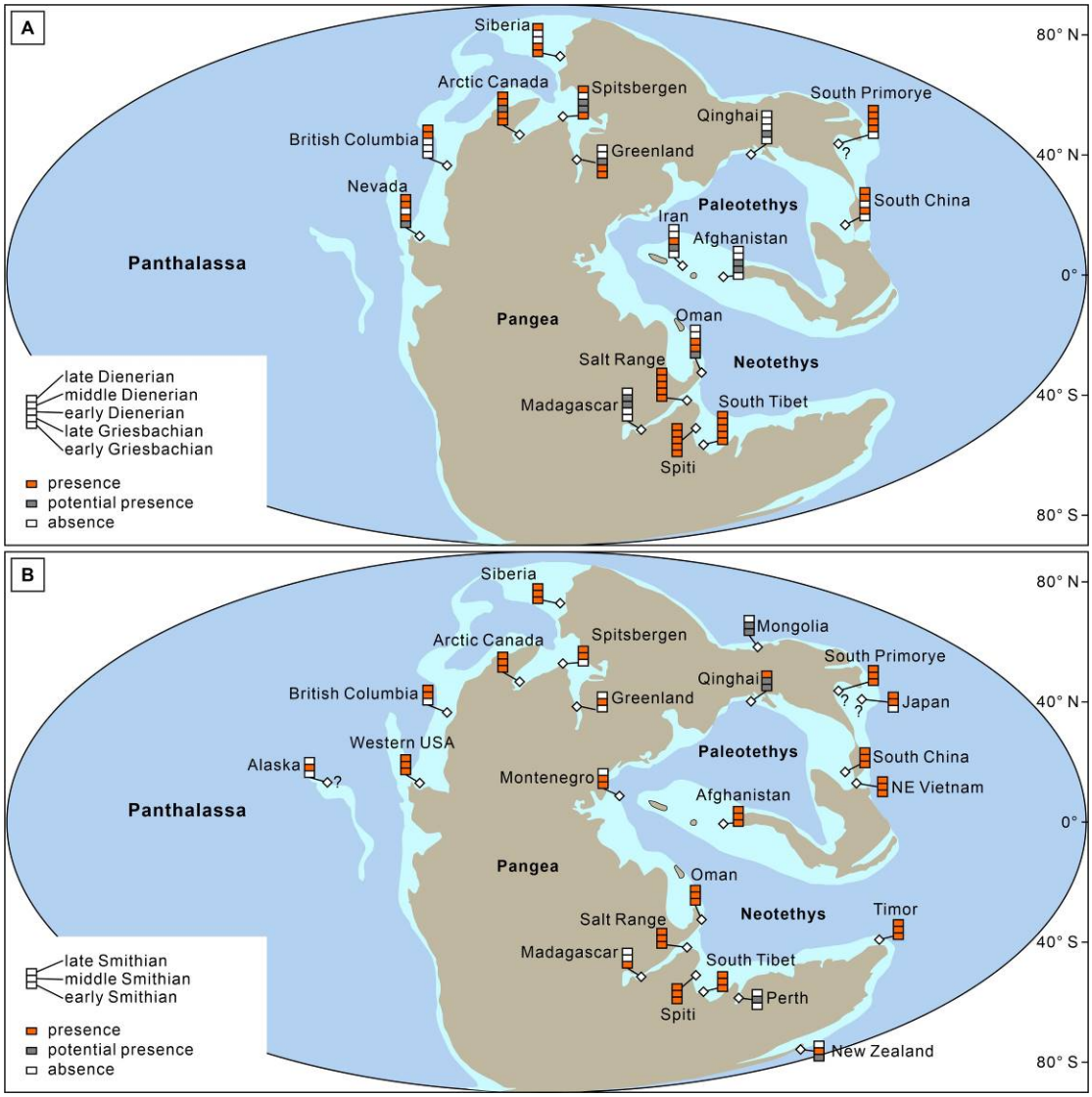

Figure 21. Main localities of Griesbachian, Dienerian (A) and Smithian (B) ammonoids. The paleogeographic maps were modified from Scotese (2014). Note that

the paleopositions of South Primorye and Japan remains unclear (see ~~e.g.,~~ Ehiro, 1998; Brayard et al., 2009).

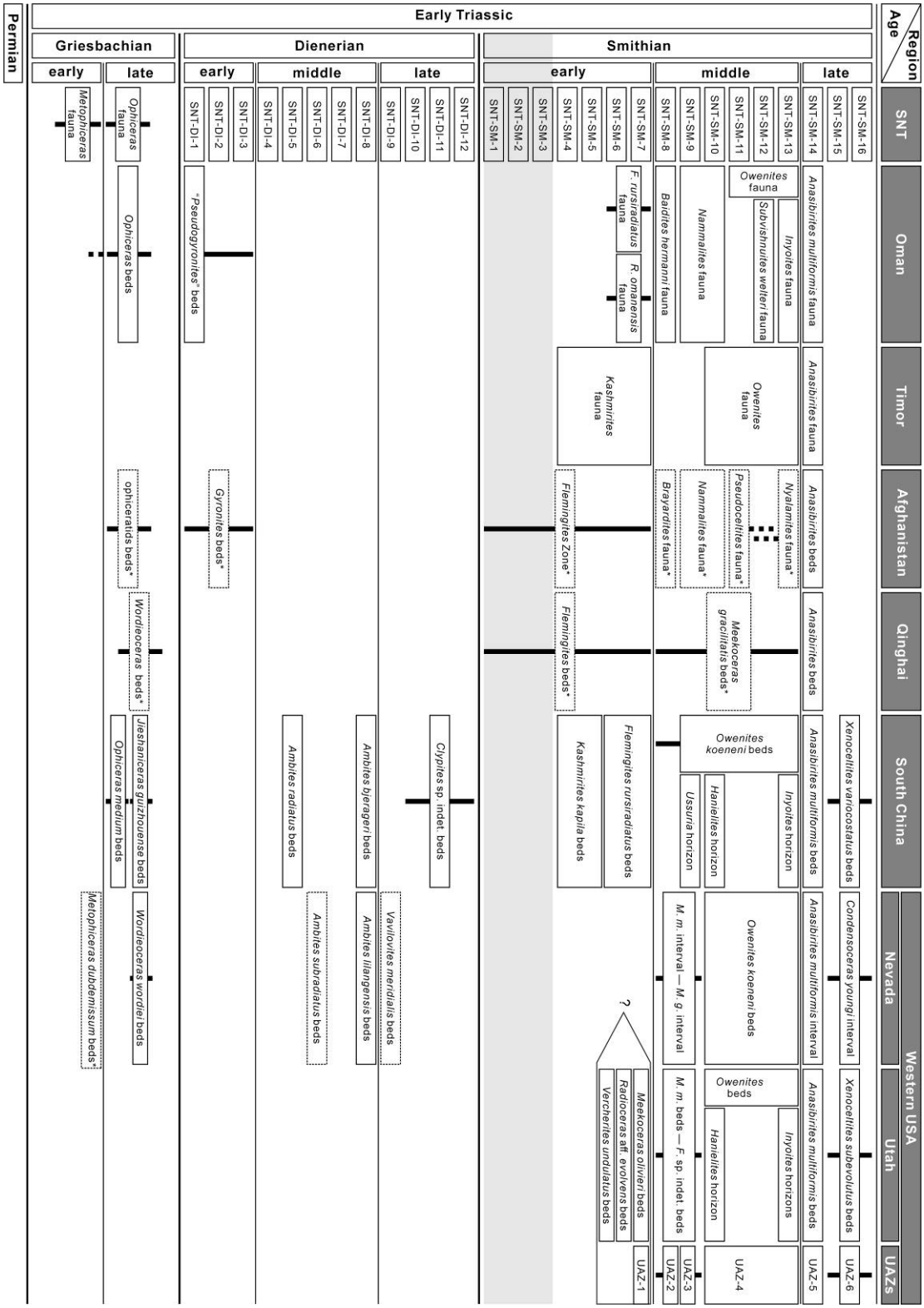

Figure 22. Global correlations of Griesbachian-Smithian ammonoid biostratigraphic scales, part I, Tethys and low latitude regions. Asterisks indicate poorly documented assemblages/faunas/beds. Vertical solid and dotted lines represent uncertainties in correlation. Grey area indicates an uncertain interval for the Dienerian/Smithian

boundary among different proposals.

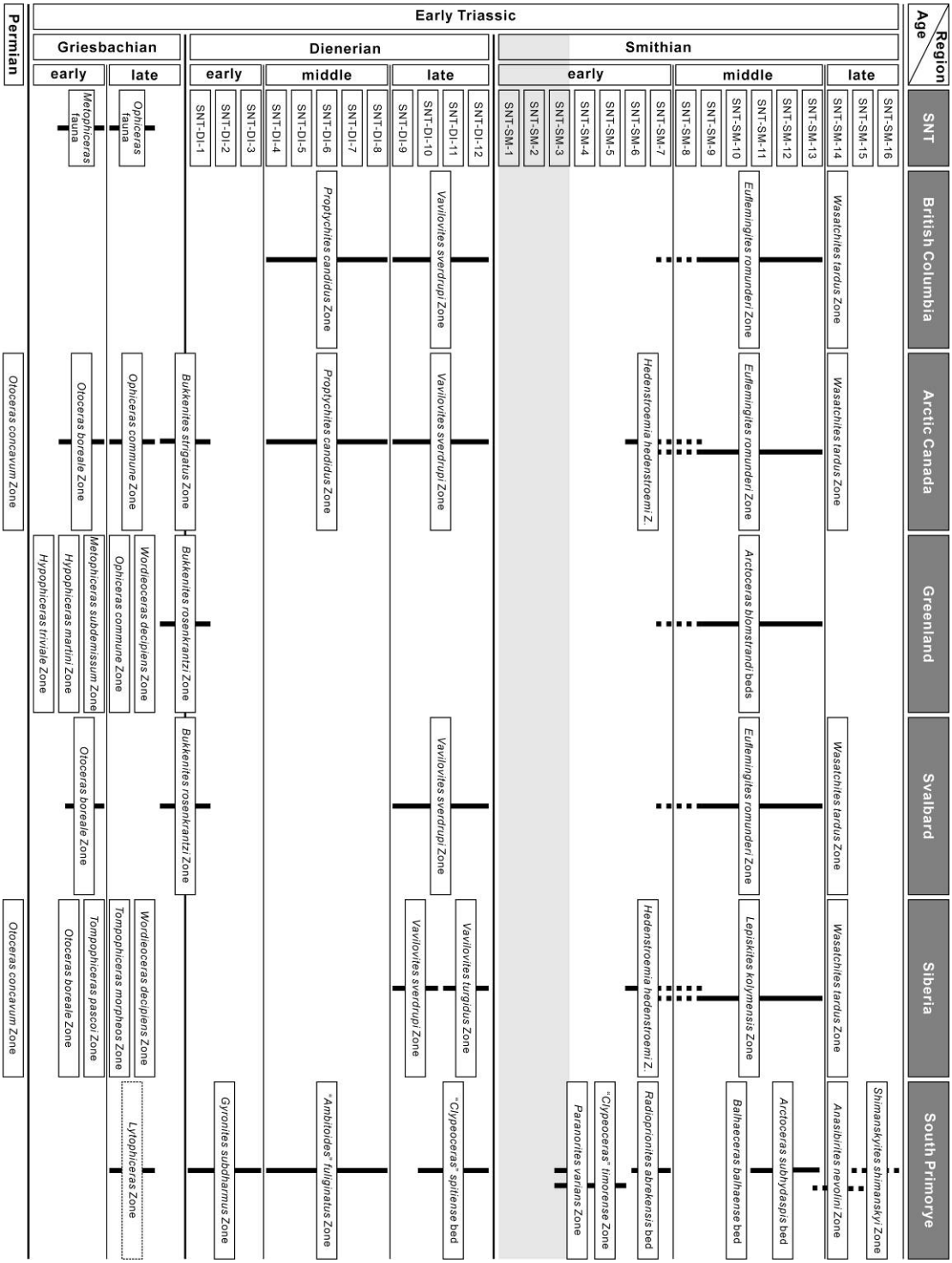

Figure 23. Global correlations of Griesbachian-Smithian ammonoid biostratigraphic scales, part II. Asterisks indicate poorly documented assemblages/faunas/beds. Vertical solid and dotted lines represent uncertainties in correlation. The *Otoceras concavum* Zone is temporarily placed in the latest Permian, see discussion in section 4.1.6. Grey area indicates an uncertain interval for the Dienerian/Smithian boundary among different proposals.

4.1.3 Qinghai, China

Qinghai Province is located in the center of the Qinghai-Tibet Plateau. Lower Triassic sediments are widely distributed within this area but are still poorly studied. Wang and Chen (1984) described an ammonoid assemblage near Maduo County, including *Cordillerites* sp., *Flemingites muthensis*, *Anotoceras costatum*, *Gyrophiceras vermiformis*, *Acanthophiceras* cf. *gibbosum*, and *Wordieoceras decipiens*. These identifications are highly questionable based on their poor preservation. In addition, this assemblage constitutes a mix of Griesbachian and Smithian taxa (Fig. 22). Further works are thus needed to fully decipher the exact taxonomic composition and stratigraphic superpositions of this assemblage.

4.1.4 South China

Griesbachian ammonoids have been rather well studied in South China (Fig. 22). However, many works are based on poorly preserved specimens (Wang, 1984; Tong et al., 2004). For instance, most Induan ammonoids are smooth without distinctive shell sculptures. Usually, flattened specimens cannot be confidently identified at the genus/species level and even at the family level. Therefore, biostratigraphic works based on poorly preserved flattened species were excluded in the following discussion.

Several works reported relatively well-preserved Griesbachian ammonoids (Mu et al., 2007; Brühwiler et al., 2008; Dai et al., 2019). Early Griesbachian ammonoids have not been reported thus far from South China. Late Griesbachian ammonoids, represented by the *Ophiceras* beds, have been described from Guangxi and Guizhou (Brühwiler et al., 2008; Dai et al., 2019). The overlying *Jieshaniceras guizhouense* beds were tentatively integrated into the latest Griesbachian since no typical Dienerian ammonoids have been found in these beds thus far (Dai et al., 2019). Conodont data from these beds also support a late Griesbachian age for these beds

(Mu et al., 2007).

4.1.5 Western USA basin

Recently, a new Griesbachian ammonoid fauna was described at Crittenden Spring, Nevada (Jenks et al., 2021). It represents the first report of a late Griesbachian assemblage from the western USA basin (Fig. 22). This assemblage contains four species: *Wordieoceras wordiei*, *Wordieoceras mullenae*, *Kyokites* cf. *K. hebeiseni* and *Ophimullericeras paullae*.

Ammonoid specimens attributed to the early Griesbachian species *Metophiceras subdemissum* and *Discophiceras subkyokticum* were also briefly reported from the Dinwoody Formation of southeastern Idaho and Montana (Newell and Kummel, 1942). However, their preservation is very poor and fragmentary. Thus, these taxonomic and age assignments are doubtful.

4.1.6 Arctic Canada

Arctic Canada is one of the key regions for Griesbachian ammonoids, where the type section of this substage is located (Tozer, 1965). Tozer (1965, 1967) proposed 4 successive ammonoid zones for the Griesbachian: *Otoceras concavum* Zone, *Otoceras boreale* Zone, *Ophiceras commune* Zone, and *Bukkenites strigatus* Zone, in ascending order (Fig. 23).

As the formal definition of the Permian-Triassic boundary is based on the first occurrence of the conodont *Hindeodus parvus* at the Meishan section, China (Yin et al., 2001), part of the initially early Griesbachian beds defined by Tozer is consequently assumed to be of late Permian age. The *Otoceras concavum* Zone and probably the lower part of the *Otoceras boreale* Zone were thus attributed to the Late Permian (Henderson and Baud, 1997). However, this age assignment is still debated (Shevyrev, 2006; Jenks et al., 2021). Baud and Beauchamp (2001) proposed a revised definition of the Griesbachian for Arctic Canada, which only includes the *Ophiceras commune* and *Bukkenites strigatus* Zones. This definition is not followed here because

H. parvus occurs within the *Otoceras boreale* Zone at Otto Fiord South (Henderson and Baud, 1997), and whether it represents the first appearance datum of *H. parvus* is unclear (Orchard, 1996; Orchard and Tozer, 1997). In any case, at least the upper part of the *Otoceras boreale* Zone belongs to the Early Triassic. At the same site, *Otoceras concavum* co-occurs with the latest Changhsingian conodont assemblage (Henderson and Baud, 1997). We thus here tentatively consider that the *Otoceras concavum* Zone corresponds to the latest Permian in Arctic Canada. It should nevertheless be noted that correlations between Griesbachian conodont and ammonoid biostratigraphical scales in Arctic Canada remain blurred with many uncertainties. This results from the scarce occurrences of conodonts at the Griesbach Creek section, the type area of the Griesbachian substage (Henderson and Baud, 1997; Orchard and Tozer, 1997).

To our knowledge, there is no coeval ammonoid fauna to the *Otoceras concavum* Zone within the Tethys. The *Otoceras boreale* Zone can be roughly correlated with the *Otoceras-Metophiceras* associations of the SNT. The *Ophiceras commune* Zone correlates with the *Ophiceras* fauna in the SNT. The *Bukkenites strigatus* Zone was thought to represent the latest Griesbachian in Arctic Canada. However, conodonts from the upper part of this zone indicate a Dienerian age (Orchard and Tozer, 1997). Thus, the *Bukkenites strigatus* Zone most likely straddles the Griesbachian/Dienerian boundary. This age assignment is also supported by ammonoid data from the SNT, as *Bukkenites* occurs in the upper *Ophiceras* fauna in South Tibet (this work) and in the early Dienerian at the Salt Range and Spiti (Ware et al., 2018a, 2018b).

4.1.7 Greenland

Greenland is another key region for Griesbachian ammonoid faunas. Indeed, it probably represents the most complete Griesbachian ammonoid succession worldwide (Spath, 1930, 1935; Trümpy, 1969). Six ammonoid zones were recognized from the Wordie Creek Formation (Bjerager et al., 2006). These are the *Hypophiceras triviale*, *Hypophiceras martini*, *Metophiceras subdemissum*, *Ophiceras commune*, *Wordieoceras decipiens* and *Bukkenites rosenkrantzi* Zones, in ascending order (Fig.

23).

The *Hypophiceras triviale* Zone was considered latest Permian in age (Bjerager et al., 2006). However, this interpretation should be taken with caution since the correlation between conodont and ammonoid biostratigraphical scales in eastern Greenland is still crude (Bjerager et al., 2006). For instance, the base of the *Hypophiceras triviale* Zone is 7 m above the base of the Wordie Creek Formation at Oksedal, northern Jameson Land, while the first occurrence (FO) of *Hindeodus parvus* occurs 23.5 m above the base of the Wordie Creek Formation (Bjerager et al., 2006). In addition, the globally reported negative $\delta^{13}C$ spike for PTB occurs at the base of the Wordie Creek Formation, predating the FO of *Hindeodus parvus* in Jameson Land (Stemmerik et al., 2001). Consequently, it is likely that the FO of *Hindeodus parvus* in Jameson Land is younger than its FO at the Meishan GSSP (Bjerager et al., 2006). We thus consider the *Hypophiceras triviale* Zone to belong to the early Griesbachian instead of the latest Permian.

The *Hypophiceras martini* and *Metophiceras subdemissum* Zones are also early Griesbachian in age. The *Ophiceras commune* and *Wordieoceras decipiens* Zones correspond to the late Griesbachian. As in Arctic Canada, the *Bukkenites rosenkrantzi* Zone probably straddles the Griesbachian/Dienerian boundary. A thorough revision of Griesbachian ammonoids in eastern Greenland is ongoing by one of the authors (D.W.).

4.1.8 Svalbard

Griesbachian ammonoids are represented by two successive zones in Svalbard: the *Otoceras boreale* and *Bukkenites rosenkrantzi* Zones (Weitschat and Dagys, 1989). The *Otoceras boreale* Zone contains *Otoceras boreale*, *Paravishnuites oxynotus*, and *Ophiceras spathi*. This association correlates with the upper part of the *Otoceras boreale* Zone from Arctic Canada (Fig. 23). As in Arctic Canada and Greenland, the age of the *Bukkenites rosenkrantzi* Zone is unclear. This zone in Svalbard represents the latest Griesbachian or the early Dienerian.

4.1.9 Siberia

Five latest Permian-Griesbachian ammonoid zones were established in Siberia (Dagys and Ermakova, 1996). These are the *Otoceras concavum*, *Otoceras boreale*, *Tompophiceras pascoi*, *Tompophiceras morpheos*, and *Wordieoceras decipiens* zones, in ascending order (Fig. 23). The *Otoceras concavum* Zone is here assigned to the latest Permian (see discussion in section 4.1.6). The *Otoceras boreale* and *Tompophiceras pascoi* Zones represent the early Griesbachian. Zakharov (1994) reported that *Otoceras concavum* co-occurs with *Otoceras boreale,* and thus merged these two zones. However, Dagys (1994b) argued that this co-occurrence was a consequence of incorrect interpretation on the taxonomy of *Otoceras concavum*. In a recent paper, Zakharov et al. (2020) admitted this misinterpretation and adopted the scheme with two distinct zones.

Ophiceras commune occurs within the overlying *Tompophiceras morpheos* Zone, thus allowing correlation of this zone with the *Ophiceras commune* Zone in eastern Greenland and Arctic Canada. The *Wordieoceras decipiens* Zone was hypothesized to correlate with the *Bukkenites strigatus* Zone in Arctic Canada (Dagys, 1994a). This is rejected here. Indeed, the *Wordieoceras decipiens* Zone in Siberia is a monospecific assemblage, and this species is not found within the *Bukkenites strigatus* Zone. In addition, *Wordieoceras decipiens* occurs below *Bukkenites* in eastern Greenland (Bjerager et al., 2006). Therefore, the *Wordieoceras decipiens* Zone in Siberia correlates with the *Wordieoceras decipiens* Zone in eastern Greenland and is older than the *Bukkenites strigatus* Zone in Arctic Canada.

4.1.10 South Primorye

A single Griesbachian zone was defined from South Primorye, the *Lytophiceras* sp. indet. Zone (Shigeta et al., 2009). It is expected to be of late Griesbachian age (Fig. 23), but the sampled specimens are somewhat poorly preserved, preventing further in-depth comparisons and correlation with other basins.

4.1.11 Iran

Griesbachian ammonoids in Iran are poorly documented and are mainly composed of ophiceratids (Bando, 1979; Korn et al., 2021), which likely indicates a late Griesbachian age. However, their general poor preservation prevents robust identifications and correlations.

4.2 Dienerian

Well-preserved Dienerian ammonoid faunas and successions are restricted to a few regions, such as the SNT. Other regions only show sporadic records of Dienerian ammonoids.

4.2.1 Oman

Only a few Dienerian ammonoids have been described from Oman. A small ammonoid fauna was reported from an exotic block at Wadi Wasit (Krystyn et al., 2003). This fauna contains *Bukkenites*? *scheibleri*, "*Proptychites*" *markhami*, "*Kymatites*" *hodgsoni*, and "*Pseudogyronites*", which is similar to the early Dienerian ammonoids in the SNT (Fig. 22). However, the co-occurring conodont taxa suggest a late Griesbachian age for beds including this ammonoid assemblage (Krystyn et al., 2003). Further correlations thus need a more detailed taxonomic revision of this fauna. Another block from the Batain Plain, eastern Oman, contains rich Dienerian-Smithian ammonoids and conodonts (Souquet and Goudemand, 2020). However, the detailed ammonoid content of this block has not yet been published.

4.2.2 Afghanistan

Ishii et al. (1971) described a *Gyronites* fauna at Khoja Ghare Wali, ca. 30 km east of Kabul. This fauna most likely indicates an early Dienerian age (Fig. 22). However, the poor preservation of this material prevents further in-depth correlation. Collignon (1973) also illustrated a specimen (pl. 5, fig. 1) from the Azrao Valley (S.E.

of Kabul) and assigned it to *Clypites typicus*, which is an iconic late Dienerian species. However, after observation of this specimen (UBGD 277233) in Collignon's collection housed at the Université de Bourgogne, France, we can reassign this specimen to *Pseudosageceras*, which ranges from the late Dienerian to the Spathian and has therefore a low biostratigraphic value.

4.2.3 South China

Occurrences of Dienerian ammonoids are scarce in South China (Fig. 22). Early Dienerian ammonoids have not been found thus far. The middle Dienerian *Ambites radiatus* and *A. bjerageri* Zones were documented in Guizhou and Guangxi (Brühwiler et al., 2008; Dai et al., 2019). The late Dienerian genus *Clypites* was found only in Guangxi (Brayard and Bucher, 2008). One specimen identified as *Proptychites* sp. indet. by Brühwiler et al. (2008) was later synonymized with *Koninckites khoorensis* by Ware et al. (2018), which adds one more occurrence of the late Dienerian ammonoid in South China.

4.2.4 Nevada

Middle and late Dienerian ammonoids are documented only from the Candelaria Hills, Nevada (Ware et al., 2011). Most of these come from float concretions and lack stratigraphic information. However, the ages of these middle and late Dienerian assemblages (Fig. 22) can be confirmed based on the occurrences of *Ambites*, *Mullericeras*, *Protychites* and *Vavilovites*. These assemblages have strong affinities with SNT faunas, suggesting frequent faunal exchanges between the Neotethys and the opposite side of the Panthalassa during that time (see also Brayard et al., 2007, 2009; Jenks et al., 2010; Monnet et al., 2013; Jenks and Brayard, 2018, for discussion of such faunal exchanges during the Early Triassic).

4.2.5 British Columbia

Two Dienerian ammonoid zones were established in British Columbia, i.e., the

Proptychites candidus and *Vavilovites sverdrupi* Zones (Tozer, 1994). The former generally indicates a middle Dienerian age (Fig. 23), while the latter corresponds to the late Dienerian (Ware et al., 2018b). The *Vavilovites sverdrupi* Zone can also be subdivided into three subzones: *Koninckites dimidiatus*, *Vavilovites obtusus*, and "*Kingites*" *discoidalis* Subzones. However, precise correlation with the SNT is difficult.

According to our observations of Tozer's collection at the Geological Survey of Canada in Vancouver, many of the Dienerian taxa in British Columbia are not the same as those found in Arctic Canada but have SNT affinities. For instance, the specimens identified by Tozer (1994) as *Proptychites candidus* and *Vavilovites sverdrupi* in British Columbia do not belong to these species found in Arctic Canada, but rather to species with SNT affinities (*Proptychites candidus* is close to *Proptychites ammonoides* and *Koninckites khoorensis*, and *Vavilovites sverdrupi* resembles *Vavilovites meridialis*). *Ambites fuliginatus* initially described by Tozer (1994) was synonymized with *Ambites lilangensis* by Ware et al. (2018a), thus suggesting the existence of a latest middle Dienerian ammonoid fauna.

4.2.6 Arctic Canada

Tozer (1965, 1967, 1994) distinguished two Dienerian ammonoid zones in Arctic Canada (Fig. 23). The lower zone is the *Proptychites candidus* Zone, which roughly corresponds to the middle Dienerian based on the occurrence of *Ambites* (Ware et al., 2018b). The upper zone is the *Vavilovites sverdrupi* Zone, roughly corresponding to the late Dienerian (Ware et al., 2018b).

4.2.7 Svalbard

Vavilovites have been documented in Svalbard (Weitschat and Dagys, 1989). This taxon indicates a late Dienerian age (Fig. 23). Early and middle Dienerian ammonoids have not been documented in Svalbard to date.

4.2.8 Siberia

Two Dienerian ammonoid zones were defined in Siberia, i.e., the *Vavilovites sverdrupi* and *Vavilovites turgidus* Zones (Dagys and Ermakova, 1996). The *Vavilovites sverdrupi* Zone is well correlated within the Boreal regions and is late Dienerian (Fig. 23). The *Vavilovites turgidus* Zone can be subdivided into two subzones: the *Vavilovites subtriangularis* and *Vavilovites umbonatus* Subzones. However, due to the strong endemicity of taxa occurring in this zone, accurate correlations are impossible. We tentatively assign this zone also to the late Dienerian since *Vavilovites* has not been documented in the early Smithian to date.

4.2.9 South Primorye

The Dienerian ammonoid succession in South Primorye was described by Shigeta et al. (2009). It includes the *Gyronites subdharmus* Zone, the *Ambitoides fuliginatus* Zone, and the "*Clypeoceras spitiense*" bed, in ascending order (Fig. 23). The *Gyronites subdharmus* Zone was interpreted to be of late Griesbachian age by Shigeta et al. (2009). This zone was later reassigned to the early Dienerian (Ware et al., 2015; Ware et al., 2018b). The *Ambitoides fuliginatus* Zone (index marker reassigned to *Mullericeras* by Ware et al., 2018b) roughly corresponds to the middle Dienerian (Ware et al., 2018b). The "*Clypeoceras spitiense*" bed (reassigned to *Clypites typicus* by Ware et al., 2018b) correlates with SNT-DI-10 and SNT-DI-11 (Fig. 22).

4.2.10 Iran

An early Dienerian ammonoid fauna from Iran was recently mentioned (Korn et al., 2021). It contains *Ussuridiscus varaha* and *Gyronites* cf. *dubius*, thus corresponding to SNT-DI-1 in SNT (Fig. 22).

4.3 Smithian

Our present knowledge of the Smithian ammonoid biochronology is more detailed than for the Griesbachian and Dienerian. This results from several published works based on extensive bed-by-bed sampling and homogenized taxonomic treatment during the last two decades (e.g., Brayard and Bucher, 2008; Brühwiler et al., 2011; Shigeta et al., 2014; Jenks and Brayard, 2018). However, regarding high-resolution scales and global correlations, some uncertainties remain, owing to the presence of endemic assemblages at some sites and the absence of revised studies for some localities.

4.3.1 Oman

Smithian ammonoids in Oman were found in isolated exotic blocks, initially deposited on sea highs with low sedimentary rates (Krystyn et al., 2003; Brosse et al., 2019). These cm- to km-sized blocks (exhibiting a "Hallstatt" facies) were redeposited into younger sediments due to tectonic instability (Baud et al., 2012). A high-resolution ammonoid biostratigraphy is thus difficult to determine due to high levels of condensation and the often lack of stratigraphic superpositions. However, after careful and detailed sampling, it is possible to construct a rather highly resolved biostratigraphic scale for a large part of the Smithian, as done, for instance, by Brühwiler et al. (2012a). These authors have defined seven Smithian ammonoid faunas (Fig. 22).

The *Rohillites omanensis* and *Flemingites rursiradiatus* faunas correspond to the late early Smithian, but information on superposition is lacking to determine their exact succession (Fig. 22). Here, we follow former works (Brühwiler et al., 2012a; Jattiot et al., 2020) and correlate them with the late early Smithian.

The *Baidites hermanni* fauna was thought to be of early middle Smithian age but with some uncertainty (Brühwiler et al., 2012a). Here, we correlate the *Baidites hermanni* fauna with the *Brayardites compressus* Zone in the SNT, according to the

following evidences: (1) *Baidites* was found in SNT-SM-8 in South Tibet; (2) *Jinyaceras*, found in this fauna, is restricted to SNT-SM-7 and SNT-SM-8 in the SNT; and (3) the occurrence of "*Paranorites jenksi*" in the *Baidites hermanni* fauna is the main evidence of its early Smithian age assignment (Brühwiler et al., 2012a). However, this is questionable, owing to its poor preservation.

The overlying *Nammalites pilatoides* fauna correlates with SNT-SM-9 and SNT-SM-10 based on the range of *Nammalites pilatoides* (Fig. 22).

The *Owenites* fauna correlates with SNT-SM-11 to SNT-SM-13 UAZs. The *Owenites* fauna can be further subdivided into different faunas. Here, we differentiate a *Subvishnuites welteri* fauna (represented by samples HB 904 and HB 905 in Brühwiler et al., 2012a). This fauna is characterized by the co-occurrence of *Subvishnuites* and *Nyalamites*, which correlates with SNT-SM-12 (Fig. 22).

The late middle Smithian *Inyoites* fauna corresponds to SNT-SM-13. The *Anasibirites multiformis* fauna correlates with SNT-SM-14 (Fig. 22).

4.3.2 Timor

Smithian ammonoids are also found in exotic blocks in Timor (Welter, 1922; Kummel, 1968b; Nakazawa and Bando, 1968; Jattiot et al., 2020). The specimens show an exquisite preservation, better than in other sampled localities worldwide. However, superposition information among blocks is sometimes lacking. Generally, blocks can be divided into three successive faunas: the *Kashmirites*, *Owenites* and *Anasibirites* faunas, corresponding to the early, middle and late Smithian, respectively (Jattiot et al., 2020). According to the taxonomic composition of each fauna, we can roughly correlate the *Kashmirites* fauna with SNT-SM-4 to SNT-SM-7 UAZs and the *Owenites* fauna with SNT-SM-8 to SNT-SM-13 UAZs (Fig. 22). The *Anasibirites* fauna correlates with SNT-SM-14.

4.3.3 Afghanistan

Rare Smithian ammonoids were described from Afghanistan (Kummel and

Erben, 1968; Collignon, 1973). Based on the available data, we can confirm that all the early, middle and late Smithian ammonoid faunas occur (Fig. 22).

Studied collections of Collignon (1973) housed at the Université de Bourgogne, Dijon, France, were also revised. Although generally poorly preserved, some specimens can be identified at the genus and species levels. The occurrence of *Flemingites* sp. indet. (pl. 3, fig. 6 in Collignon, 1973, UBGD 277253) suggests the probable occurrence of an early Smithian ammonoid assemblage (Fig. 22).

Middle Smithian ammonoids were relatively well documented by Kummel and Erben (1968). They are generally grouped into the *Owenites* Zone. According to illustrations provided by Kummel and Erben (1968), we expect the occurrences of the *Nammalites*, *Pseudoceltites* and *Nyalamites* faunas but lack a detailed taxonomic composition and precise superposition (Fig. 22). One Collignon's specimen (pl. 3, fig. 5 in Collignon, 1973, UBGD 277252), initially assigned to *Flemingites muthianus*, is actually a specimen of *Brayardites*. Thus, an almost complete middle Smithian succession is potentially present in Afghanistan. In addition, this succession appears identical to the SNT. However, this remains to be confirmed during future access on outcrops.

Kummel and Erben (1968) also described an unusual *Anasibirites* fauna, which contains a mixed assemblage of middle Smithian and late Smithian taxa. This probably results from a sampling, reworking, or condensation bias. Further work is therefore needed to clarify the exact composition of this fauna. We nevertheless consider in this work that part of this fauna correlates at least with other *Anasibirites* beds worldwide (Fig. 22).

4.3.4 Qinghai, China

Smithian ammonoids have scarcely been documented in Qinghai Province, China (Fig. 22). A poorly preserved specimen of *Flemingites muthianus* was found near Maduo County (Wang and Chen, 1984). If this assignment is correct, it suggests an early Smithian age for beds containing this specimen. *Meekoceras gracilitatis* was

946 also reported from this area (Wang and Chen, 1984), which suggests the occurrence of
947 middle Smithian beds. The late Smithian genus *Anasibirites* was found at the
948 Naocangjiangou section (He et al., 1986) and indicates the presence of a late Smithian
949 fauna (Fig. 22).

950 **4.3.5 South China**

951 Smithian ammonoids have been well documented from Guangxi (Chao, 1959;
952 Brayard and Bucher, 2008; Dai et al., 2021). Materials from other localities in South
953 China are usually poorly preserved (Tong et al., 2004) and are thus excluded from the
954 following discussion. To date, 5 intervals have been recognized (Brayard and Bucher,
955 2008). They are the early Smithian *Kashmirites kapila* and *Flemingites rursiradiatus*
956 beds, the middle Smithian *Owenites koeneni* beds and the late Smithian *Anasibirites*
957 *multiformis* and *Xenoceltites variocostatus* beds (Fig. 22).

958 The *Kashmirites kapila* beds correlate with SNT-SM-4 and SNT-SM-5,
959 according to the occurrence of *K. kapila* in both Guangxi and SNT (Fig. 22). The
960 *Flemingites rursiradiatus* beds were assigned to the early middle Smithian in some
961 previous works (Brayard et al., 2013; Jenks et al., 2015). However. According to the
962 initial subdivisions of the Smithian (Brühwiler et al., 2010a), the age of these beds
963 should be the late early Smithian (Fig. 22).

964 The *Owenites koeneni* beds are middle Smithian and can be subdivided into three
965 horizons: the *Ussuria*, *Hanielites*, and *Inyoites* horizons. The *Inyoites* horizon
966 correlates with SNT-SM-13 based on the occurrence of *Inyoites* in both regions, while
967 precise correlations of the former two horizons with UAZs in the SNT remain
968 uncertain (Fig. 22).

969 The early late Smithian *Anasibirites multiformis* beds correlate with SNT-SM-14.
970 The *Xenoceltites variocostatus* beds correspond to SNT-SM-15 and SNT-SM-16 (Fig.
971 22).

4.3.6 Northeastern Vietnam

Four Smithian ammonoid beds have been recognized in northeastern Vietnam (Shigeta et al., 2014), which are rather similar to those found in South China. They are the early Smithian *Flemingites rursiradiatus* beds, the middle Smithian *Urdyceras tulongensis* beds and *Owenites koeneni* beds, and the late Smithian *Xenoceltites variocostatus* beds. *Urdyceras tulongensis* beds correlate with SNT-SM-8. The early late Smithian *Anasibirites* fauna has not yet been reported from northeastern Vietnam.

4.3.7 Western USA basin

The western USA basin is one of the key regions for Smithian ammonoids. It has been studied since the beginning of the last century (Hyatt and Smith, 1905; Smith, 1932; Kummel and Steele, 1962) and recently provided new ammonoid findings (Jenks et al., 2010; Brayard et al., 2013; Jattiot et al., 2017; Jenks and Brayard, 2018; Brayard et al., 2020, 2021). Middle and late Smithian ammonoid faunas are well documented, while early Smithian assemblages are less well-known owing to the lack of well-preserved specimens (Fig. 22).

Ten Smithian ammonoid beds are recognized in Utah (Brayard et al., 2013, 2020, 2021). Brayard et al. (2013) initially tentatively assigned the six following beds to the early Smithian: *Vercherites undulatus* beds, *Radioceras* aff. *Evolvens* beds, *Meekoceras olivieri* beds, *Meekoceras millardense* beds, *Preflorianites-Kashmirites* beds, and *Inyoites beaverensis* beds. However, the material from these beds is often poorly preserved, leaving many uncertainties on age attribution (Fig. 22).

Based on recently sampled well-preserved material from Crittenden Spring, Nevada, and comparison with conodont occurrences, it appears that *Meekoceras millardense* is middle Smithian (Jenks and Brayard, 2018; Maekawa and Jenks, 2021). Co-occurring ammonoids (e.g., *Juvenites* and *Proharpoceras*) also suggest a middle Smithian age. Thus, the *Meekoceras millardense* beds are middle Smithian, but it is not certain that these beds represent the earliest middle Smithian in the western US basin (Fig. 22). The ammonoid content of the three beds below the *Meekoceras*

millardense beds (*Vercherites undulatus*, *Radioceras* aff. *evolvens* and *Meekoceras olivieri* beds), are dominated by paranoritids, and *Meekoceras olivieri* is potentially closer to *Vercherites*. We thus leave them as early Smithian (Fig. 22). Additional well-preserved material is mandatory to determine their exact superposition.

Middle Smithian ammonoids are abundant in the western USA basin and were most often included into a single interval, i.e., the *Meekoceras gracilitatis* Zone (Kummel and Steele, 1962). However, it has been shown that this zone can be subdivided into more horizons or subzones with different stratigraphic resolutions depending on sampling effort and taxonomic revisions (Brayard et al., 2013; Jattiot et al., 2017; Jenks and Brayard, 2018). Ten middle Smithian interval zones have, for instance, been recognized from Crittenden Spring, northeastern Nevada (Jenks and Brayard, 2018), with some uncertainties in correlating this high-resolution scale at a global scale.

Jattiot et al. (2017) postulated 6 UAZs for the Smithian of the western US basin, which were recently confirmed at the basin scale (Brayard et al., 2021). UAZ 1 is characterized by a single species, *Meekoceras olivieri*, resembling *Vercherites* (see previous paragraph). Thus, UAZ 1 most likely represents the early Smithian. UAZs 2 and 3 were assigned to the early Smithian based on the occurrence of *Kashmirites stepheni*. However, this material is rather poorly preserved, and its attribution may be questionable. In addition, the co-occurring species *Meekoceras gracilitatis* suggests a middle Smithian age. Overall, UAZs 2 and 3 can likely be included in the middle Smithian. UAZ 4 is middle Smithian, and UAZs 5 and 6 are late Smithian.

Late Smithian ammonoids were also commonly reported from the western USA basin (e.g., Mathews, 1929; Jattiot et al., 2017; Brayard et al., 2021). Two successive assemblages can be recognized. The lower one corresponds to the UAZ 5 of Jattiot et al. (2017) and is dominated by prionitids, such as *Anasibirites*, *Wasatchites*, *Hemiprionites*, and *Gurleyites*. The upper zone is equal to the UAZ 6 of Jattiot et al. (2017) and is characterized by the co-occurrence of xenoceltitids and *Pseudosageceras* (Brayard et al., 2021).

Widmann et al. (2020) recently introduced a new latest Smithian zone above the

xenoceltitids-*Pseudosageceras* assemblage and below the first Spathian ammonoid assemblage. However, the detailed taxonomic composition of this new zone has not yet been described, and no specimens have been illustrated. Based on present data, this zone would have no equivalent worldwide.

4.3.8 British Columbia

Two Smithian ammonoid zones have been recognized in British Columbia, i.e., the *Euflemingites romunderi* and *Anawasatchites tardus* Zones (Tozer, 1994). The *Euflemingites romunderi* Zone roughly corresponds to the middle Smithian, while the *Anawasatchites tardus* Zone correlates with the early late Smithian SNT-SM-14 and worldwide (Fig. 23). A second late Smithian zone potentially exists in British Columbia, as suggested by *Pseudosageceras plicatum*, which closely resembles ?*Pseudosageceras bullatum* from the late Smithian in Nevada (Jattiot et al., 2017). Unfortunately, this specimen occurs in a floated block (Tozer, 1994), preventing further age determination and correlation.

4.3.9 Arctic Canada

Tozer (1965, 1967, 1994) identified 3 zones in Arctic Canada, i.e., the *Hedenstroemia hedenstroemi*, *Euflemingites romunderi*, and *Anawasatchites tardus* Zones, in ascending order (Fig. 23). The *Hedenstroemia hedenstroemi* Zone can be tentatively roughly correlated with the late early Smithian to early middle Smithian interval (see discussion in subsection 6.3.10). The *Euflemingites romunderi* and *Anawasatchites tardus* Zones correspond to the middle and early late Smithian, respectively.

4.3.10 Siberia

Three Smithian ammonoid zones can be distinguished in Siberia (Fig. 23), i.e., the *Hedenstroemia hedenstroemi*, *Lepiskites kolymensis* and *Wasatchites tardus* Zones (Dagys, 1994a). The *Hedenstroemia hedenstroemi* Zone was tentatively correlated

with the early Smithian in several previous works but with very large uncertainty (Brayard et al., 2013; Jenks et al., 2015; Jenks and Brayard, 2018). There is no firm known occurrence of *Hedenstroemia* from the earliest Smithian of well-sampled regions, such as the Salt Range (Brühwiler et al., 2011). In the SNT, the oldest occurrence of *Hedenstroemia* is in SNT-SM-6. Although the *Hedenstroemia* species from Siberia differ from the Salt Range species, we can therefore hypothesize that the Boreal *Hedenstroemia hedenstroemi* Zone roughly correlates with the late early Smithian in the SNT. This deserves more work to be confirmed. In addition, another genus, *Anaxenaspis*, co-occurring in the *Hedenstroemia hedenstroemi* Zone, suggests a middle Smithian age, as it occurs in the middle Smithian of, e.g., the Salt Range and Spiti (Brühwiler et al., 2012b, 2012c). Overall, the *Hedenstroemia hedenstroemi* Zone may span the late early Smithian to early middle Smithian interval (Fig. 23).

The overlying *Lepiskites kolymensis* Zone is middle Smithian, as it contains *Juvenites*, *Meekoceras, Arctoceras* and *Euflemingites*, but accurate correlations with other basins are problematic. The *Wasatchites tardus* Zone corresponds to the early late Smithian (Fig. 23).

4.3.11 Greenland

Smithian ammonoids are scarcely reported from Greenland with the single occurrence of *Arctoceras blomstrandi* (Lindström et al., 2020), suggesting a middle Smithian age (Fig. 23).

4.3.12 Svalbard

Middle and late Smithian ammonoids have been well documented from Svalbard (Tozer and Parker, 1968; Korchinskaya, 1972; Weitschat and Hamburg, 1978; Weitschat and Dagys, 1989; Piazza et al., 2017; Hansen et al., 2021). Two assemblages can be distinguished. The lower one is characterized by the occurrences of *Arctoceras* and *Euflemingites* and represents the middle Smithian (Fig. 23). This interpretation is also supported by organic carbon isotopic values (Hansen et al.,

2021). The upper assemblage is dominated by early late Smithian prionitids, such as *Anasibirites* and *Wasatchites*, and thus correlates worldwide.

4.3.13 South Primorye

Seven Smithian ammonoid zones/beds were established in South Primorye (Shigeta et al., 2009; Smyshlyaeva and Zakharov, 2012, 2013, 2015; Zakharov et al., 2013, 2021). The *Paranorites varians* Zone was interpreted to be of Dienerian age (Shigeta et al., 2009). However, *Paranorites* occurs in the early Smithian from South China and the Salt Range (Brayard and Bucher, 2008; Brühwiler et al., 2012c), suggesting that the *Paranorites varians* Zone is potentially of Smithian age (Fig. 23). In addition, the conodont *Eurygnathodus costatus*, co-occurring in this zone, also suggests an early Smithian age, at least younger than SNT-SM-3 (see Krystyn et al., 2017).

The "*Clypeoceras*" *timorense* Zone most likely correlates with SNT-SM-3 to SNT-SM-5 interval in the SNT (Fig. 23), based on their faunal similarity. This interpretation is based on: (1) "*Clypeoceras*" *timorense* illustrated by Shigeta et al. (2009) resembles *Radioceras evolvens* (found in SNT-SM-5), both in shell shape and suture line. We thus consider them here as potential synonyms. (2) *Ussuriflemingites primoriensis* found in the "*Clypeoceras*" *timorense* Zone is close to *Vercherites vercheri* (occurring in SNT-SM-3), except for fewer indentations on its suture lobes. This taxon thus suggests a middle early Smithian age as well.

The *Radioprionites abrekensis* bed is difficult to correlate with other regions. *Radioprionites* is closer to early Smithian paranoritids than to prionitids. Its overall shell shape resembles some paranoritids (e.g., *Paranorites*) found in the SNT, and its suture lines show a somewhat long auxiliary series, also close to paranoritids (e.g., *Radioceras* and *Paranorites*). Based on the strong affinity of *Radioprionites abrekensis* to paranoritids and the absence of typical middle Smithian taxa occurring in this bed, we thus tentatively correlate it with the late early Smithian.

The *Balhaeceras balhaense* bed was correlated to SNT-SM-10 by Brühwiler et al.

(2012c). We agree with this interpretation as: (1) *Hemiprionites* sp. indet. occurring in this bed was synonymized with *Shigetaceras* (occurring exclusively in SNT-SM-10) by Brühwiler et al. (2012c). (2) *Balhaeceras balhaense* is close to *Galfettites omani*, which has been found in SNT-SM-9 and SNT-SM-10 (Fig. 19). Overall, the taxonomic composition similarity between the *Balhaeceras balhaense* bed and SNT-SM-10 supports this correlation.

The *Arctoceras subhydaspis* bed can be roughly constrained to SNT-SM-11 to SNT-SM-13 (Fig. 23), since it is younger than the *Balhaeceras balhaense* bed, and no typical late Smithian taxa were found in this bed. More precise correlation is not possible based on present data.

The *Anasibirites nevolini* Zone corresponds to the early late Smithian. However, its content exhibits an unusual mixture of both typical middle Smithian and early late Smithian taxa (Zakharov et al., 2013, 2021), which is not recorded in other basins.

A recently described *Shimanskyites shimanskyi* Zone (Zakharov et al., 2013) can be roughly assigned to the second part of the late Smithian (Fig. 23).

4.3.14 Japan

A few Smithian ammonoids have been described from the Lower Triassic in Kyushu, Japan. They can be grouped into two zones: the middle Smithian *Owenites* and late Smithian *Anasibirites* Zones (Kummel and Sakagami, 1960; Bando, 1964). Bando (1970) described two poorly preserved ammonoid assemblages form the Osawa Formation in Kitakami Massif. He identified three genera, *Meekoceras*, *Flemingites*, and *Euflemingites* in the lower assemblage. This assemblage could be early-middle Smithian age, but with great uncertainty due to poor preservation of these specimens. The upper assemblage is monospecific, containing "*Glyptophiceras* cf. *gracile*", which was re-assigned to a Spathian ammonoid *Deweveria kovalenkoi* by Shigeta (2022). Therefore, whether Smithian ammonoids exist in Kitakami Massif remains to be clarified.

4.3.15 Montenegro

Montenegro represents one of the rare regions in western Tethys yielding Smithian ammonoids. Đaković (2017) and Đaković et al. (2022) described a moderately-rich ammonoid assemblage from screes.. These authors assigned it to the middle Smithian. However, based on available data, this assemblage may encompass the late Dienerian to the middle Smithian interval. Indeed, the presence of *Parahedenstroemia* suggest a potential late Dienerian age. *Parahedenstroemia* was indeed documented from the late Dienerian at South Primorye (Shigeta et al., 2009) and the Candelaria Hills, Nevada (Ware et al., 2011). Other genera, such as *Lingyunites*, *Owenites* and *Truempyceras,* occurring in this assemblage better suggest an early to middle Smithian age. More specimens from *in situ* sampling are needed to solve this conundrum.

4.3.16 Northwestern Caucasus

A middle Smithian ammonoid assemblage was reported from the northwestern Caucasus (Shevyrev, 1995). It includes *Inyoites*, *Dieneroceras*, *Meekoceras*, *Arctoceras*, *Subvishnuites*, *Parussuria*, *Lanceolites*, *Juvenites*, and *Owenites*. Due to the lack of stratigraphic information about their superpositions, more detailed correlations are impossible. This fauna shows an apparent strong affinity with both the SNT and the western USA basin, indicating frequent biotic exchanges between Tethys and Panthalassa during the middle Smithian (Brayard et al., 2009).

4.3.17 New Zealand

Kummel (1968a) described a small Smithian ammonoid assemblage from New Zealand, which contains four species: *Owenites* cf. *koeneni*, *Flemingites* cf. *lidacensis*, *Subvishnuites welteri*, and *Wyomingites* cf. *aplanatus*, suggesting an early to middle Smithian age. However, the preservation of sampled specimens is very poor, preventing further comparisons.

5 Correlations with conodont biostratigraphy

Apart from ammonoids, conodonts also play a significant role in Early Triassic biochronology. For instance, the GSSP of the Permian/Triassic boundary was defined by the first occurrence of conodont *Hindeodus parvus* (Yin et al., 2001). Generally, ammonoids and conodonts are somewhat congruent for defining stage/substage boundaries in the Early Triassic (Orchard and Tozer, 1997). Within the Southern Neotethys, detailed correlations await similar high-resolution scales for conodonts (Fig. 20).

At the base of the Griesbachian, the conodont *Hindeodus parvus* appears in the same horizon as *Otoceras woodwardi* in Spiti (Krystyn and Orchard, 1996). At the Selong section, *Hindeodus parvus* also co-occurs together with "*Otoceras latilobatum*" (Wang and Wang, 1995). This suggests that *Hindeodus parvus* co-occurs with *Otoceras* in the Southern Neotethys. However, in Boreal regions, *Otoceras* apparently occurs slightly earlier than *Hindeodus parvus* (Henderson and Baud, 1997).

The Griesbachian/Dienerian boundary corresponds to the first appearances of the ammonoid *Gyronites* and the conodont *Sweetospathodus kummeli* in the Salt Range (Romano et al., 2013; Ware et al., 2018b), Spiti (Ware et al., 2018a; Sun et al., 2021) and South Tibet (Wang and Wang, 1995). The *Sweetospathodus kummeli* Zone corresponds to the whole early Dienerian and correlates with SNT-DI-1, SNT-DI-2, and SNT-DI-3. The first regional occurrence of the conodont *Neospathodus dieneri* seems congruent with that of *Ambites*, but may be slightly younger in the Salt Range (Romano et al., 2013).

Regarding the base of the Smithian, the first appearance of the ammonoid *Flemingites bhargavai* is coeval to that of the conodont *Novispathodus waageni* in the Salt Range (Brühwiler et al., 2012c; Romano et al., 2013). However, Krystyn et al. (2007, 2017) found in Spiti that *Novispathodus waageni* occurs ~60 cm higher than *Flemingites bhargavai*, and corresponds to the base of the *Flemingites* gr. *nanus* Zone

(=SNT-SM-4). If we adopt this conodont proposal, the Induan/Olenekian boundary will be three ammonoid UAZs higher than the *Flemingites bhargavai* Zone (Figs. 19, 20, 22-24). Their correlation remains unclear in South Tibet, due to the lack of fossiliferous limestones at the base of the Smithian in the studied sections. Thus far, a single Smithian conodont zone has been defined in Selong, the *Novispathodus waageni* Zone, roughly corresponding to the whole unit D of the Kangshare Formation (Wang and Wang, 1995). Goudemand et al. (2019) mentioned several regional Smithian conodont zones in the Salt Range, which can be easily correlated with ammonoids according to their positions in the same sections. However, the detailed taxonomic composition of these conodont zones is still unpublished. Another difficulty in Smithian correlating ammonoid and conodont scales in the SNT is the heterogeneous definitions of conodont zones. For instance, the compositions and definitions of Smithian conodont zones in the Salt Range and Spiti are quite different (Fig. 20). Similar to ammonoids, high-resolution biostratigraphical works on conodonts in different regions using a standard quantitative method, such as the UA method (e.g., Leu et al., 2022), are therefore necessary to propose robust correlations between ammonoid and conodont zones.

6 Correlation with oxygen and carbon isotopic curves

The global average surface temperature during the Early Triassic was potentially the highest in the Phanerozoic (Scotese et al., 2021), representing an extremely hot climate. Early Triassic carbon cycle and sea surface temperature experienced large fluctuations (Payne et al., 2004; Tong et al., 2007; Sun et al., 2012; Romano et al., 2013; Song et al., 2013; Goudemand et al., 2019). However, the detailed tempo of some of these perturbations remains poorly constrained. Here, we compiled the published Early Triassic oxygen and carbon isotopic data from the southern Neotethys and correlated them with the newly established high-resolution ammonoid UA zones (Fig. 24).

Four negative (N1–N4) and three positive (P1–P3) carbon isotopic excursions have been reported in the Early Triassic (Song et al., 2013), of which three negative (N1–N3) and two positive (P1–P2) excursions are encompassed in the studied interval. In the absence of biostratigraphical scales, these excursions can be used as a supplementary tool for global stratigraphic correlations (Song et al., 2013; Zhang et al., 2019).

In the SNT, N1 occurs during the early Griesbachian, and is followed by a gradual increase from the early Griesbachian to the middle Dienerian SNT-DI-4. P1 potentially occurs in SNT-DI-4, followed by a possible N2 inSNT-DI-11. However, the currently available isotopic data for this interval in the SNT are too scarce to be certain. Carbon isotopes display a rapid increase across the Dienerian/Smithian boundary and reach P2 during SNT-SM-4. After P2, carbon isotopes show a gradual decrease until N3 at the end of the middle Smithian. From the late Smithian to the Spathian, the carbon isotope curves exhibit a remarkable increase and reached P3 during the earliest Spathian. The Smithian/Spathian boundary (SSB) based on SNT ammonoids is thus located close to the recent high-resolution proposal of Leu et al. (2022) based on conodont AUs from South China.

Similarly to the carbon isotopic oscillations, the Early Triassic oxygen isotopic composition of conodont apatite also displays large fluctuations, reflecting sea surface temperature changes (Sun et al., 2012; Romano et al., 2013; Goudemand et al., 2019). Based on available data, three warm periods (W1–W3) and three relatively cooler intervals (C1–C3) occur from the Griesbachian to the early Spathian (Romano et al., 2013; Goudemand et al., 2019). Across the Permian/Triassic boundary, a rapid increase (W1) in SST has been documented at many sites, such as South China (Joachimski et al., 2012; Chen et al., 2016) and northwestern Iran (Schobben et al., 2014). However, W1 has not been formally reported from southern Neotethys due to the lack of data on the oxygen isotopes of the Changhsingian. C1 occurs during the late Griesbachian to the early Dienerian UAZ SNT-DI-2. Thereafter, the second warm period (W2) corresponds to SNT-DI-3 to SNT-DI-7. The transition from W2 to C2 has not been well-documented due to the lack of conodont apatite oxygen isotopic data in

SNT-DI-8 and SNT-DI-9. C2 begins roughly in SNT-DI-10 and persists until SNT-SM-6. From SNT-SM-6 to SNT-SM-7, oxygen isotopes exhibit a rapid and marked decrease, reflecting the beginning of the third warm period (W3). It persists until the early late Smithian SNT-SM-14. From the SNT-SM-15 to the early Spathian, oxygen isotope displays a remarkable increase, suggesting a cooling event (C3). Similar sea surface temperature changes have been reported in South China (Leu et al. 2022).

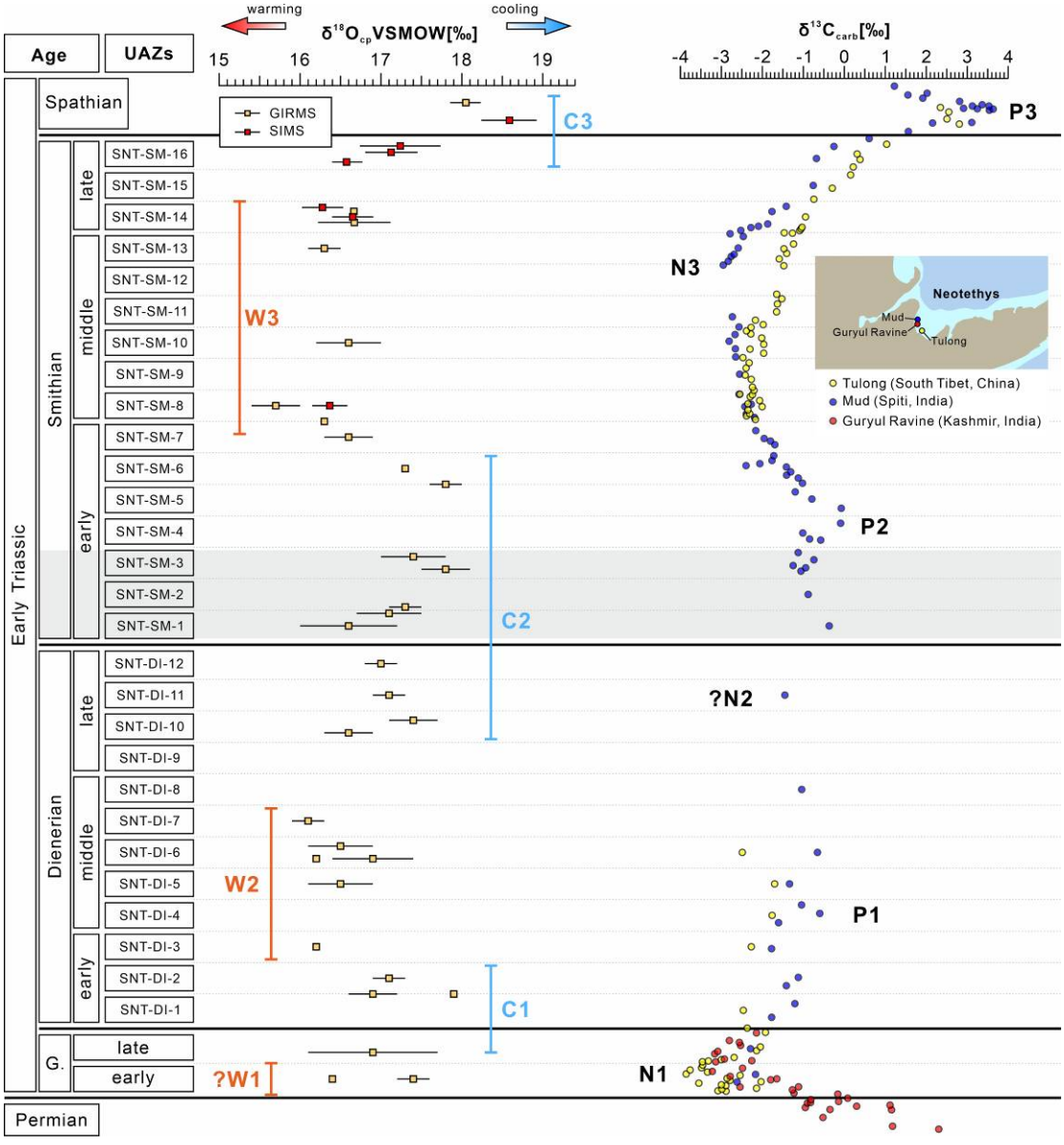

Figure 24. Correlations of ammonoid biostratigraphy with oxygen and carbon isotopic records in the southern Neotethys. Oxygen isotopic data (mean values with one standard deviation) of conodont apatite from Romano et al. (2013) and Goudemand et al. (2019). Carbon isotopic records were compiled from four sections, Tulong (Brühwiler et al., 2009), Mud (Sun et al., 2021), and Guryul Ravine (Wang et al.,

2019). Grey area indicates an uncertain interval for the Dienerian/Smithian boundary among different proposals.

7. Conclusions

The main conclusions of this work are summarized as follows:

(1) Based on exhaustive bed-by-bed sampling and a revised taxonomy, we identified 140 species from the Kangshare Formation in South Tibet covering the Griesbachian-Smithian interval. Twenty-two UAZs were recognized by means of the UA method, largely improving the known resolution of the Early Triassic ammonoid biostratigraphy in South Tibet.

(2) The synthetic analysis of the new ammonoid data from South Tibet and two other basins, i.e., Spiti (India) and the Salt Range (Pakistan), resulted in an unprecedented high-resolution Dienerian and Smithian ammonoid biostratigraphic scale, including 12 UAZs for the Dienerian and 16 UAZs for the Smithian, including a new UAZ (ST-18 in South Tibet; SM-12 at the SNT scale).

(3) These new UAZs can be well correlated within the SNT and provide a robust time calibration for carbon cycle and temperature fluctuations.

(4) Within the SNT, ammonoids and conodont biostratigraphy are in relatively good agreement to define stage/substage boundaries. However, high-resolution analyses using quantitative biostratigraphical methods on conodonts from this area await further work to achieve good correlation between conodonts and ammonoid biostratigraphies.

(5) Comprehensive global correlations for the Griesbachian, Dienerian, and Smithian ammonoid biostratigraphy are discussed in depth. We found that the originally suggested earliest Smithian *Hedenstroemia hedenstroemi* Zone in Arctic regions can be correlated to the late early Smithian age.

Despite the marked progresses of Early Triassic ammonoid biostratigraphy in recent decades and in this work, many uncertainties remain in the detailed correlation

of the zonal scheme from different basins and the definitions of the stage/substage boundaries. Additional work with similarly extensive high-resolution sampling and quantitative method in other basins is still needed to obtain comparable highly resolved biostratigraphic scales and more robust correlations.

Acknowledgments: We thank Daoliang Chu, Yunfen Huang, and Huyue Song for their assistance in the field. We are grateful for the help from the Forestry Bureau, Department of Land and Resources and Everest Protection Agency in Tibet, China. Daojun Yuan and Cheng Ji are acknowledged for their help in accessing the Early Triassic ammonoid collections at the Nanjing Institute of Geology and Palaeontology. Jérôme Thomas is thanked for access to the Early Triassic ammonoid collections stored at the Université de Bourgogne. Leopold Krystyn is acknowledged for access to the Early Triassic ammonoid collections from the Himalayas deposited in the Department of Palaeontology, University of Vienna. Hugo Bucher is thanked for access to the Early Triassic ammonoid collections stored at the Paläontologisches Institut und Museum, University of Zurich. David Ware acknowledges Michael J. Orchard and John-Paul Zonneveld from the Geological Survey of Canada in Vancouver for access to Tozer's collections. Marco Balini (Milano) and an anonymous reviewer are thanked for their constructive comments on earlier version of the manuscript

Funding: This research was funded by the National Natural Science Foundation of China (92155201, 41821001), the Strategic Priority Research Program of Chinese Academy of Sciences (XDB26000000), the 111 Project (B08030), and the Fundamental Research Funds for National University, China University of Geosciences (Wuhan) and China Scholarship Council (202006410051). This work was also supported by a BQR of the Université de Bourgogne (to X.D. and A.B.).

Author contributions:

Xu Dai: Conceptualization, Investigation, Methodology, Writing - original draft

Arnaud Brayard: Conceptualization, Supervision, Writing - review & editing

David Ware: Validation, Writing - review & editing

Shouyi Jiang: Investigation, Writing - review & editing

Mingtao Li: Investigation, Writing - review & editing

Fengyu Wang: Investigation, Writing - review & editing

Xiaokang Liu: Investigation, Writing - review & editing

Haijun Song: Conceptualization, Investigation, Supervision, Writing - review & editing

References

Balini, M., Lucas, S.G., Jenks, J.F. and Spielmann, J.A., 2010. Triassic ammonoid biostratigraphy: an overview. In: S.G. Lucas (Editor), The Triassic Timescale. The Geological Society of London London, pp. 221–262.

Bando, Y., 1964. The Triassic stratigraphy and ammonite fauna of Japan. The science reports of the Tohoku University. Second series, Geology, 36(1): 1–A30.

Bando, Y., 1970. Lower Triassic ammonoids from the Kitakami Massif. Transactions and proceedings of the Paleontological Society of Japan. New series, 79: 337–354.

Bando, Y., 1979. Upper Permian and Lower Triassic Ammonoids from Abadeh, Central Iran. Memoir of the Faculty of Education, Kagawa University, 29: 103–138.

Baud, A. and Beauchamp, B., 2001. Proposals for the redefinition of the Griesbachian substage and for the base of the Triassic in the Arctic regions. International Symposium on the Global Stratotype of the Permian-Triassic Boundary and the Paleozoic-Mesozoic Events: 26–28.

Baud, A., Richoz, S., Beauchamp, B., Cordey, F., Grasby, S., Henderson, C.M., Krystyn, L. and Nicora, A., 2012. The Buday'ah Formation, Sultanate of Oman: A Middle Permian to Early Triassic oceanic record of the Neotethys and the late Induan microsphere bloom. Journal of Asian Earth Sciences, 43: 130–144.

Benton, M.J. and Wu, F., 2022. Triassic Revolution. Frontiers in Earth Science, 10: 899541.

Bjerager, M., Seidler, L., Stemmerik, L. and Surlyk, F., 2006. Ammonoid stratigraphy and sedimentary evolution across the Permian–Triassic boundary in East Greenland. Geological Magazine, 143(5): 635–656.

Brayard, A. and Bucher, H., 2008. Smithian (Early Triassic) ammonoid faunas from northwestern Guangxi (South China): taxonomy and biochronology. Fossils and Strata, 55: 1–184.

Brayard, A., Bucher, H., Escarguel, G., Fluteau, F., Bourquin, S. and Galfetti, T., 2006. The Early Triassic ammonoid recovery: Paleoclimatic significance of diversity gradients. Palaeogeography, Palaeoclimatology, Palaeoecology, 239(3–4): 374–395.

Brayard, A., Bylund, K.G., Jenks, J.F., Stephen, D.A., Olivier, N., Escarguel, G., Fara, E. and Vennin, E., 2013. Smithian ammonoid faunas from Utah: implications for Early Triassic biostratigraphy, correlation and basinal paleogeography. Swiss Journal of Palaeontology, 132(2): 141–219.

Brayard, A., Escarguel, G. and Bucher, H., 2007. The biogeography of Early Triassic ammonoid faunas: Clusters, gradients, and networks. Geobios, 40(6): 749–765.

Brayard, A., Escarguel, G., Bucher, H. and Brühwiler, T., 2009. Smithian and Spathian (Early Triassic) ammonoid assemblages from terranes: Paleoceanographic and paleogeographic implications. Journal of Asian Earth Sciences, 36: 420–433.

Brayard, A., Jenks, J.F. and Bylund, K.G., 2019. Ammonoids and nautiloids from the earliest Spathian Paris Biota and other early Spathian localities in southeastern Idaho, USA. Geobios, 54: 13–36.

Brayard, A., Jenks, J.F., Bylund, K.G., Olivier, N., Vennin, E., Stephen, D.A., Escarguel, G. and Fara, E., 2021. Latest Smithian (Early Triassic) ammonoid assemblages in Utah (western USA basin) and their implications for regional biostratigraphy, biogeography and placement of the Smithian/Spathian boundary. Geobios, 69: 1–23.

Brayard, A., Krumenacker, L.J., Botting, J.P., Jenks, J.F., Bylund, K.G., Fara, E., Vennin, E., Olivier, N., Goudemand, N., Saucede, T., Charbonnier, S., Romano, C., Doguzhaeva, L., Ben, T., Hautmann, M., Stephen, D.A., Thomazo, C. and Escarguel, G., 2017. Unexpected Early Triassic marine ecosystem and the rise of the Modern evolutionary fauna. Science Advances, 3(2): e1602159.

Brayard, A., Olivier, N., Vennin, E., Jenks, J.F., Bylund, K.G., Stephen, D.A., McShinsky, D., Goudemand, N., Fara, E. and Escarguel, G., 2020. New middle and late Smithian ammonoid faunas from the Utah/Arizona border: New evidence for calibrating Early Triassic transgressive-regressive trends and paleobiogeographical signals in the western USA basin. Global and Planetary Change, 192: 103251.

Brosse, M., Bucher, H., Baud, A., Frisk, Å.M., Goudemand, N., Hagdorn, H., Nutzel, A., Ware, D. and Hautmann, M., 2019. New data from Oman indicate benthic high biomass productivity coupled with low taxonomic diversity in the aftermath of the Permian–Triassic Boundary mass extinction. Lethaia, 52(2): 165–187.

Brühwiler, T., Brayard, A., Bucher, H. and Guodun, K., 2008. Griesbachian and Dienerian (Early Triassic) Ammonoid Faunas from Northwestern Guangxi and Southern Guizhou (South China). Palaeontology, 51(5): 1151–1180.

Brühwiler, T., Bucher, H., Brayard, A. and Goudemand, N., 2010a. High-resolution biochronology and diversity dynamics of the Early Triassic ammonoid recovery: The Smithian faunas of the Northern Indian Margin. Palaeogeography Palaeoclimatology Palaeoecology, 297(2): 491–501.

Brühwiler, T., Bucher, H. and Goudemand, N., 2010b. Smithian (Early Triassic) ammonoids from Tulong, South Tibet. Geobios, 43(4): 403–431.

Brühwiler, T., Bucher, H., Goudemand, N. and Galfetti, T., 2012a. Smithian (Early Triassic) ammonoid faunas from Exotic Blocks from Oman: taxonomy and biochronology. Palaeontographica Abteilung A: 13–107.

Brühwiler, T., Bucher, H. and Krystyn, L., 2012b. Middle and late Smithian (Early Triassic) ammonoids from Spiti, India. Special Papers in Palaeontology Series(88): 115–174.

Brühwiler, T., Bucher, H., Roohi, G., Yaseen, A. and Rehman, K., 2011. A new early Smithian ammonoid fauna from the Salt Range (Pakistan). Swiss Journal of Palaeontology, 130(2): 187–201.

Brühwiler, T., Bucher, H., Ware, D., Hermmann, E., Hochuli, P.A., Roohi, G., Rehman, K. and Yaseen, A., 2012c. Smithian (Early Triassic) ammonoids from the Salt Range. Special Papers in Palaeontology Series, 88: 1–114.

Brühwiler, T., Goudemand, N., Galfetti, T., Bucher, H., Baud, A., Ware, D., Hermann, E., Hochuli, P.A. and Martini, R., 2009. The Lower Triassic sedimentary and carbon isotope records from Tulong (South Tibet) and their significance for Tethyan palaeoceanography. Sedimentary Geology, 222: 314–332.

Brühwiler, T., Ware, D., Bucher, H., Krystyn, L. and Goudemand, N., 2010c. New Early Triassic ammonoid faunas from the Dienerian/Smithian boundary beds at the Induan/Olenekian GSSP candidate at Mud (Spiti, Northern India). Journal of Asian Earth Sciences, 39(6): 724–739.

Burgess, S.D., Bowring, S. and Shen, S.-z., 2014. High-precision timeline for Earth's most severe extinction. Proceedings of the National Academy of Sciences of the United States of America, 111(9): 3316–3321.

Chao, K., 1959. Lower Triassic ammonoids from Western Kwangsi, China. Palaeontol. Sinica Science Press, 355 pp.

Chen, B., Joachimski, M.M., Wang, X.-d., Shen, S.-z., Qi, Y.-p. and Qie, W.-k., 2016. Ice volume and paleoclimate history of the Late Paleozoic Ice Age from conodont apatite oxygen isotopes from Naqing (Guizhou, China). Palaeogeography, Palaeoclimatology, Palaeoecology, 448: 151–161.

Collignon, M., 1973. Ammonites du Trias inférieur et moyen d'Afghanistan. Annales de Paléontologie, 59: 127–163.

Dagys, A., 1994a. Lower Triassic stage, substage and zonal scheme of North-Eastern Aisa. Mémoires de Géologie (Lausanne), 22: 15–23.

Dagys, A., 1994b. Zonation of eastern Boreal Lower Triassic and Induan/Olenekian boundary. Albertiana, 15: 19–23.

Dagys, A. and Ermakova, S., 1996. Induan (Triassic) ammonoids from North-Eastern Asia. Revue de Paléobiologie, 15: 401–447.

Dai, X. and Song, H., 2020. Toward an understanding of cosmopolitanism in deep time: a case study of ammonoids from the middle Permian to the Middle Triassic. Paleobiology, 46(4): 533–549.

Dai, X., Song, H., Brayard, A. and Ware, D., 2019. A new Griesbachian–Dienerian (Induan, Early Triassic) ammonoid fauna from Gujiao, South China. Journal of Paleontology, 93(1): 48–71.

Dai, X., Yuan, Z., Brayard, A., Li, M., Liu, X., Jia, E., Du, Y., Song, H. and Song, H., 2021. Calibrating the late Smithian (Early Triassic) crisis: New insights from the Nanpanjiang Basin, South China. Global and Planetary Change, 201: 103492.

Dai, X., Davies, J.H.F.L., Yuan, Z., Brayard, A., Ovtcharova, M., Xu, G., Liu, X., Smith, C.P.A., Schweitzer, C.E., Li, M., Perrot, M.G., Jiang, S., Miao, L., Cao, Y., Yan, J., Bai, R., Wang, F., Guo, W., Song, H., Tian, L., Dal Corso, J., Liu, Y., Chu, D. and Song, H., 2023. A Mesozoic fossil lagerstätte from 250.8 million years ago shows a modern-type marine ecosystem. Science, 379(6632): 567–572.

Đaković, M., 2017. New Early Triassic (Smithian) ammonoids from Gornji Brčeli (southern Montenegro). Austrian Journal of Earth Sciences, 110(2): 96–104.

Đaković, M., Krystyn, L. and Sudar, M., 2022. The Middle Smithian (Early Triassic) ammonoids of Gornji Brčeli (Southern Montenegro). Rivista Italiana di Paleontologia e Stratigrafia. 128(2): 411–430.

Dal Corso, J., Song, H., Callegaro, S., Chu, D., Sun, Y., Hilton, J., Grasby, S.E., Joachimski, M.M. and Wignall, P.B., 2022. Environmental crises at the Permian–Triassic mass extinction. Nature Reviews Earth & Environment, 3(3): 197–214.

Diener, C., 1897. The Cephalopoda of the Lower Trias. Palaeontologia Indica, 15(2): 1–181.
Ehiro, M., 1998. Permian ammonoid fauna of the Kitakami Massif northeast Japan-Biostratigraphy and Paleobiogeography. Palaeoworld, 9: 113–122.
Ehiro, M., Sasaki, O., and Kano, H., 2016. Ammonoid fauna of the upper Olenekian Osawa Formation in the Utatsu area, South Kitakami Belt, Northeast Japan. Paleontological Research, 20(2): 90–104.
Ehiro, M., 2022. Latest Olenekian (Early Triassic) ammonoids from the uppermost part of the Osawa Formation (Inai Group) in the South Kitakami Belt, Northeast Japan. Paleontological Research, 26(2): 137–157.
Gaetani, M., Jacobsshagen, V., Nicora, A., Kauffmann, G., Tselepidis, V., Sestini, N.F., Mertmann, D. and Skourtsis-Coroneou, V., 1992. The Early-Middle Triassic boundary at Chios (Greece). Rivista Italiana di Paleontologia e Stratigrafia, 98(2): 181–204.
Galfetti, T., Bucher, H., Martini, R., Hochuli, P.A., Weissert, H., Crasquin-Soleau, S., Brayard, A., Goudemand, N., Brüehwiler, T. and Guodun, K., 2008. Evolution of Early Triassic outer platform paleoenvironments in the Nanpanjiang Basin (South China) and their significance for the biotic recovery. Sedimentary Geology, 204(1–2): 36–60.
Galfetti, T., Bucher, H., Ovtcharova, M., Schaltegger, U., Brayard, A., Bruehwiler, T., Goudemand, N., Weissert, H., Hochuli, P.A., Cordey, F. and Guodun, K., 2007a. Timing of the Early Triassic carbon cycle perturbations inferred from new U-Pb ages and ammonoid biochronozones. Earth and Planetary Science Letters, 258(3–4): 593–604.
Galfetti, T., Bucher, H., Ovtcharova, M., Schaltegger, U., Brayard, A., Brühwiler, T., Goudemand, N., Weissert, H., Hochuli, P.A., Cordey, F. and Guodun, K., 2007b. Timing of the Early Triassic carbon cycle perturbations inferred from new U-Pb ages and ammonoid biochronozones. Earth and Planetary Science Letters, 258(3–4): 593–604.
Goudemand, N., 2014. Note on the conodonts from the Induan-Olenekian boundary. Albertiana, 42: 49–51.
Goudemand, N., Romano, C., Leu, M., Bucher, H., Trotter, J.A. and Williams, I.S., 2019. Dynamic interplay between climate and marine biodiversity upheavals during the Early Triassic Smithian-Spathian biotic crisis. Earth-Science Reviews, 195: 169–178.
Grasby, S.E., Beauchamp, B., Embry, A. and Sanei, H., 2013. Recurrent Early Triassic ocean anoxia. Geology, 41(2): 175–178.
Griesbach, C.L., 1880. Palaeontological notes on the Lower Trias of the Himalayas. Geological Survey of India Records 13(2): 83–113.
Guex, J., Galster, F. and Hammer, Ø., 2016. Discrete Biochronological Time Scales. Springer International Publishing, Switzerland, 160 pp.
Guex, J., Hungerbühler, A., Jenks, J.F., O'Dogherty, L., Atudorei, V., Taylor, D.G., Bucher, H. and Bartolini, A., 2010. Spathian (Lower Triassic) ammonoids from western USA (Idaho, California, Utah and Nevada). Mémoires de Géologie de Lausanne, 49: 1–81.
Hammer, Ø., Harper, D.A. and Ryan, P.D., 2001. PAST: paleontological statistics software package for education and data analysis. Palaeontologia Electronica, 4(1): 9.
Hansen, B.B., Bucher, H., Schneebeli-Hermann, E. and Hammer, Ø., 2021. The middle Smithian (Early Triassic) ammonoid *Arctoceras blomstrandi*: conch morphology and ornamentation in relation to stratigraphy. Papers in Palaeontology, 7(3): 1435–1457.
He, G., Wang, Y. and Chen, G., 1986. Early and Middle Triassic of Mt. Burhan Budai, Central Qinghai,

Carboniferous and Triassic strata and fossils from the southern slope of Mt. Burhan Budai, Qinghai Nanking, pp. 171–274.

Henderson, C.M. and Baud, A., 1997. Correlation of the Permian-Triassic boundary in Arctic Canada and comparison with Meishan, China. Proceedings of the 30th International Geological Congres (Beijing, 1996), 11: 143–152.

Hermann, E., Hochuli, P.A., Mehay, S., Bucher, H., Brühwiler, T., Ware, D., Hautmann, M., Roohi, G., ur-Rehman, K. and Yaseen, A., 2011. Organic matter and palaeoenvironmental signals during the Early Triassic biotic recovery: The Salt Range and Surghar Range records. Sedimentary Geology, 234(1–4): 19–41.

Hsu, J., 1976. Discovery of Glossopteris flora in southern Xizang and its significance to geology and paleogeography. Scientia Geologica Sinica, 4: 323–331.

Hyatt, A. and Smith, J.P., 1905. The Triassic cephalopod genera of America. U.S. Geol. Surv., prof. pap, 40: 1–394.

Ishii, K.-i., Fischer, J. and Bando, Y., 1971. Notes on the Permian-Triassic boundary in Eastern Afghanistan. Journal of Geosciences, 14(1): 1–18.

Jattiot, R., Bucher, H. and Brayard, A., 2020. Smithian (Early Triassic) ammonoid faunas from Exotic Blocks from Timor: taxonomy and biochronology. Palaeontographica Abteilung A, 317(1–6): 1–137.

Jattiot, R., Bucher, H., Brayard, A., Brosse, M., Jenks, J.F. and Bylund, K.G., 2017. Smithian ammonoid faunas from northeastern Nevada: implications for Early Triassic biostratigraphy and correlation within the western USA basin. Palaeontographica Abteilung A, 309: 1–89.

Jenks, J., Guex, J., Hungerbühler, A., Taylor, D.G. and Bucher, H., 2013. Ammonoid biostratigraphy of the early Spathian *Columbites parisianus* Zone (Eary Triassic) at Bear Lake Hot Springs, Idaho. New Mexico Museum of Natural History and Science, 61: 268–283.

Jenks, J.F. and Brayard, A., 2018. Smithian (Early Triassic) ammonoids from Crittenden Springs, Elko County, Nevada: taxonomy, biostratigraphy and biogeography. New Mexico Museum of Natural History and Science Bulletin, 78: 1–175.

Jenks, J.F., Brayard, A., Brühwiler, T. and Bucher, H., 2010. New Smithian (Early Triassic) ammonoids from Crittenden Springs, Elko County, Nevada: implications for taxonomy, biostratigraphy and biogeography. Bulletin of New Mexico Museum of Natural History & Science, 48: 1–41.

Jenks, J.F., Maekawa, T., Ware, D., Shigeta, Y., Brayard, A. and Bylund, K.G., 2021. Late Griesbachian (Early Triassic) ammonoids and nautiloids from the Dinwoody Formation at Crittenden Springs, Elko county, Nevada. New Mexico Museum of Natural History and Science, 86: 1–23.

Jenks, J.F., Monnet, C., Balini, M., Brayard, A. and Meier, M., 2015. Biostratigraphy of Triassic Ammonoids. In: C. Klug, I. Kruta, D. Korn, R.H. Mapes and K.D. Baets (Editors), Ammonoid Paleobiology: From macroevolution to paleogeography. Springer, Netherlands, pp. 329–388.

Ji, C., Zhang, C., Jiang, D., Bucher, H., Motani, R. and Tintori, A., 2015. Ammonoid age control of the Early Triassic marine reptiles from Chaohu (South China). Palaeoworld, 24(3): 277–282.

Jin, Y., Shen, S., Zhu, Z., Mei, S. and Wang, W., 1996. The Selong Xishan section, candidate of the global stratotype section and point of the Permian-Triassic boundary. In: H. Yin (Editor), The Palaeozoic-Mesozoic Boundary Candidates of the Global Stratotype Section and Point of the Permian-Triassic Boundary. China University of Geosciences Press, Wuhan, pp. 127–137.

Joachimski, M.M., Lai, X., Shen, S., Jiang, H., Luo, G., Chen, B., Chen, J. and Sun, Y., 2012. Climate

warming in the latest Permian and the Permian-Triassic mass extinction. Geology, 40(3): 195–198.

Joachimski, M.M., Müller, J., Gallagher, T.M., Mathes, G., Chu, D., Mouraviev, F., Silantiev, V., Sun, Y. and Tong, J., 2022. Five million years of high atmospheric CO2 in the aftermath of the Permian-Triassic mass extinction. Geology, 50(6): 650–654.

Kiparisova, L.D. and Popov, Y.N., 1956. Subdivision of the lower series of the Triassic system into stages. Doklady Academy Sciences U.S.S.R., 109: 842–845.

Klein, C. and Korn, D., 2016. Quantitative analysis of the late Famennian and early Tournaisian ammonoid stratigraphy. Newsletters on Stratigraphy, 49/1: 1–26.

Korchinskaya, M.V., 1972. Biostratigraphy of Triassic deposits of Svalbard. Bulletin of Canadian Petroleum Geology, 20(4): 742–749.

Korn, D., Leda, L., Heuer, F., Salimi, H.M., Farshid, E., Akbari, A., Schobben, M., Ghaderi, A., Struck, U., Gliwa, J., Ware, D. and Hairapetian, V., 2021. Baghuk Mountain (Central Iran): high-resolution stratigraphy of a continuous Central Tethyan Permian–Triassic boundary section. Fossil Record, 24: 1–22.

Krafft, A.V. and Diener, C., 1909. Lower Triassic cephalopoda from Spiti. Malla Johar, and Byans. Palaeontologia Indica, 15: 1–186.

Krystyn, L. and Orchard, M.J., 1996. Lowermost Triassic ammonoid and conodont biostratigraphy of Spiti, India. Albertiana, 17: 10–21.

Krystyn, L., Orchard, M.J. and Richoz, S., 2017. Revised conodont and ammonoid biochronology of the N. waageni-date based IOB in the GSSP candidate section of Mud (Spiti, Himalaya). Geo.Alp., 14: 127.

Krystyn, L., Richoz, S., Baud, A. and Twitchett, R.J., 2003. A unique Permian–Triassic boundary section from the Neotethyan Hawasina Basin, Central Oman Mountains. Palaeogeography, Palaeoclimatology, Palaeoecology, 191(3–4): 329–344.

Krystyn, L., Richoz, S. and Bhargava, O.N., 2007. The Induan-Olenekian Boundary (IOB) in Mud—an update of the candidate GSSP section M04. Albertiana, 36: 33–45.

Kummel, B., 1968a. New Zealand Triassic ammonoids. New Zealand Journal of Geology and Geophysics, 3(3): 486–509.

Kummel, B., 1968b. Scythian ammonoids from Timor. Museum of Comparative Zoology, 283: 1–21.

Kummel, B. and Erben, H.K., 1968. Lower and Middle Triassic cephalopods from Afghanistan. Palaeontographica Abteilung A: 95–148.

Kummel, B. and Sakagami, S., 1960. Mid-Scythian ammonites from Iwai formation, Japan. Museum of Comparative Zoology, 126: 1–11.

Kummel, B. and Steele, G., 1962. Ammonites from the *Meekoceras gracilitatus* Zone at Crittenden Spring, Elko County, Nevada. Journal of Paleontology, 36(4): 638–703.

LEU 2022

Li, M., Song, H., Algeo, T.J., Wignall, P.B., Dai, X. and Woods, A.D., 2018a. A dolomitization event at the oceanic chemocline during the Permian-Triassic transition. Geology, 46(12): 1043–1046.

Li, M., Song, H., Tian, L., Woods, D.A., Dai, X. and Song, H., 2018b. Lower Triassic deep sea carbonate precipitates from South Tibet, China. Sedimentary Geology, 376: 60–71.

Li, M., Song, H., Wignall, P.B., She, Z., Dai, X., Song, H. and Xiao, Q., 2019a. Early Triassic oceanic red beds coupled with deep sea oxidation in South Tethys. Sedimentary Geology, 391: 105519.

Li, M., Song, H., Woods, A.D., Dai, X. and Wignall, P.B., 2019b. Facies and evolution of the carbonate factory during the Permian–Triassic crisis in South Tibet, China. Sedimentology, 59: 646–678.

Lindström, S., Bjerager, M., Alsen, P., Sanei, H. and Bojesen-Koefoed, J., 2020. The Smithian–Spathian boundary in North Greenland: implications for extreme global climate changes. Geological Magazine, 157(10): 1547–1567.

Lyu, Z., Orchard, M.J., Chen, Z.-Q., Henderson, C.M. and Zhao, L., 2020. A proposed ontogenesis and evolutionary lineage of conodont *Eurygnathodus costatus* and its role in defining the base of the Olenekian (Lower Triassic). Palaeogeography Palaeoclimatology Palaeoecology, 559: 109916.

Maekawa, T. and Jenks, J.F., 2021. Smithian (Olenekian, Early Triassic) conodonts from ammonoid-bearing limestone blocks at Crittenden Springs, Elko County, Nevada, USA. Paleontological Research, 25(3): 201–245.

Mathews, A.A.L., 1929. The Lower Triassic cephalopod fauna of the Fort Douglas area, Utah. Walker Museum Memoirs 1(1): 1–46.

Mojsisovics, E., Waagen, W.H. and Diener, C., 1895. Entwurf einer Gliederung der pelagischen sedimente des Trias-Systems. Sitzungsberichte der kaiserlichen Akademie der Wisseenchaften Wien, mathematisch–naturwissenschaftliche Classe. 104(1): 1271–1302

Monnet, C. and Bucher, H., 2005. Anisian (Middle Triassic) ammonoids from North America: quantitative biochronology and biodiversity. Stratigraphy, 2(4): 281–296.

Monnet, C., Bucher, H., Brayard, A. and Jenks, J.F., 2013. Globacrochordiceras gen. nov (Acrochordiceratidae, late Early Triassic) and its significance for stress-induced evolutionary jumps in ammonoid lineages (cephalopods). Fossil Record, 16(2): 197–215.

Mu, A.-T., Wen, S.-H., Wang, Y., Chang, P.-K. and Yin, C.-X., 1973. Stratigraphy of the Mount Jolmo Lungma region in Southern Tibet, China. Scientia Sinica, 16(1): 96–111.

Mu, L., Zakharov, Y.D., Li, W. and Shen, S., 2007. Early Induan (Early Triassic) cephalopods from the Daye Formation at Guiding, Guizhou Province, South China. Journal of Paleontology, 81(5): 858–872.

Nakazawa, K. and Bando, Y., 1968. Lower and Middle Triassic ammonites from Portuguese Timor. Memoirs of the Faculty of Science, Kyoto University, Series of Geol. & Mineral., 34(2): 83–114.

Newell, N.D. and Kummel, B., 1942. Lower Eo-Triassic stratigraphy, western Wyoming and southeast Idaho. Geological Society of America Bulletin, 53: 937–996.

Orchard, M.J., 1996. Conodont fauna from the Permian-Triassic boundary: observations and reservations. Permophiles, 28: 36–39.

Orchard, M.J., 2010. Triassic conodonts and their role in stage boundary definition. In: S.G. Lucas (Editor), The Triassic Timescale. The Geological Society of London London, pp. 139–161.

Orchard, M.J., Nassichuk, W.W. and Rui, L., 1994. Conodonts from the lower Griesbachian *Otoceras latilobatum* bed of Selong, Tibet and the position of the Permian-Triassic boundary. Canadian Society or Petroleum Geologists, Memoir 17: 823–843.

Orchard, M.J. and Tozer, E.T., 1997. Triassic conodont biochronology, its calibration with the ammonoid standard, and a biostratigraphic summary for the Western Canada Sedimentary Basin. Bulletin of Canadian Petroleum Geology, 45(4): 675–692.

Ovtcharova, M., Goudemand, N., Hammer, O., Guodun, K., Cordey, F., Galfetti, T., Schaltegger, U. and Bucher, H., 2015. Developing a strategy for accurate definition of a geological boundary

through radio-isotopic and biochronological dating: The Early-Middle Triassic boundary (South China). Earth-Science Reviews, 146: 65–76.

Pan, H. and Shen, S., 2008. Late Permian (Lopingian) gastropods from the Qubuerga Formation at the Qubu section in the Mt. Everest (Qomolangma) Region, Southern Tibet (Xizang), China. Journal of Paleontology, 82(5): 1038–1042.

Payne, J.L., Lehrmann, D.J., Wei, J., Orchard, M.J., Schrag, D.P. and Knoll, A.H., 2004. Large perturbations of the carbon cycle during recovery from the end-Permian extinction. Science, 305(5683): 506–509.

Piazza, V., Hammer, Ø. and Jattiot, R., 2017. New late Smithian (Early Triassic) ammonoids from the Lusitaniadalen Member, Vikinghøgda Formation, Svalbard. Norwegian Journal of Geology, 97(2): 105–117.

Posenato, R., 1992. Tirolites (Ammonoidea) from the Dolomites, Bakony and Dalmatia: taxonomy and biostratigraphy. Eclogae Geologicae Helvetiae, 85(3): 893–929.

Raup, D.M., 1979. Size of the permo-triassic bottleneck and its evolutionary implications. Science, 206(4415): 217–218.

Romano, C., Goudemand, N., Vennemann, T.W., Ware, D., Schneebeli-Hermann, E., Hochuli, P.A., Brüehwiler, T., Brinkmann, W. and Bucher, H., 2013. Climatic and biotic upheavals following the end-Permian mass extinction. Nature Geoscience, 6(1): 57–60.

Sakagami, S., Sciunnach, D. and Garzanti, E., 2006. Late Paleozoic and Triassic bryozoans from the Tethys Himalaya (N India, Nepal and S Tibet). Facies, 52: 279–298.

Schobben, M., Joachimski, M.M., Korn, D., Leda, L. and Korte, C., 2014. Palaeotethys seawater temperature rise and an intensified hydrological cycle following the end-Permian mass extinction. Gondwana Research, 26(2): 675–683.

Scotese, C.R., 2014. Atlas of Middle & Late Permian and Triassic Paleogeographic maps, maps 43–48 from volume 3 of the PALEOMAP Atlas for ArcGIS (Jurassic and Triassic) and maps 49–52 from volume 4 of the PALEOMAP PaleoAtlas for ArcGIS (Late Paleozoic). Mollweide Projection, PALEOMAP Project, Evanston, IL.

Scotese, C.R., Song, H., Mills, B.J. and van der Meer, D.G., 2021. Phanerozoic paleotemperatures: The earth's changing climate during the last 540 million years. Earth-Science Reviews, 215: 103503.

Sepkoski, J.J., 1981. A factor analytic description of the Phanerozoic marine fossil record. Paleobiology, 7(1): 36–53.

Shen, S., Archbold, N.W., Shi, G.-R. and Chen, Z.-Q., 2000. Permian brachiopods from the Selong Xishan section, Xizang (Tibet), China. Part 1: Stratigraphy, Strophomenida, Productida and Rhynchonellida. Geobios, 33(6): 725–752.

Shen, S., Archbold, N.W., Shi, G.-R. and Chen, Z.-Q., 2001. Permian brachiopods from the Selong Xishan section, Xizang (Tibet), China. Part 2: Palaeobiogeographical and Palaeontological implications, Spiriferida, Athyridida and Terebratulida. Geobios, 34(2): 157–182.

Shen, S., Cao, C., Henderson, C.M., Wang, X., Shi, G.R., Wang, Y. and Wang, W., 2006. End-Permian mass extinction pattern in the northern peri-Gondwanan region. Palaeoworld, 15: 3–30.

Shen, S., Cao, C., Shi, G.R., Wang, X. and Mei, S., 2003a. Lopingian (Late Permian) stratigraphy, sedimentation and palaeobiogeography in southern Tibet. Newsletters on stratigraphy, 39(2–3): 157–179.

Shen, S., Mu, L. and Zakharov, Y.D., 2004. *Roadoceras* (Permian Ammonoidea) from the Qubuerga

Formation in the Mt. Everest Area in Southern Tibet. Gondwana Research, 7(3): 863–869.
Shen, S., Shi, G.-R. and Archbold, N.W., 2003b. Lopingian (Late Permian) brachiopods from the Qubuerga Formation at the Qubu section in the Mt. Qomolangma region, southern Tibet (Xizang), China. Palaeontographica Abteilung a-Palaozoologie-Stratigraphie, 268(1–3): 49–101.
Shevyrev, A.A., 1995. Triassic ammonites of northwestern Caucasus. Trudy Paleontologiceskogo Instituta (Akademija Nauk SSR), 264: 1–174.
Shevyrev, A.A., 2006. Triassic Biochronology: State of the Art and Main Problems. Stratigraphy and Geological Correlation, 14(6): 629–641.
Shigeta, Y., 2022. Revision of early Spathian (late Olenekian, Early Triassic) ammonoids from the Osawa Formation at Akaushi in the Motoyoshi area, South Kitakami Belt, Northeast Japan. Paleontological Research, 26(4): 405–419.
Shigeta, Y., Komatsu, T., Maekawa, T. and Tran, H.D., 2014. Olenekian (Early Triassic) stratigraphy and fossil assemblages in northeastern Vietnam, 45. National Museum of Nature and Science, 1–309 pp.
Shigeta, Y., Zakharov, Y.D., Maeda, H. and Popov, A.M., 2009. The Lower Triassic System in the Abrek Bay Area, South Primorye, Russia, 38. National Museum of Nature and Science, Tokyo, 218 pp.
Smith, C.P.A., Laville, T., Fara, E., Escarguel, G., Olivier, N., Vennin, E., Goudemand, N., Bylund, K.G., Jenks, J.F., Stephen, D.A., Hautmann, M., Charbonnier, S., Krumenacker, L.J. and Brayard, A., 2021. Exceptional fossil assemblages confrm the existence of complex Early Triassic ecosystems during the early Spathian. Scientific Reports, 11: 19657.
Smith, J.P., 1932. Lower Triassic ammonoids of North America. USGS Professional Paper, 167: 1–199.
Smyshlyaeva, O. and Zakharov, Y., 2012. New representatives of the family Melagathiceratidae (Ammonoidea) from the Lower Triassic of South Primorye. Paleontological Journal, 46(2): 142–147.
Smyshlyaeva, O. and Zakharov, Y.D., 2013. New members of the family Flemingitidae (Ammonoidea) from the Lower Triassic of South Primorye. Paleontological Journal, 47(3): 247–255.
Smyshlyaeva, O. and Zakharov, Y.D., 2015. New lower triassic ammonoids from South Primorye. Paleontological Journal, 49(2): 111–120.
Song, H., Huang, S., Jia, E., Dai, X., Wignall, P.B. and Dunhill, A.M., 2020. Flat latitudinal diversity gradient caused by the Permian–Triassic mass extinction. Proceedings of the National Academy of Sciences of the United States of America, 117(30): 17578–17583.
Song, H., Tong, J., Algeo, T.J., Horacek, M., Qiu, H., Song, H., Tian, L. and Chen, Z.-Q., 2013. Large vertical $\delta^{13}C$ DIC gradients in Early Triassic seas of the South China craton: implications for oceanographic changes related to Siberian Traps volcanism. Global and Planetary Change, 105: 7–20.
Song, H., Wignall, P.B. and Dunhill, A.M., 2018. Decoupled taxonomic and ecological recoveries from the Permo-Triassic extinction. Science Advances, 4(10): eaat5091.
Song, H., Wignall, P.B., Tong, J., Bond, D.P., Song, H., Lai, X., Zhang, K., Wang, H. and Chen, Y., 2012. Geochemical evidence from bio-apatite for multiple oceanic anoxic events during Permian–Triassic transition and the link with end-Permian extinction and recovery. Earth and Planetary Science Letters, 353: 12–21.
Souquet, L. and Goudemand, N., 2020. Exceptional basal-body preservation in some Early Triassic

conodont elements from Oman. Palaeogeography, Palaeoclimatology, Palaeoecology, 549: 109066.

Spath, L.F., 1930. The Eo-Triassic invertebrate fauna of East Greenland. Meddelelser om Grønland, 83: 1–90.

Spath, L.F., 1935. Additions to the Eo-Triassic invertebrate fauna of East Greenland. Meddelelser om Grønland, 98: 1–115.

Stanley, S.M., 2016. Estimates of the magnitudes of major marine mass extinctions in earth history. Proceedings of the National Academy of Sciences of the United States of America, 113(42): E6325–E6334.

Stemmerik, L., Bendix-Almgreen, S.E. and Piasecki, S., 2001. The Permian–Triassic boundary in central East Greenland: past and present views. Bulletin of the Geological Society of Denmark, 48: 159–167.

Sun, Y., Joachimski, M.M., Wignall, P.B., Yan, C., Chen, Y., Jiang, H., Wang, L. and Lai, X., 2012. Lethally hot temperatures during the Early Triassic greenhouse. Science, 338(6105): 366–370.

Sun, Y.D., Richoz, S., Krystyn, L., Grasby, S.E., Chen, Y.L., Banerjee, D. and Joachimski, M.M., 2021. Integrated bio-chemostratigraphy of Lower and Middle Triassic marine successions at Spiti in the Indian Himalaya: Implications for the Early Triassic nutrient crisis. Global and Planetary Change, 196: 103363.

Tong, J., Zakharov, Y.D., Orchard, M.J., Yin, H., and Hansen, H.J., 2003. A candidate of the Induan-Olenekian boundary stratotype in the Tethyan region. Science in China Series D: Earth Sciences, 46: 1182–1200.

Tong, J., Zakharov, Y.D. and Wu, S., 2004. Early Triassic ammonoid succession in Chaohu, Anhui Province. Acta Palaeontologica Sinica, 43(2): 192–204.

Tong, J., Zuo, J. and Chen, Z.Q., 2007. Early Triassic carbon isotope excursions from South China: Proxies for devastation and restoration of marine ecosystems following the end-Permian mass extinction. Geological Journal, 42(3–4): 371–389.

Tozer, E.T., 1965. Lower Triassic stages and Ammonoid zones of Arctic Canada. Paper of the Geological Survey of Canada, 65-12: 1–14.

Tozer, E.T., 1967. A standard for Triassic time. Bulletin of the Geological Survey of Canada, 156: 1–141.

Tozer, E.T., 1994. Canadian Triassic ammonoid faunas. Geological Survey of Canada, 467: 1–663.

Tozer, E.T. and Parker, J.R., 1968. Notes on the Triassic biostratigraphy of Svalbard. Geological Magazine, 105(6): 526–542.

Trümpy, R., 1969. Lower Triassic ammonites from Jameson Land (East Greenland). Meddelelser om Grønland, 168: 77–116.

Visscher, H., 1992. The new STS Triassic stage nomenclature. Albertiana, 10: 1.

Wang, L., Wignall, P.B., Sun, Y., Yan, C., Zhang, Z. and Lai, X., 2017. New Permian-Triassic conodont data from Selong (Tibet) and the youngest occurrence of *Vjalovognathus*. Journal of Asian Earth Sciences, 146: 152–167.

Wang, X.D., Cawood, P.A., Zhao, H., Zhao, L.S., Grasby, S.E., Chen, Z.Q. and Zhang, L., 2019. Global mercury cycle during the end-Permian mass extinction and subsequent Early Triassic recovery. Earth and Planetary Science Letters, 513: 144–155.

Wang, Y., 1984. Earliest Triassic ammonoid faunas from Jiangsu and Zhejiang and their bearing on the definition of Permo-Triassic boundary. Acta Palaeontologica Sinica, 23(3): 257–269.

Wang, Y. and Chen, G., 1984. The Triassic ammonoid horizons in Qinghai Province. Tibetan Plateau Geology Anthology, 14: 137–146.

Wang, Y. and He, G., 1976. Triassic ammonoids from the Mount Jolmo Lungma region. In: A report of scientific expedition in the Mount JolmoLungma region (1966-1968), Palaeontology, 3: 223–502.

Wang, Y., Sun, D. and He, G., 1980. New insights in stratigraphy of the Himalaya. Journal of Stratigraphy, 4(1): 55–59.

Wang, Z. and Wang, Y., 1995. Permian-Lower Triassic conodonts from Selong Xishan of Nyalam, S. Tibet, China. Acta Micropalaeontologica Sinica, 12(4): 333–348.

Ware, D., Bucher, H., Brayard, A., Schneebeli-Hermann, E. and Brühwiler, T., 2015. High-resolution biochronology and diversity dynamics of the Early Triassic ammonoid recovery: the Dienerian faunas of the Northern Indian Margin. Palaeogeography, Palaeoclimatology, Palaeoecology, 440: 363–373.

Ware, D., Bucher, H., Brühwiler, T. and Krystyn, L., 2018a. Dienerian (Early Triassic) ammonoids from Spiti (Himachal Pradesh, India). Fossil & Strata, 63: 177–241.

Ware, D., Bucher, H., Brühwiler, T., Schneebeli-Hermann, E., Hochuli, P.A., Roohi, G., Rehman, K. and Yaseen, A., 2018b. Griesbachian and Dienerian (Early Triassic) ammonoids from the Salt Range, Pakistan. Fossil & Strata, 63: 11–175.

Ware, D., Jenks, J.F., Hautmann, M. and Bucher, H., 2011. Dienerian (Early Triassic) ammonoids from the Candelaria Hills (Nevada, USA) and their significance for palaeobiogeography and palaeoceanography. Swiss Journal of Geosciences, 104(1): 161–181.

Waterhouse, J.B., 1994. The Early and Middle Triassic ammonoid succession of the Himalayas in western and central Nepal Part 1. Stratigraphy, classification and early Scythian ammonoid systematics. Palaeontographica Abteilung A, 232: 1–83

Waterhouse, J.B., 1996a. The Early and Middle Triassic ammonoid succession of the Himalayas in western and central Nepal Part 2. Systematic Studies of the early middle Scythian. Palaeontographica Abteilung A, 241: 27–100.

Waterhouse, J.B., 1996b. The Early and Middle Triassic ammonoid succession of the Himalayas in western and central Nepal Part 3. late middle Scythian ammonoids. Palaeontographica Abteilung A, 241: 101–167.

Waterhouse, J.B., 1999. The Early and Middle Triassic ammonoid succession of the Himalayas in western and central Nepal Part 4. late Scythian. Palaeontographica Abteilung A, 254: 101–190.

Weitschat, W. and Dagys, A., 1989. Triassic biostratigraphy of Svalbard and a comparison with NE-Siberia. Mitteilungen aus dem Geologisch-Paläontologischen Institut der Universität Hamburg, 68: 179–213.

Weitschat, W. and Hamburg, U.L., 1978. Biostratigraphy of the uppermost part of the Smithian Stage (Lower Triassic) at the Botneheia, W-Spitsbergen. Mitteilungen Geologisch-Paläontologischen Institut Universität Hamburg, 48: 85–100.

Welter, O.A., 1922. Die Ammoniten der unteren Trias von Timor. Paläontol. Timor, 11: 83–160.

Widmann, P., Bucher, H., Leu, M., Vennemann, T., Bagherpour, B., Schneebeli-Hermann, E., Goudemand, N. and Schaltegger, U., 2020. Dynamics of the largest carbon isotope excursion during the Early Triassic biotic recovery. Frontiers in Earth Science, 8: 196.

Wu, K., Tong, J., Metcalfe, I., Liang, L., Xiao, Y. and Tian, L., 2020. Quantitative stratigraphic

correlation of the Lower Triassic in South China based on conodont unitary associations. Earth-Science Reviews, 200: 102997.

Wu, Y., Chu, D., Tong, J., Song, H., Dal Corso, J., Wignall, P.B., Song, H., Du, Y. and Cui, Y., 2021. Six-fold increase of atmospheric pCO2 during the Permian–Triassic mass extinction. Nature communications, 12(1): 1–8.

Xiao, Y., Suzuki, N. and He, W., 2018. Low-latitudinal standard Permian radiolarian biostratigraphy for multiple purposes with Unitary Association, Graphic Correlation, and Bayesian inference methods. Earth-Science Reviews, 179: 168–206.

Yin, A. and Harrion, T.M., 2000. Geologic evolution of the Himalayan-Tibetan orogen. Annual review of earth and planetary sciences, 28: 211–280.

Yin, H., Zhang, K., Tong, J., Yang, Z. and Wu, S., 2001. The global stratotype section and point (GSSP) of the Permian-Triassic boundary. Episodes, 24(2): 102–114.

Yuan, D., Zhang, Y. and Shen, S., 2018. Conodont succession and reassessment of major events around the Permian-Triassic boundary at the Selong Xishan section, southern Tibet, China. Global and Planetary Change, 161: 194–210.

Zakharov, Y.D., 1994. Proposals on revision of the Siberian standard for the Lower Triassic and candidate stratotype section and point for the Induan-Olenekian boundary. Albertiana, 14: 44–51.

Zakharov, Y.D., Biakov, A.S., Horacek, M., Kutygin, R.V., Sobolev, E.S. and Bond, D.P., 2020. Environmental control on biotic development in Siberia (Verkhoyansk Region) and neighbouring areas during Permian–Triassic large igneous province activity. In: J. Guex, J.S. Torday and W.B. Miller Jr. (Editors), Morphogenesis, Environmental Stress and Reverse Evolution. Springer Nature Switzerland: 197–231.

Zakharov, Y.D., Bondarenko, L., Smyshlyaeva, O.P. and Popov, A.M., 2013. Late Smithian (Early Triassic) ammonoids from the *Anasibirites nevolini* Zone of South Primorye, Russian Far East. In: L.H. Tanner, J.A. Spielmann and S.G. Lucas (Editors), The Triassic System. New Mexico Museum of Natural History and Science, 61: 597–612.

Zakharov, Y.D., Bondarenko, L.G., Popov, A.M. and Smyshlyaeva, O.P., 2021. New findings of latest Early Olenekian (Early Triassic) fossils in South Primorye, Russian Far East, and their stratigraphical significance. Journal of Earth Science, 32(3): 554–572.

Zakharov, Y.D., Shigeta, Y., Popov, A.M., Sokarev, A.N., Buryi, G.I., Golozubov, V.V., Panasenko, E.S. and Dorukhovskaya, E.A., 2000. The candidates of global stratotypes of the boundary of the Induan and Olenekian stages of the Lower Triassic in southern Primorye. Albertiana, 24: 12–26.

Zhao, L., Orchard, M.J., Tong, J., Sun, Z., Zuo, J., Zhang, S. and Yun, A., 2007. Lower Triassic conodont sequence in Chaohu, Anhui Province, China and its global correlation. Palaeogeography, Palaeoclimatology, Palaeoecology, 252(1-2): 24–38.

Zhang, C., Bucher, H. and Shen, S.-Z., 2017. Griesbachian and Dienerian (Early Triassic) ammonoids from Qubu in the Mt. Everest area, southern Tibet. Palaeoworld, 26(4): 650–662.

Zhang, L., Orchard, M.J., Brayard, A., Algeo, T.J., Zhao, L., Chen, Z.-Q. and Zhengyi, L., 2019. The Smithian/Spathian boundary (late Early Triassic): A review of ammonoid, conodont, and carbon-isotopic criteria. Earth-Science Reviews, 195: 7–36.

Zhang, M., 1976. A new species of Helicoprionid shark from Xizang. Scientia Geologica Sinica, 4: 332–336.

1843 Zhang, Y.-C., Shi, G.R. and Shen, S.-Z., 2013. A review of Permian stratigraphy, palaeobiogeography
1844 and palaeogeography of the Qinghai–Tibet Plateau. Gondwana Reaserch, 24: 55–76.
1845 Zhang, S.-H., Shen, S.-Z. and Erwin, D.H., 2022. Latitudinal diversity gradient dynamics during
1846 Carboniferous to Triassic icehouse and greenhouse climates. Geology, 50(10): 1166–1171.